Numerical Modeling of Methane Decomposition for Hydrogen Production in a Fluidized Bed Reactor

by

Maryam Younessi Sinaki

A thesis
presented to the University of Waterloo
in fulfillment of the
thesis requirement for the degree of
Doctor of Philosophy
in
Mechanical Engineering

Waterloo, Ontario, Canada, 2014

AUTHOR'S DECLARATION

I hereby declare that I am the sole author of this thesis. This is a true copy of the thesis, including any required final revisions, as accepted by my examiners.

I understand that my thesis may be made electronically available to the public.

Abstract

The decomposition of methane for hydrogen production is an attractive alternative to the established method of reforming. This process considerably reduces the emission of greenhouse gases, and its overall efficiency and cost are competitive. The decomposition of methane is performed with a catalyst to produce a substantial amount of hydrogen, and decrease the operating temperature. Between different catalysts available, carbon is selected in this study due to its low rate of decay and advantages such as low cost and availability. Also, a fluidized bed reactor operating in the particulate regime is employed due to the efficient contact between the catalyst and the gas. Consequently, hydrogen production from the thermocatalytic decomposition of methane in a particulate fluidized bed reactor of carbon particles is investigated.

To obtain an appropriate design and operation for this process, the effect of different operating parameters and catalyst properties should be investigated on the performance. This aim can be achieved by modeling. A number of models with different complexities have been proposed for this process. Considering the objective of this thesis, a complex kinetic model is required to represent the effect of the catalyst properties. In literature, the kinetics is generally modeled with a global equation using experimental parameters. Since investigation on the effect of the properties of the catalyst is not feasible with this method, the detailed kinetic model with a surface reaction mechanism is employed in this study. Investigation on this surface mechanism is very limited, and only one of the models available in literature is determined to be appropriate. Nevertheless, this model has some important drawbacks. The major problem is that the specific surface area is considered as the only catalyst property affecting the activity of carbon. Experimental studies suggest that the activity of this catalyst is a function of its specific surface area and number of active sites, and neglecting either of these properties can lead to a high inaccuracy. Consequently, a new kinetic model is developed where a modified form of the available mechanism is used, and the number of active sites and the specific surface area of the catalyst are considered in the rate equations. It is noted that although several experimental investigations have been performed on the origin of the active sites, their quantity has not been acceptably determined yet. A method is presented in this study to estimate the number of active sites with the developed model and

experimental data. To the best knowledge of the author, this is the first model to incorporate the effect of this parameter for carbon catalysts in the decomposition of methane and quantify its value. Another important problem of the model available in literature is its dependency on experimental measurements for determining the hydrodynamic characteristics of the fluidized bed. In this study, the hydrodynamics of the reactor is modeled with empirical correlations to obtain a complete representation of the process within the required accuracy, with minimal experimental requirements.

The model is used to investigate the effect of different operating parameters and catalyst properties on the amount of the initial methane conversion. The operating parameters studied are the temperature, residence time, gas velocity, and composition of the feed gas. The catalyst properties considered are the particle size and pore volume, the number of active sites, and the percentage of fine particles in the bed. The effect of the variations of each of these factors in a certain range is investigated for a fluidized bed reactor operating at the onset of fluidization at nominal condition. The onset of fluidization is maintained by changing the inlet flow rate in a reactor of a specific size. The results show that, considering the range of variations in this study, the procedures that cause the highest improvement in conversion are: increasing the residence time, decreasing the size of particles, adding fine particles to the bed, increasing the temperature, using catalysts with high surface areas or large number of active sites, changing the inlet gas composition, and using catalysts with large pore volumes, respectively. It is noted that all of these improvements are associated with higher initial or operating costs. Therefore, changing each of these factors beyond a certain value is faced with economic and technical barriers. Consequently, the possibility and efficiency of using two factors simultaneously for achieving higher conversions was also investigated. The results can be used as a guideline to choose between several catalysts considering their characteristics, or to suggest appropriate operating conditions.

Acknowledgements

First and foremost, I would like to express my sincere gratitude to my supervisor, Professor Feridun Hamdullahpur, for guiding this thesis with his extensive knowledge. I thank him for his continuous support and valuable advice during my PhD program.

I would like to thank Dr. A. M. Al Taweel of Dalhousie University for serving as my external examiner, as well as my committee members Dr. Xianguo Li, Dr. Fue Sang Lien and Dr. Eric Croiset.

I gratefully acknowledge the financial support of the Natural Sciences and Engineering Research Council of Canada (NSERC), Toyota Motor Manufacturing Canada (TMMC), Sun Microsystems of Canada, and Gabriel David Warshaw Memorial Fund.

I would also like to thank Dr. Edgar Matida for his suggestions during the early phase of this research.

I extend my deepest gratitude to my parents, Parvaneh and Abbas, for their support and encouragement in every phase of my life and for understanding me and being there for me throughout the years. Thanks to my brothers, Mohammad and Ahmadreza, for their encouragements.

Last but not least, I am so thankful to my husband, Siamak, and my son, Arman, for their love and support, for sharing their happiness with me, and for making my hard times easier. I am deeply grateful for having a wonderful family.

Dedication

To my beloved husband Siamak,

To the joy of my life, my son Arman,

And to my precious parents Parvaneh and Abbas.

Table of Contents

List of Tables

List of Figures

Nomenclature

Notations

A_s : Surface area of the particles per volume, m^2/m^3

C : Molar concentration of gaseous species, mol/m^3

d_p : Diameter of the catalyst particles, m

d^* : Dimensionless diameter

E_a : Activation Energy, J/mol

f_s : Ratio of number density of active of catalyst to that of ordered carbon

F_{45} : Mass fraction of particles smaller than 45 μm

g : Acceleration of gravity, m/s^2

HR : Hausner ratio

i : Number of carbon atoms in a particle

K_i : Constant parameters used in the calculation of u_{mf} (i = 1 to 4)

k : Per-site rate coefficient of surface reactions or rate constant, 1/mol s

k_B : Boltzmann constant, 1.3807×10^{-23} m^2 kg/s^2 K^1

k_o : Pre-exponential factor

L_0 : Height of the bed, m

m : Mass of reactant, kg

M_r : r^{th} moment, $1/m^3$

MW : Molecular weight, kg/mol

n : Order of reaction

N_A : Avogadro's number, 6.022×10^{23} 1/mol

N_i : Number density of size i particles, $1/m^3$

P : Pressure, atm

r : Reaction rate, mol/m^3 s

R : Universal gas constant, 8.314 J/mol K

S_{BET} : Specific surface area of the catalyst, m^2/kg

T	:	Temperature, K
u	:	Velocity of the fluid, m/s
u*	:	Dimensionless velocity
u_t	:	Terminal velocity, m/s
u_t'	:	Velocity that creates a void fraction equal to unity, m/s
v	:	Pore volume, cm^3/gr
X_{CH4}	:	Methane conversion
x_{H2}	:	Mole fraction of hydrogen produced
Y	:	Mass fraction

Greek Letters

γ	:	Collision efficiency
ε	:	Void fraction of the reactor
μ	:	Viscosity of the gas, kg/m s
ρ	:	Density, kg/m^3
ϕ	:	Sphericity
τ	:	Residence time of the gas in the reactor, s
χ	:	Number density of surface sites, $1/m^2$
$\dot{\omega}$	:	Molar production rate, mol/m^3 s

Subscripts

a	:	Adsorbed
as	:	Active sites
comp	:	Value of a variable with a specific composition
f	:	Final value
g	:	Gas
i	:	Number of reaction
in	:	Reactor inlet
k	:	Number of species
mb	:	Minimum bubbling
mf	:	Minimum fluidization

o	:	Initial value
os	:	Surface sites on ordered carbon
p	:	Catalyst particles
ref	:	Nominal value
T	:	Value of a variable at a specific temperature T
u	:	Value of a variable at a specific velocity u
V	:	Changes with respect to variable V
ρ	:	Value of a variable with a specific density ρ

Chapter 1
Introduction

Hydrogen is an attractive fuel for the future. The application of this fuel considerably reduces greenhouse gas emissions compared to current methods of producing energy [1]. One of the challenges in the way of broader commercial scale utilization of hydrogen is the presence of obstacles associated with the methods of producing this gas. Hydrogen can be produced from different substances, such as water [2, 3] and biomass [4, 5]. However, due to economic and technical constraints, fossil fuels have been found to be the most appropriate source at the present time and in the foreseeable future [6, 7]. The most established method of hydrogen production is currently the reforming of methane [8, 9]. The efficiency of this method is rather high [10], but it has the disadvantage of producing a significant amount of CO_2 gas as a by-product [11]. The separation of carbon dioxide from hydrogen and its subsequent sequestration are complex and increase the cost of the overall process. The alternative method of decomposition of methane has been proposed for hydrogen production [6, 12-14]. This method has the benefit of considerably reducing the CO_2 produced. It is therefore more appropriate with regard to environmental concerns, and also simplifies the overall process. Comparison of these two methods shows that the decomposition of methane is an attractive alternative to the established reforming process and a valuable field of research as a technology for hydrogen production in the future [6, 15].

In order to produce a substantial amount of hydrogen, the decomposition of methane is either performed with a catalyst [16-18], or at high temperatures commonly obtained from solar energy conversion [19, 20]. The catalysts used in this process are classified into two main groups of metals and carbons. The application of transition metal catalysts, such as Ni or Co, in the decomposition of methane for the production of carbon dates back to several decades ago [21]. These catalysts have a high initial activity and considerably decrease the operating temperature. However, they are rapidly deactivated due to the deposition of carbon, which removal results in the production of large amounts of CO_2. On the other hand, carbon catalysts, which were originally proposed by Muradov [14], remain active for a longer period, and also enable the use of the deposited carbon as a marketable by-product. The use of carbonaceous catalysts also offers other advantages such as durability, availability and low cost.

Fluidized bed reactors have been proposed for this process to obtain a high contact between the catalyst and the gas. This type of reactor allows a high mass and heat transfer, and provides the possibility of removing the produced carbon in continuous operation [22]. The optimal operation of the fluidized bed is achieved in the particulate regime due to the uniform mixing. Consequently, hydrogen production from the thermocatalytic decomposition of methane in a particulate fluidized bed reactor of carbon particles is investigated in this study.

1.1. Motivation

In order to achieve an appropriate design and operation for the process of thermocatalytic decomposition of methane with carbon catalysts, a sound understanding of the performance of this process should be obtained. Consequently, the variations of the amount of hydrogen production with important factors, such as operating parameters and catalyst properties, should be investigated. Several experimental studies have been performed to provide such an insight. Although the results of these studies are valuable, the ranges investigated are limited, and expanding these results is expensive. Also, investigation on some factors, mainly some of the properties of the catalyst, is not feasible experimentally. Therefore, it is important to develop an adequate model for representing the amount of hydrogen from this process while considering the main affecting factors.

A limited number of models have been proposed for the thermocatalytic decomposition of methane over carbon catalysts in fixed and fluidized beds [23-26]. Some numerical studies have also been performed on this reaction in solar reactors, where methane is seeded with carbon particles mainly to improve heat transfer [27-33]. In most of these investigations, the kinetics of the process has been modeled with an empirical power law, where the apparent order of the reaction and the required parameters are determined experimentally for each different type of carbon catalyst. These models have been used to study the temperature distribution and the effect of parameters such as temperature and flow rate on methane conversion. However, since the properties of the catalysts were not considered in these models, investigation on the effect of employing different catalysts and modifying the catalyst properties is not feasible with this method. To overcome this limitation, a detailed model is needed for the kinetics of the reaction, with proper inclusion of the properties of the catalyst. Information concerning the detailed kinetic modeling of the process of decomposition of methane with carbon catalysts is very limited. A detailed model has been proposed [25] for fluidized bed reactors with a plausible surface reaction mechanism. However, this model has some shortcomings. First, it cannot be employed as a standalone application, since it is reliant on experimental measurements, specifically the hydrodynamics characteristics of the fluidized bed. Also, the only catalyst property considered in this study to represent the difference between the activities of various carbon types is the surface area of the catalyst, which according to experiments is not adequate.

Experimental studies have been performed on the characteristics of the catalyst to find the main properties affecting the amount of hydrogen production [34-41]. These studies suggest that the discrepancies observed in the activity of various types of carbon catalysts can be explained by the differences in the specific surface areas and the number of active sites. The active sites are the sites on the surface of the catalyst that are more prone to react with the surrounding gas. The number of active sites is consequently one of the main catalyst properties to consider in the modeling of the process. This factor is different in various types of carbon catalysts, where it is generally accepted that defects and irregularities on the surface form active sites [18, 34, 39]. Hence, the number of active sites is a function of the characteristics of the surface of the catalyst. Although methods have been suggested for obtaining a comparative amount of the number of active sites on different type of carbon

catalysts for methane decomposition [34], a general method has not yet been established to find this value. As discussed earlier, this factor has not been included in existing models. Consequently, one of the important limitations of the existing models is the lack of consideration of the catalyst properties necessary to differentiate between the activities of various types of carbon.

1.2. Objective

The objective of this study is to develop a model to investigate the variations of the production of hydrogen under the influence of factors that can be modified to obtain an optimal design and operation. The main factors to be investigated can be classified into two groups of operating parameters and catalyst properties. The effect of operating parameters such as temperature can be investigated with simplified kinetic models. However, the effect of the properties of the catalyst particles is not considered in these models. Consequently, a detailed kinetic model should be used to include the effect of these parameters and enable the study of the application of different types of carbon catalysts and the investigation of the effect of their properties.

One of the aims in this study is to include the number of active sites on the surface of the catalyst in the model. This parameter has been proposed as one of the main properties that can explain the difference between the activities of several types of carbon catalyst available. However, it has not been acceptably determined yet, and its effect has not been considered in any of the existing models. Therefore, the intent is to include the number of active sites in the model, to estimate this value for different types of catalysts, and to investigate its effect on the amount of hydrogen production under various conditions.

It is noted that an important feature sought in this study is to obtain the variations of hydrogen production with minimal recourse to experiment by developing a standalone model. Therefore, the kinetics of the reaction should be coupled with the hydrodynamics model to determine the characteristics of the fluidized bed reactor.

1.3. Outline

This thesis consists of five chapters. The process of decomposition of methane for hydrogen production and its advantages are presented in Chapter 2. Also, the incentives of using a fluidized bed reactor and carbon catalysts are discussed, and the main characteristics of this type of reactor are introduced. A literature review is then provided for the different methods of modeling the process. The development of the new model is presented in Chapter 3. The interaction of gas phase species is first modeled based on combustion mechanisms and the effect of the catalyst is then added with a detailed kinetic model that take into consideration the main catalyst properties. The hydrodynamics model of the fluidized bed is also described in this chapter. Chapter 4 focuses on the results obtained with the developed model. The effects of different operating parameters and the main properties of carbon catalysts are presented in this chapter. The contributions of this study are summarized in Chapter 5 and some potential future works are suggested.

Chapter 2
Literature Review

Hydrogen is a clean and effective fuel for the future. It is known as a clean fuel since it only produces water as a by-product, in contrast to conventional fuels with high greenhouse gas emissions. In addition, it has the potential to yield a higher efficiency compared to traditional methods of energy production when used in fuel cells [10]. These motivations have directed many studies to investigate on hydrogen as the clean energy source for the future. In order to make hydrogen a marketable fuel, the fields of production, storage, and utilization of this gas should progress further.

Considering that hydrogen cannot be directly obtained from the environment, methods should be designed for producing this gas using natural resources. The main sources for hydrogen production are water, biomass, and fossil fuels. Water might be thought to be an ideal source for hydrogen. However, methods that use water are either too expensive, or are in the early phase of development [42]. Biomass is another promising source that can be used to produce hydrogen with the method of reforming [43, 44]. This method also requires considerable development because of the fast deactivation of the catalysts used in the process and the low hydrogen production [45]. Fossil fuels, specifically natural gas, are currently the most attractive and accessible resource for hydrogen production in terms of economics and technological feasibility. Most of the required hydrogen worldwide is produced from fossil fuels and this trend is expected to continue in the next decades [7, 46]. It is noted that

methane, which is the main component of natural gas, is the preferred source of hydrogen among different hydrocarbons due to its high hydrogen content and lower cost.

Different methods of hydrogen production from methane have been developed. Methane steam reforming is currently the most common method to produce hydrogen. The main problem of this method is the large amount of carbon dioxide produced. Methane decomposition has been suggested as an alternative to this method, since it almost completely eliminates carbon dioxide emissions. In this chapter, the methods of steam reforming and methane decomposition are briefly described and rationales for choosing the latter method in this study are explained. The different catalysts available for decreasing the operating temperature of the decomposition of methane are presented. The effect of their properties on the performance of the process is then investigated. Next, the fluidized bed is presented as the suitable reactor for this process due to its advantages over other available reactors. Finally, the different aspects for modeling methane decomposition in a fluidized bed of carbon particles are explained, and the models available in literature along with their shortcomings are presented.

2.1. Hydrogen Production from Methane

The main methods of hydrogen production from methane are steam reforming and thermal decomposition. In this section, these processes and the additional units required in a hydrogen production plant using these methods are presented. Their benefits and disadvantages are then explained, followed by an overall comparison.

2.1.1. Methane Steam Reforming

Reforming of methane is currently the most economic and widely used way to produce hydrogen. In this process, the endothermic reaction of steam and methane produces hydrogen and carbon monoxide, as shown in the following reaction.

$$CH_4 + H_2O \rightarrow CO + 3H_2 \qquad \Delta H^{o}_{298} = +206.1 \ \text{kJ/mol}$$

The catalytic steam reforming of methane usually takes place over a nickel catalyst at a temperature range of 1100 to 1300 K [47]. The reaction is highly endothermic requiring a heat input for the reaction, and additional energy for producing steam from liquid water.

Since reforming produces a mixture of hydrogen and carbon monoxide, some additional processes must be added to obtain pure hydrogen. The schematic diagram of a hydrogen production plant with reforming is shown in Fig. 2-1.

In this plant, the first process that follows reforming is water gas shift, where the remaining energy of the incompletely burned carbon in CO is used to extract an additional mole of hydrogen from steam as follow:

$$CO + H_2O \rightarrow CO_2 + H_2 \qquad \Delta H^{\circ}_{298} = -41 \ \text{kJ/mol}$$

The next process is the removal of CO_2 from the gas mixture to obtain a clean hydrogen stream. The total CO_2 emissions from reforming process could reach up to 0.3–0.4 m^3 per m^3 of hydrogen produced [48]. Therefore, if the process of steam reforming is to be used for hydrogen production and meet the requirements of lowering greenhouse gas emissions, the CO_2 by-product should be sequestered. Sequestration of this gas is an energy intensive process, involving the capture, pressurization, transportation and injection of liquid CO_2 under the ocean or underground, in depleted natural gas wells or geologic formations. The CO_2 capture and storage highly increases the cost of hydrogen production. It is noted that the technical feasibility of CO_2 sequestration has been proven on large-scale systems [49]. However, many concerns still exist with regard to the safety and problems associated with this procedure, and the duration of CO_2 retention [50, 51].

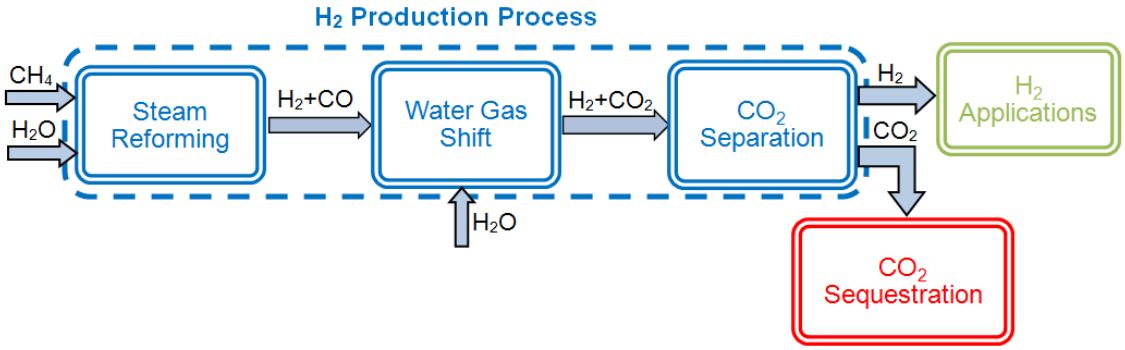

Fig. 2-1: Schematic of a hydrogen production plant with reforming process.

2.1.2. Methane Thermal Decomposition

An alternative route for hydrogen production is methane decomposition. This method, which has received much attention in recent years, eliminates CO_2 emission and its only by-product is carbon. It is therefore considered an environmentally attractive approach for the production of hydrogen from natural gas. In this process, methane is heated to a high temperature in an air-free and water-free environment, and decomposes to carbon and hydrogen through the following reaction:

$$CH_4 \rightarrow C + 2H_2 \qquad \Delta H^{\circ}_{298} = +75.6 \ \text{kJ/mol}$$

Methane decomposition is a moderately endothermic process that occurs at high temperatures in excess of 1500 K. This temperature can decrease with the use of catalysts.

A schematic representation of the hydrogen production plant with the methane decomposition process is shown in Fig. 2-2. Since this process produces no CO or CO_2 by-products, it eliminates the need for water gas shift and CO_2 removal stages required by conventional hydrogen production plants. Therefore, the overall CO_2 emission is significantly reduced and the process is less complex. In addition to hydrogen, the process produces the important by-product of carbon. Carbon can be marketed, or stored for future use.

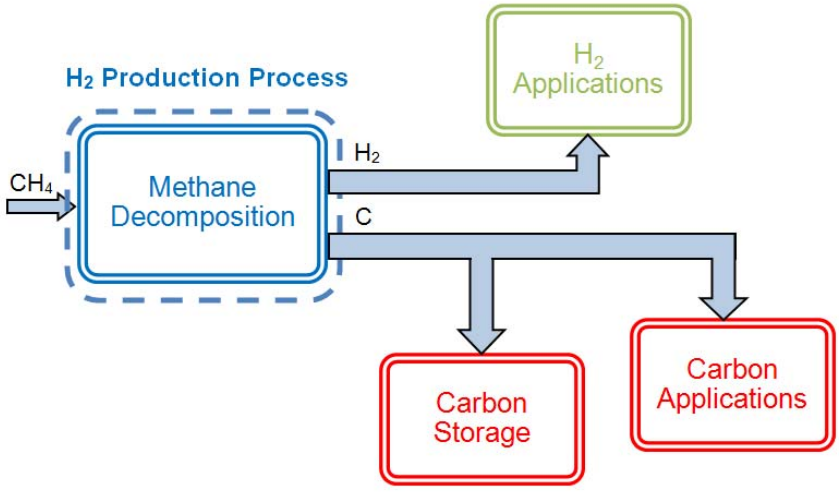

Fig. 2-2: Schematic of a hydrogen production plant with methane decomposition process.

2.1.3. Comparison of Steam Reforming and Methane Decomposition

To meet the requirements of a clean fuel, hydrogen should be produced with a method with little or no CO_2 emission. As a conclusion, steam reforming with carbon dioxide sequestration, or the alternative method of methane decomposition should be used. In this section, these two processes are compared considering their efficiency, cost of hydrogen produced, and environmental impact.

A comparison of the efficiencies shows that steam reforming is more efficient than methane decomposition; however, adding the procedure of separation and sequestration of CO_2 lowers the net efficiency of this process to around 60%, which is very close to the efficiency of methane decomposition [8, 15, 48]. It is also noted that the carbon by-product from the decomposition of methane encloses a large amount of energy, and has the potential to be used in future technologies such as carbon direct fuel cells. This application would further increase the overall efficiency of using the methane decomposition process.

The cost of hydrogen produced from the decomposition of methane and steam reforming without CO_2 sequestration is compared in Fig. 2-3. Since the carbon by-product from the decomposition of methane is a marketable product, its selling price affects the overall cost of the produced hydrogen. It is observed that methane decomposition is initially more expensive than steam reforming without CO_2 sequestration. However, if the produced carbon is marketed at a price of around $350/kg or more, the former process becomes economical. It is noted that the carbon by-product can be used as a substitute for petroleum coke with a market value of $310–460/ton. Also, other markets are available for this product offering a higher price [8]. However, the amount of carbon required in these applications is much lower than the amount that would be produced by large scale production of hydrogen as a fuel. Therefore, determining a proper application for the produced carbon is an important step in the commercialization of the decomposition of methane. It is noted that the above economic comparison was made while considering the process of steam reforming without CO_2 sequestration. When the addition of this procedure is considered to lower greenhouse gas emission, the price of hydrogen from both technologies is very close even without considering marketing of the carbon by-product.

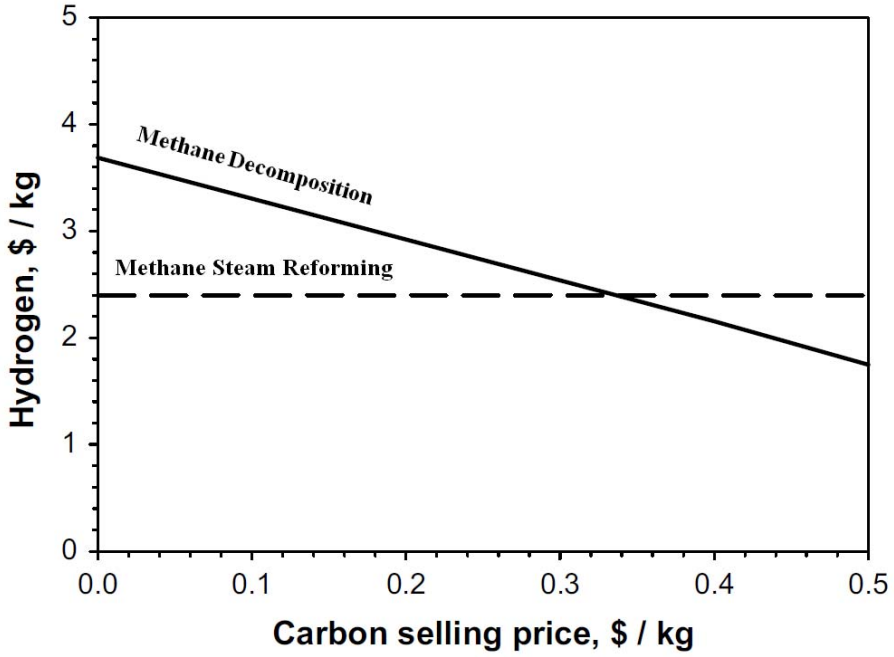

Fig. 2-3: Price of hydrogen produced from thermal decomposition of methane and methane steam reforming as a function of carbon selling price (Reprinted from [8]**, with permission from the International Journal of Hydrogen Energy).**

A thorough comparison of the environmental impact of the steam reforming and methane decomposition was performed by Dufour *et al.* [7]. This study shows that although CO_2 sequestration reduces the emission of this gas from steam reforming, it creates an additional negative environmental impact due to its high energy requirements. It can be concluded that, considering the environmental factor, the method of methane decomposition is more appropriate than steam reforming, even with the addition of the process of CO_2 sequestration.

Overall, methane thermal decomposition has great potential benefits in producing fuel with lower amounts of greenhouse gas emission. Also, since CO and CO_2 are not present in the outlet gas from this process, it is more beneficial for certain kinds of fuel cells that are sensitive to the presence of these gases. Nevertheless, this process is in an early stage of development compared to the established method of steam reforming, and requires development of an efficient process. The aforementioned advantages of methane decomposition versus reforming certainly justifies spending the effort in developing the production of hydrogen with this method.

2.2. Thermocatalytic Decomposition of Methane

The technology of methane decomposition was evaluated to be an attractive method for hydrogen production. In order to produce a substantial amount of hydrogen, this process is either performed with a catalyst, or at high temperatures commonly obtained from solar energy. A drawback of the non-catalytic decomposition of methane is the production of undesired by products, such as ethane, ethylene and acetylene, which are thermodynamically favoured at high temperatures. Also, in addition to the high energy required, special materials and equipments should be used due to the operating conditions of this process. The application of a catalyst considerably reduces the temperature and eliminates these problems. The different choices of catalyst are discussed in this section. The effect of their properties is then investigated to identify the main ones affecting the performance of this process. Another important subject in the investigation of the catalytic decomposition of methane is the selection of a suitable reactor. This topic is subsequently discussed, and the operation of the selected reactor is described.

2.2.1. Catalyst

The homogeneous decomposition of methane occurs at high temperatures (>1500 K), due to very strong C–H bonds. In order to develop an efficient process and reduce the temperature, an appropriate catalyst is required. The selection of an efficient and durable catalyst is an essential step for the development of this process.

Metals, such as Ni, Fe, Co, Pd, have been investigated as appropriate catalysts for methane decomposition since early 60's [52]. While the activation energy for non-catalytic methane decomposition was reported in the range of 370 to 433 kJ/mol [53], metal catalysts lower this value to around 60 kJ/mol [54]. The comparison between these values shows the efficiency of using this type of catalyst. Accordingly, the reaction temperature can be lowered to a value around 1000 K or below with metal catalysts. On the other hand, these catalysts have a major drawback, which is their rapid deactivation. This occurs with the carbon lay down on the catalyst surface, which blocks the active surface sites. In order to reactivate the catalysts, carbon is usually burned off of the surface, or in some cases is gasified with steam [55]. Although these methods solve the deactivation problem, they both

result in the production of large amounts of CO_2, creating a negative aspect for the overall process.

Considering the problems associated with the use of metals, carbon was suggested as an alternative catalyst [14] and the technical feasibility of the application of this catalyst has been demonstrated [56]. The activation energy of methane decomposition is lowered to 140–238 kJ/mol when appropriate carbon catalysts are used [40]. Although carbons can have a considerable catalytic effect on the process, their initial activity is low compared to metals. However, these catalysts have been accepted as a suitable alternative to metal catalysts due to several advantages. One of the benefits of using carbon is the slow rate of deactivation. These catalysts can therefore be used for a longer period. Furthermore, the carbon by-product can be marketed to reduce the cost. Methods have also been proposed to activate this by-product and use it in the process. In contrast to metal catalysts, handling of the carbon by-product does not produce any considerable amount of CO_2, and the emission of this gas is mitigated. Some of the other benefits of carbon as a catalyst are its availability, durability, low cost, high temperature resistance, and tolerance to harmful impurities in the feedstock [39].

Two different group of carbon have been found to be suitable catalysts for the process of decomposition of methane: activated carbons and carbon blacks. Activated carbon is a form of carbon that has been processed to create a high surface area by increasing its porosity. It has a high initial activity compared to other carbons. Although the deactivation rate of this catalyst is slower than metals, it eventually becomes inactivate, but over a longer period. The typical trend of deactivation of this catalyst can be observed in an example illustrated in Fig. 2-4. The other carbon proposed as a suitable catalyst for methane decomposition is carbon black. Carbon black is an elemental carbon formed in the incomplete combustion of heavy hydrocarbons in hot flames. The surface area of carbon blacks is relatively high, but it is generally smaller than that of activated carbons. The initial activity of carbon blacks is also lower than activated carbons [14, 41]. This catalyst experiences a similar initial deactivation. However, as observed in the example presented in Fig. 2-4, the deactivation of carbon black does not continue till its complete inactivity. Instead, it reaches a quasi steady state with an intermediate activity that is preserved for a long time [35, 38, 41, 57, 58].

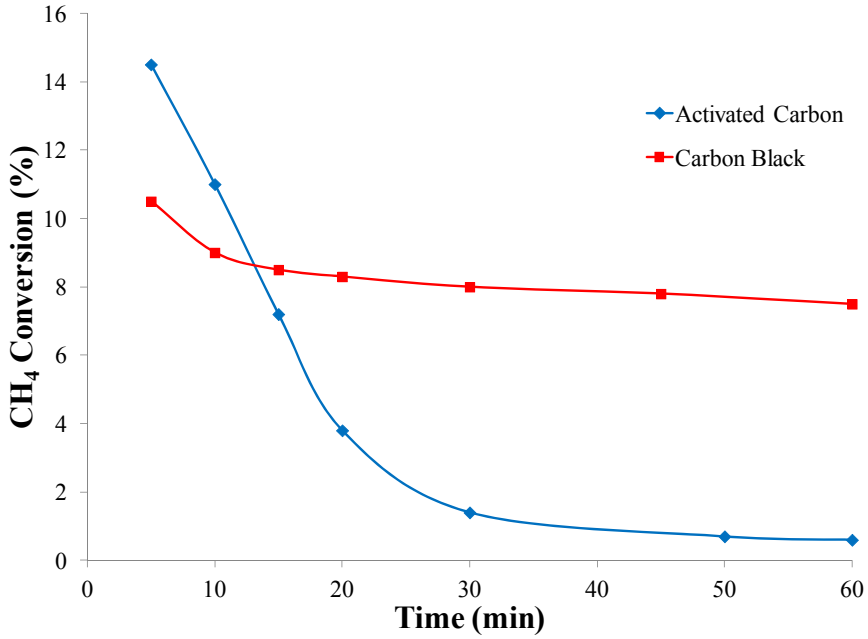

Fig. 2-4: Variations of methane conversion with time over an activated carbon and a carbon black at 1173 K. Data from references [40] **and** [41]**.**

Multiple experimental investigations have been performed on the decomposition of methane over these two groups of carbon, as well as several other samples of carbon, to study the effect of their properties on the catalytic activity. The most important of these properties are discussed in the following subsections.

Specific Surface Area

Experimental studies have been performed on the initial activity of different types of carbon, such as activated carbon, carbon blacks, acetylene black, graphite and cokes, with a wide range of surface areas from 8 and 3000 m^2/g. The initial reaction rate of methane decomposition over several types of carbon is plotted against their specific surface area in Fig. 2-5. The results show that the highest activities are usually associated with large surface areas [34, 39, 59, 60]. However, a deeper investigation on different samples of the same group, like activated carbons [39, 40, 60, 61] or carbon blacks [35, 37, 41] reveals many exceptions to this trend. It is concluded that the surface area is most probably a determining factor in the activity of the carbon catalyst; however, other factors should also be considered to explain the discrepancies observed [56, 61].

As discussed earlier, the activity of carbon blacks reaches a quasi stable condition after a certain time. It is interesting to note that experimental data show that, contrary to the initial activity, the stable activity of different types of carbon black is related to the specific surface area of the fresh catalyst [36, 38]. As shown in Fig. 2-6, the stable activity of different carbon blacks increases linearly with the specific surface area, until it reaches a maximum at high surface areas and then remains constant. While other researchers have postulated that the slope of this line depends on the kind of carbon black characterized by its application, like color, rubber, and conductive blacks, Fig. 2-6 shows that when the reaction rate at similar operating conditions are compared, all samples reasonably follow the same line.

Porosity

Experimental studies show that the pore volume and the pore size distribution do not directly affect the initial activity of the catalyst. It should be mentioned that since particles with high porosities generally have a large surface area, a large pore volume usually result in a high activity. However, a direct correlation is not observed. On the other hand, the pore volume and size distribution play an important role in the rate of decay and long-term behaviour of

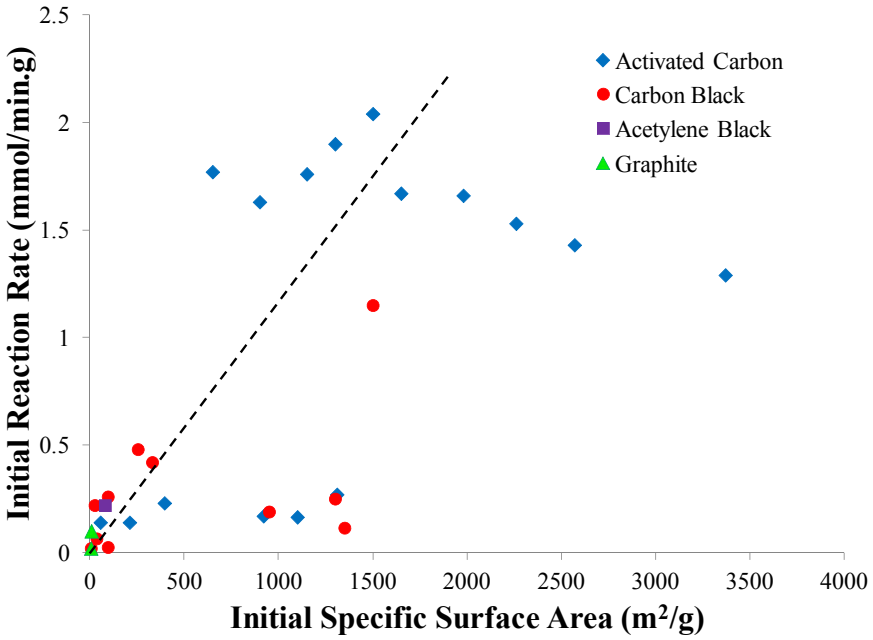

Fig. 2-5: Initial reaction rate versus specific surface area of the fresh catalyst at 1123 K. Data from references [61]**,** [37]**,** [56]**, and** [60]**.**

the catalyst [26, 40, 41, 62, 63]. In general, deactivation of the catalyst during the process is due to the loss of surface area with the deposition of carbon. The decay in the activity is faster when the deposited carbon causes blocking of the surface pores [61]. Hence, in the early stages of the process, the size of the pores plays an important role in the rate of deactivation. When the catalyst is covered with small pores, the growth of carbon blocks the mouth of the pores and causes a rapid decay [41]. Consequently, activated carbons that mainly consist of micro- and mesopores (<50 nm) deactivate rapidly. On the other hand, when a significant portion of the surface area is formed by larger pores, similar to most carbon blacks, the surface is more accessible during the reaction and the decay proceeds more slowly [35, 37, 39].

Structural Order

The general comparison of the catalytic activity of carbons with a broad range of crystallinity, from ordered graphite to disordered amorphous carbons, shows that a lower order results in a higher activity. This trend is also observed when carbons within a group with closer properties are compared [18, 34, 37]. A few exceptions are present in the latter case. However, since the activity of carbons with similar surface areas changes proportionally with their structural order,

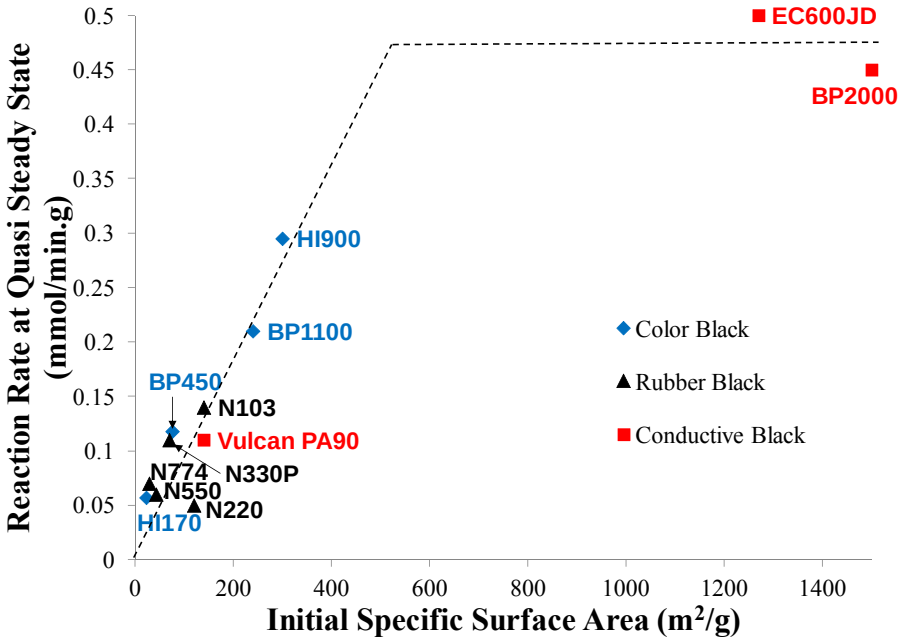

Fig. 2-6: Reaction rate at quasi steady state versus specific surface area of the fresh catalyst at 1123 K. Data from references [36, 38, 64, 65]**, in some cases with some calculations.**

these deviations can be attributed to the effect of the surface area.

The correlation between the activity and structural order can be explained by considering that the surface of amorphous carbon is composed of sections of graphite positioned in different directions [39, 66]. The free valances in the surface sites located at the corners and edges of the sections of graphite make these sites more prompt to react with the surrounding gas, and increases their activity. Therefore, a high disorder is accompanied with a larger number of active sites, and therefore has a higher activity. It is noted that, as observed in Fig. 2-7, the edges of graphite sections can be in the form of armchair and zigzag edges. The armchair edge and the corners are more active than the zigzag edge. As the order of the carbon decreases, the number of corners and armchair edges increases, and higher activities are obtained [62].

The changes in the surface structure of different carbon catalysts were investigated during the process to obtain the effect of the degree of order on the deactivation of the catalyst. Comparison of the structure of the fresh and deactivated catalyst shows that this property remains nearly unchanged. It is concluded that the deactivation is not related to the order of carbon, which confirms that the blockage of pores and reduction of the effective surface area is the main mechanism of deactivation [35, 37, 61].

Concentration of Defects

Several types of defects can be found on the surface of graphitic carbon materials. These defects can be categorized into two groups of vacancies and topological defects [67-69]. Vacancies correspond to cases where one or several carbon atoms are missing in the graphene structure. Topological defects indicate the presence of polygonal structures other than hexagonal. The most common of these defects are di-vacancies, mono-vacancies, and Stone-Wales

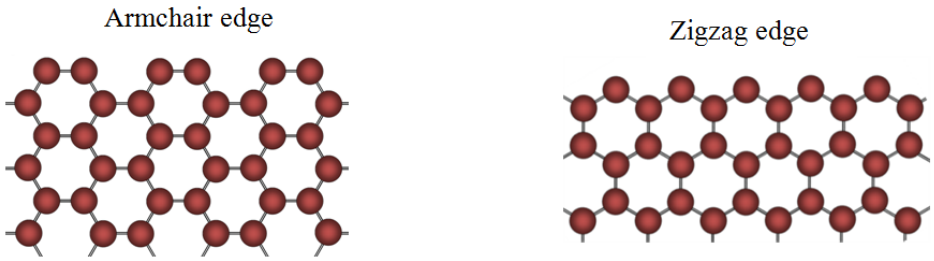

Fig. 2-7: Schematic representation of the different edges of graphite sections.

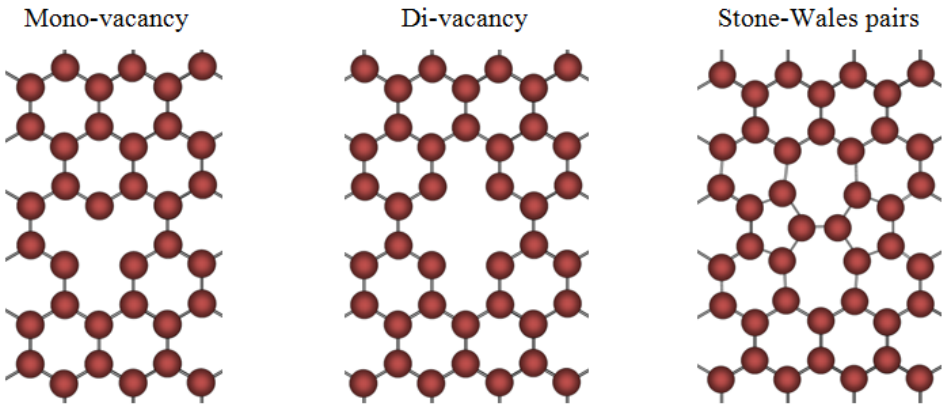

Fig. 2-8: Schematic representation of common defects on graphene layer.

defects, which are illustrated in Fig. 2-8. Experimental and theoretical studies have shown that these defects are numerous and stable on the surface of graphitic carbons [70, 71].

The amount of defects on the surface of carbon has been quantified in some experimental studies to investigate its effect on the activity of the catalysts. The results show that carbons with larger amounts of defects demonstrate a higher activity [18, 34]. Some deviation are observed, which can again be justified by the effect of the surface area. The increase of activity caused by the different types of defects is due to the decrease in electronic stability caused by the irregular structure and the higher tendency of the carbon particles adjacent the defects to react with the surrounding gas.

Number of Active Sites

In the discussion about the structural order and amount of defects of the catalyst, several types of high energy sites were presented. Due to the presence of their free valences, these sites have a high tendency to interact with surrounding species to reach an energetic stability by satisfying their valence requirement. Consequently, these surface sites are more prompt to influence the reactions of the surrounding gas species and are recognized as the active sites in the process of methane decomposition. Since the effect of both the structural order and amount of defects on the catalyst surface are caused by the active sites, they are combined into one single factor of number of active sites to simplify the investigation. As explained earlier, experimental studies revealed that the number of these sites largely affects the activity of the catalyst. This factor has been determined to be the reason behind the deviations of certain catalysts from the trend of variations of activity with the surface area

observed in Fig. 2-5. Consequently, this parameter is considered as one of the main factors in the analysis of the process of decomposition of methane over carbon [37-41, 56, 61].

It is evident that the number of active sites is a function of the structural order and the density of defects on the surface of carbon catalysts. However, no method has been established to determine this value. It is emphasized that due to the importance of the number of active sites, this value should be determined, and used in investigation on the catalytic activity of carbon.

2.2.2. Reactor

The selection of an appropriate reactor is an important step to obtain an optimal performance for a process. The most common reactors used for the catalytic decomposition of methane are the fixed bed and fluidized bed reactors, which are schematically illustrated in Fig. 2-9. In both of these reactors, methane gas flows through the bed of catalyst particles in an upward direction, and partially decomposes to carbon and hydrogen in the reaction zone. The produced carbon is deposited on the catalyst particles, while the flow of hydrogen-rich gas leaves the reactor from the top through a filter. In the fixed bed, the catalyst particles are stationary. Conversely, in the fluidized bed, the gas flow creates a fluid-like motion in the particles and an efficient gas-solid mixture is created. The major problem of using a fixed bed in this process is that the produced carbon deposits on the catalyst particles and the reactor eventually becomes clogged after a while. Also, since the produced carbon and deactivated catalyst cannot be removed during the process, it cannot operate continuously. On the other hand, the fluidized bed eliminates the problem of clogging, due to the motion of the particles. Also, the removal and insertion of catalyst particles is feasible in this reactor, which allows for a continuous operation. A method has been proposed by Muradov for the continuous operation of the fluidized bed reactor [22]. In this method, the particles larger than a specific size are withdrawn from the bottom of the fluidized bed reactor, while fresh catalyst is added to maintain a specific amount of particles. It is noted that the fluidized bed also has other unique characteristics that make it efficient. One of the main advantages of fluidized bed is that it provides a very high contact area between the particles and the gas. This system also enhances mixing of the gas and particles. These characteristics increase the heat and mass transfer, and improve the reaction rates.

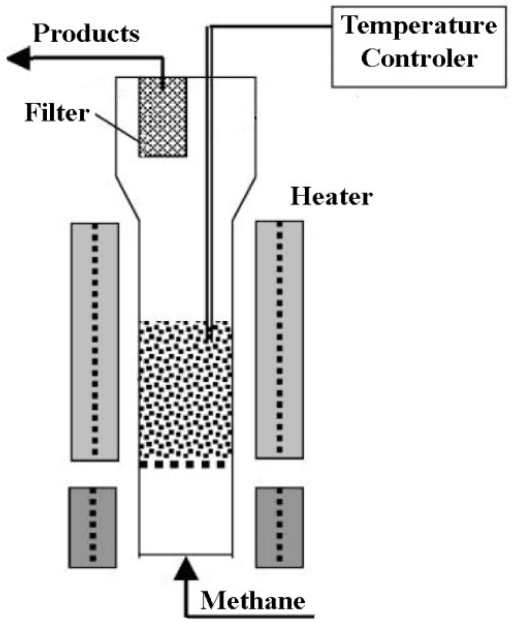

Fig. 2-9: Schematic representation of methane decomposition process using fluidized bed reactors (Reprinted from [60]**, with permission from the International Journal of Hydrogen Energy).**

The application of several other types of reactors, namely tubular, fluid wall, and spouted bed reactors were also compared with fluidized bed reactors [60]. Due to the problems associated with each of these reactors, such as clogging, low decomposition rate, and added complexity of the process, the fluidized bed was chosen as the most appropriate reactor for this process.

The performance of a process which is carried out in a fluidized bed depends on its operating regime, which specifies the behavior of the gas and particles in the reactor and their interaction. Since the regimes that can occur in a reactor depend on the properties of the solid phase, the classification of the particles is also important in this investigation. In this section, a brief explanation is presented about the different flow regimes and the classification of particles in a fluidized bed.

Flow Regimes

A fluidized bed can operate under various flow regimes. A graphical representation of the different possible regimes is illustrated in Fig. 2-10. When a gas flows upward through a bed of solid particles at low velocities, the particles lie on each other in a fixed bed. When the flow rate increases and the gas velocity reaches the incipient velocity, fluidization is initiated.

Further increase in the gas velocity causes a homogeneous expansion of the bed of particles, called the particulate regime. When the minimum bubbling velocity is reached, bubbles of gas are formed in the bed, through which a portion of the gas is by-passed; this phase is the bubbling regime. Depending on the properties of the particles, there may be no particulate regime in the fluidization of the particles. In this case the bubbles are formed at the incipient gas velocity.

With the increase in gas velocity, the size of the bubbles will increase until they are comparable with the width of the bed, creating the slugging regime. A higher increase in the gas velocity will make the bubbles to blast violently, making the bubbles and bed surface indistinguishable; this phase is called the turbulent regime. Solids entrainment will occur at a larger velocity in the fast fluidization regime, with a dilute upward flow in the core and descending streams at the wall. At the transport velocity, particles flow out of the bed, and a pneumatic conveying is observed.

It is noted that the particulate regime is the most appropriate for catalytic reactions, since it provides a uniform gas-solid mixture and a high contact between the catalyst particles and the gas, and therefore leads to an efficient reaction.

Particles Classification

The general sequence of fluidization observed in Fig. 2-10 does not occur in all conditions.

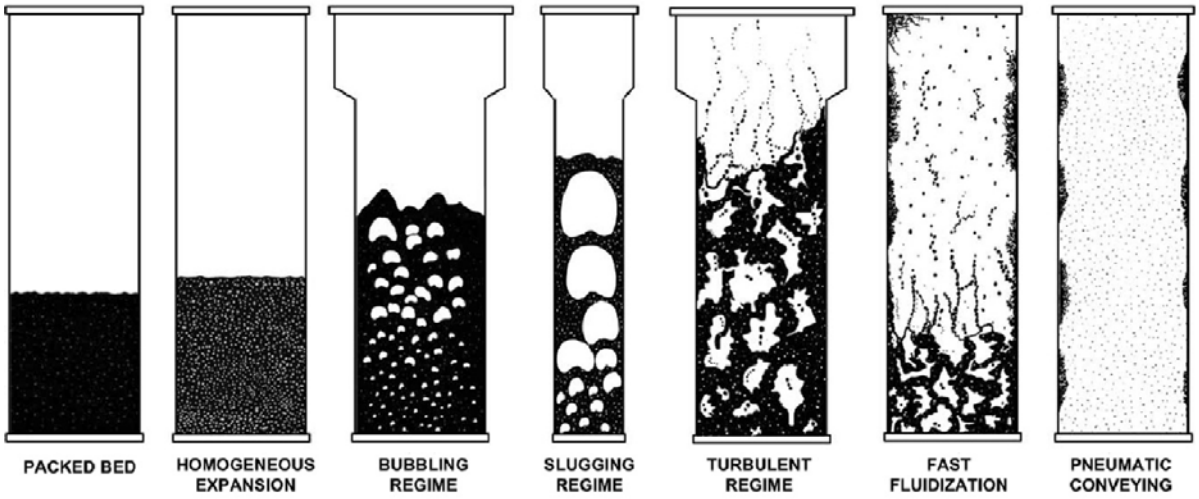

Fig. 2-10: Fluidized bed flow regimes (Reprinted from [72]**).**

The regimes that are encountered depend on the properties of the particles used. Therefore, the particles should be categorized into different groups to identify the type of fluidization that is achievable. Accordingly, a practical classification has been suggested by Geldart [73]. In this classification particles are categorized into four different groups based on their size and the difference between particle and gas densities, as observed in Fig. 2-11. The behavior of all the particles in a group is closely similar. Although updated methods have been proposed for calculating the limits of each group, the classification remains unchanged and is still applied to differentiate solid particles in various fields. The four groups of particles in Geldart's classification are briefly described below, from small to large sizes.

Group C- the particles in this group are cohesive powders that are very difficult to fluidize. When a gas flows in a bed of group C particles, instead of fluidizing the particles, channels are formed in the particle bed through which the gas escapes. This behavior is due to the high cohesive force between the particles. An example of particles in this group is cement.

Group A- these particles have a small mean size. One of the main features of this group

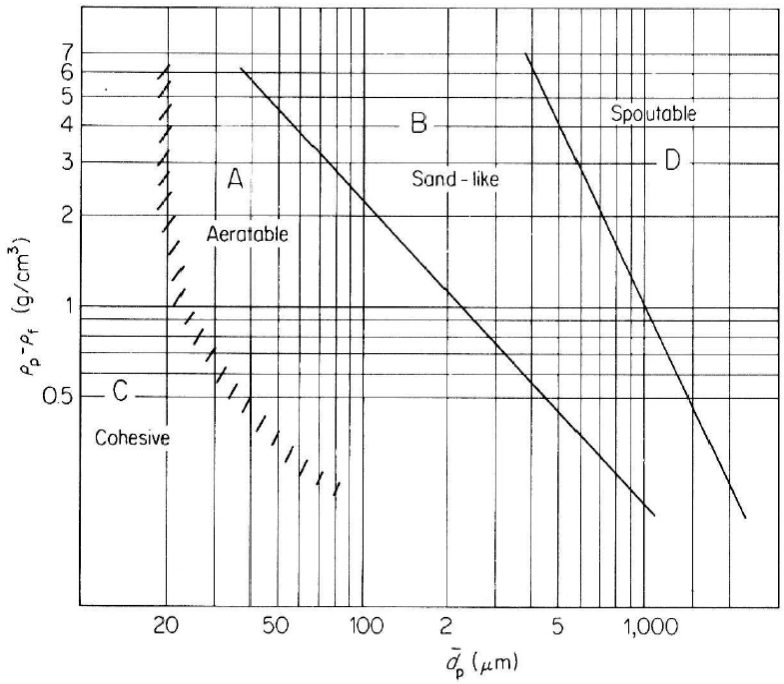

Fig. 2-11: Classification of powders by Geldart (Reprinted from [73]**, with permission from Elsevier).**

is the possibility to operate in a particulate regime. As explained in the previous section, a uniform mixture is obtained in this regime, and a high contact between the particle and gas is achieved. Catalysts are usually from this group of particles due to the benefits that it offers.

Group B- most of the solid particles with a medium size and density are located in this group. When these particles are fluidized, bubbles form at the incipient velocity and no particulate expansion is observed. Examples of powder from this group are building sand and table salt.

Group D- this group consists of large and dense particles. Bubbles are formed at incipient velocity. These particles have the ability to form a spouting bed when the gas flows through a central orifice. Rice and coffee beans are examples of group D particles.

According to practical considerations, the particles in a catalytic process are usually selected from Geldart's group A. The properties of the carbon catalyst used in methane decomposition indicate that these particles are also from group A. Therefore, operation in the particulate regime, which was selected as the efficient regime in the previous section, is feasible and will be considered throughout this study.

2.3. Modeling

The decomposition of methane in a fluidized bed of carbon catalyst particles was selected as a suitable process for producing hydrogen. This process should be modeled to predict the variations of the amount of hydrogen production with operating parameters and catalyst properties, and achieve the aim of this thesis. To study the performance of the decomposition of methane, three different aspects should be considered for a complete model: 1) the reactor should be modeled by developing and solving the governing equations required to obtain the desired results. 2) The kinetics of the chemical reaction should be added to include the extent of the variations of the hydrogen production with different factors due to the changes in the reaction rates. 3) The hydrodynamics of the reactor should also be modeled to incorporate the effect of the characteristics of the fluidized bed reactor on the performance. Several models have been developed to represent the decomposition of methane with carbon particles, where these aspects of modeling were considered [23-33, 74-76]. Some of these studies are dedicated to cases where carbon is used for its catalytic effect on the reaction. On the other

hand, a number of these models were developed for solar reactors where the inlet methane flow is seeded with carbon particles, mainly to improve heat transfer. It should be noted that the catalytic activity of carbon particles is still observed as a secondary benefit in these cases. Therefore, the effect of carbon is considered as part of the kinetic model in most of these studies. Depending on the objective of the investigation, different levels of complexity are required for the governing equations, kinetics, and hydrodynamics models. In this section, the different models for each of these aspects are described, along with a literature review.

2.3.1. Reactor Model

The complexity of the conservation equations in the reactor depends on the aim of using the model, as well as the type of reactor. The perfectly mixed reactor and the plug flow reactor are very common models used to develop and simplify the conservation equations. In the perfectly mixed reactor, the particles and gas are assumed to form a perfectly homogeneous mixture. In the plug flow reactor, no mixing is considered in the axial direction, while the properties are assumed uniform in the direction perpendicular to the flow. When higher complexities are required, one, two, or even three dimensional governing equations are developed.

Different levels of complexity have been used for the conservation equations in existing models of the catalytic decomposition of methane over carbon. The plug flow and well stirred reactor models were used in several studies [27, 31, 33, 76]. Trommer *et al.* [33] used both of these models to obtain the initial amount of hydrogen production in a vortex-flow solar reactor seeded with carbon particles. The effect of temperature on the chemical conversion was investigated for various residence times. Hirsch and Steinfeld [76] modeled a seeded solar reactor with a plug flow assumption. The effect of particle size and temperature on conversion was examined. A well stirred assumption was used by Dunker *et al.* [25] to model the conversion in a fluidized bed of carbon black particles. The effect of pressure, temperature and residence time was studied. Ozalp *et al.* [31] determined the effect of temperature and the influence of inert gas composition in the feed gas on the conversion of the process. Plug flow and mixed flow reactors were considered to model the solar reactor in this study. Ozalp *et al.* [27] also used the commercial software Chemkin to model a plug flow reactor and study the effect of carbon loading on the temperature distribution in solar

reactors. Muradov *et al.* [26] modeled the methane conversion over carbon in bubbling and turbulent fluidized beds. The conservation equations for these two types of reactor were modeled in the direction of the flow. The model was used to investigate the effect of temperature and the expanded bed height on methane conversion. Maag *et al.* [32] studied a solar reactor with a one dimensional transient model. The mass and energy conservation equations and heat transfer were coupled. The particle phase was treated as a constant number, variable diameter, monodisperse particle population in the calculations of the heat transfer. The effect of particle volume fraction and diameter as well as the composition of the inlet gas (methane and argon) on the temperature and its distribution in the reactor were investigated. Patrianakos *et al.* [30] also developed a one dimensional model for seeded solar reactors. The formation and growth of the fresh and seed particles were modeled, and the particle phase was treated as a polydisperse particle population. The distribution of the amount and size of carbon particles in the direction of the flow were determined. This model was also used in a different study [29] to investigate the effect of seeding on the hydrogen and carbon particle production rates. The model of Patrianakos *et al.* was upgraded to a two-dimensional model by Caliot *et al.* [28]. The flow, energy and species transport, as well as radiative heat transfer and carbon particle growth were considered. This model was used to study the spatial non uniformities in particle formation and growth in the reactors. Chen *et al.* [24] used the commercial software COMSOL Multiphysics 4.0a to model a two-dimensional fixed bed for the decomposition of methane over one type of activated carbon. The effect of wall temperature, reactant flow rate, and reactor diameter were determined on the conversion and temperature distribution. Bautista *et al.* [75] used two-dimensional conservation equations to predict the decomposition temperature of methane gas in a planar stagnation-point flow over a catalytic carbon surface.

It is noted that the complex conservation models are usually applied for the determination of temperature, species concentration, or reaction rate distribution in the reactor. In this study, the objective is to investigate the effect of different factors on the overall conversion, and variations of properties in the different axial directions of the reactor are insignificant. Also, a particulate fluidized bed with a uniform mixture and constant temperature is selected for the reactor. Consequently, a well stirred reactor is suitable for this investigation.

2.3.2. Kinetic Model

The objective of modeling the kinetics is to determine the rate of hydrogen production from the chemical reaction. To model the kinetics of the catalytic decomposition of methane, the amount of hydrogen production from the interaction of the gas phase species and the effect of the addition of the catalyst should be coupled. The modeling of these phenomena can be accomplished with two different approaches: by using a global equation or with a detailed model using a reaction mechanism. These two models are discussed in this section.

Global Equation

One of the methods of modeling the kinetics of a process is the use of an empirical global equation. In this method, equation (2-1), or a similar equation, is used to predict the reaction rate, r_A, of the process.

$$r_A = -\frac{dC_A}{dt} = k_n P_A^n \qquad \textbf{(2-1)}$$

In this equation, C_A and P_A are the concentration and partial pressure of the gas reactant species A, respectively, k_n is the rate constant, and n the order of the reaction. It is noted that the rate law for heterogeneous reactions is written as a function of the partial pressure, as opposed to homogeneous reactions where the concentration is used. The values of k_n and n are determined experimentally.

The order of the reaction, n, is considered a constant parameter. This value is obtained experimentally by changing the partial pressure of methane while maintaining a constant flow rate. The diluents used for this purpose are usually argon [38, 40, 41] and nitrogen [63, 77]. The reaction rate obtained in each case is plotted against the partial pressure in a log-log graph, and the slope of the resulting line determines the value of the order of reaction. Experimental studies have been performed to determine the reaction order over several types of active carbons and black carbons. The results show that the order of reaction is around 0.5 to 0.7 for fresh activated carbons [39, 40, 63, 77-79], and 0.4 to 0.6 for fresh carbon blacks [39, 77]. It is noted that this value changes during the process. Since carbon blacks demonstrate a quasi steady state after an initial drop in their activity, the reaction order in this

state has also been studied for this group of carbons. This value was found to be closer to unity compared to the order of reaction of the fresh catalyst, with values between 0.7 and 1 [36, 38, 41].

The value of k_n is determined as a function of temperature, with an Arrhenius type equation as follow:

$$k_n = k_o \exp(-\frac{E_a}{RT}) \quad \textbf{(2-2)}$$

In this equation, k_o and E_a are the pre-exponential factor and activation energy, respectively, and can be found experimentally. T is the reactor temperature, and R the universal ideal gas constant. The activation energy and pre-exponential factor are determined with the Arrhenius plot of the normal logarithm of the rate constant versus 1/T. This plot is obtained by performing experiments at different temperatures and calculating the rate constant with the resulting data. The initial activation energy of activated carbons has been found to be in a range from 140 to 200 kJ/mol [26, 40, 64, 77] and that of carbon blacks between 205 to 238 kJ/mol [26, 77].

The kinetics is studied in most of the existing models for the decomposition of methane over carbon, either if carbon is used as a catalyst or as a mean to increase heat transfer. When active carbon and carbon blacks are used as the catalyst, the reaction can be modeled with a half order power law, as obtained in experimental studies discussed above. This can also be observed in the models where these types of carbon were used. Muradov *et al.* [26] used a half-order rate law for their model, which was intended for a fluidized bed of activated carbon particles. The rate coefficient was estimated as a constant, and the activation energy of 201 kJ/mol was used. Serrano *et al.* [74] modeled the kinetics of methane decomposition over some mesoporous carbons and two carbon black catalysts with a power law. They determined the reaction order, and the activation energy to be in the range of 0.46 to 0.5, and 178 to 259 kJ/mol, respectively. Chen *et al.* [24] used a half order power law, with an activation energy of 140 kJ/mol to represent the reaction over activated carbon.

On the other hand, a different reaction order is used in studies on solar reactors. Trommer *et al.* [33] used a first degree power law to model the decomposition of methane

seeded with carbon particles in a solar reactor. The kinetic parameters were obtained experimentally and the activation energy used was in the range of 147-162 kJ/mol. The same kinetics model was used in several other studies on solar reactors [31, 32, 76]. Patrianakos *et al.* [29, 30] also modeled the kinetics of the reaction in a solar reactor. In contrast to previous models, this study considered separate models for the conversion from homogeneous and heterogeneous phases of the reaction. Nevertheless, both of these phases were modeled with a first order rate law with coefficients obtained from experiments, and activation energies of 400 and 150 kJ/mol, respectively. Another distinction of this model is the inclusion of the surface area of the particles in the rate equation. However, this parameter was not considered a property of carbon, and was instead derived by assuming a spherical shape for the particles. This model was also used by Caliot *et al.* [28]. The difference between the order of reaction in cases where the carbon is used as a catalyst or in a solar reactor cannot be justified by the type of reactor used, since the kinetics of a process is independent of this factor. However, this discrepancy can be explained by considering that the carbon used in solar reactors have different properties that create a reaction order equal to unity.

The global equation provides a simple model for studying the kinetics of a process. However, it depends on experimental values, which vary with the type of catalyst and with time. As a result, it cannot be generalized for the use of different type of carbons. Also, since the properties of the catalyst are not considered in this model, it cannot be used to determine the effect of these factors on the performance of the process.

Detailed Model

Another method of modeling the kinetics of a reaction is the detailed kinetic model. This model provides the ability to investigate different catalysts and the effect of their properties on the overall performance of the process. This method uses a reaction mechanism, by combining the different consecutive and parallel reactions of several species that participate in the process. The rate of each of these elementary reactions is obtained with rate coefficients estimated with theoretical or experimental methods. The production rate of each species is determined by considering the effect of each elementary reaction and their rates. The individual governing equations for the species are then coupled to determine the final product. The detailed model provides a better understanding of the reaction and enables the

investigation of the contribution of each different species and catalyst site. However, it is more complex than the application of a global equation and requires more computational work.

In contrast to the power law model, research on the detailed modeling of methane decomposition over carbon catalyst is very limited. Muradov [39] has proposed that the reaction likely starts with the dissociative adsorption of methane on active sites followed by a series of surface stepwise dissociation reactions leading to elemental carbon and hydrogen, as follow:

Mechanism A

$$(CH_4)_g \rightarrow (CH_3)_a + (H)_a$$

$$(CH_{3-x})_a \rightarrow (CH_{2-x})_a + (H)_a \qquad 0 < x < 2$$

$$(C)_a \rightarrow \frac{1}{n}(C_n)_c$$

$$2(H)_a \rightarrow (H_2)_g$$

where the subscripts a, c and g denote adsorbed, crystalline and gaseous species, respectively. This mechanism will be referred as mechanism A. The major problem of mechanism A is that it has not been validated in any study for carbon catalysts. This mechanism was used in a model developed by Bautista *et al.* [75] for methane decomposition over carbon, where the rate of elementary reactions were directly taken from the mechanism of combustion over platinum. However, no comparison was performed with any experimental data, and the model was not validated.

It should be mentioned that mechanism A was suggested in earlier studies for methane decomposition over metals and was successfully used for modeling this process [80-82]. It is also interesting to note that this mechanism is similar to models of combustion with metal catalysts. Since the decomposition of methane is considered as a part of the combustion process, this similarity is rational. At the same time, this can suggest that the model of the decomposition of methane over carbon should also be similar with combustion over this catalyst. A study on the models of hydrocarbons combustion over soot, which is a type of

carbon, shows that the mechanism of this process differs greatly with mechanism A and is based on a completely different approach. Considering this fact, it is likely that the methane decomposition follows a different mechanism that can be obtained considering the similarities of this process with combustion. This approach was used by Dunker *et al.* [25] to develop a mechanism for this purpose. This model is based on the mechanism of soot formation and growth in combustion developed by Appel *et al.* [83]. Two types of surface sites are considered: carbon atoms saturated with hydrogen, C_s–H, and carbon radicals, $C_s\bullet$. The mechanism for surface growth in this study is based on the H-abstraction/C_2H_2-addition reaction sequence, which is well known as the mechanism of aromatic ring growth. The reaction of combination of H with the surface carbon radical is added, and the following mechanism is obtained.

Mechanism B

$$C_s - H + H \rightleftarrows C_s\bullet + H_2$$

$$C_s\bullet + C_2H_2 \rightarrow C_s - H + H$$

$$C_s\bullet + H \rightarrow C_s - H$$

A number of additional surface reactions were added to mechanism B to account for the differences between the process of combustion and decomposition of methane. The mechanism of Dunker *et al.* was validated with experiments and also used in a separate study conducted by Ozalp *et al.* [27] to investigate the performance of a solar reactor seeded with carbon particles.

Although the model of Dunker *et al.* is suitable for the detailed kinetic model of the decomposition of methane over carbon, it has some weaknesses. The major problem of this model is that the only catalyst property considered to represent the difference between the activities of various carbon types is the surface area of the catalyst, which according to the discussion in section 2.2.1 is not adequate. In order to correctly account for the difference between various catalysts, the number of active sites should be considered in the model. It is also noted that this model cannot be used as a standalone application, since it is reliant on experimental measurements for some input values, specifically the hydrodynamics characteristics of the fluidized bed.

2.3.3. Hydrodynamics Model

The prediction of the hydrodynamics characteristics of the fluidized bed reactor is one of the required steps in this study. As discussed earlier, the particulate regime was selected as the appropriate operating regime for the reactor of the catalytic decomposition of methane. Since the velocity of the flow is restricted to values between the minimum bubbling and minimum fluidization velocities, these values should be estimated to determine the allowable limits of operation. Also, the variations of the flow and properties of the catalyst create different amounts of expansion in the bed, affecting the volume ratio of the catalyst particles to the reacting gas. This value is an important variable in a catalytic reaction and should also be determined in this section.

Different models can be used for representing the hydrodynamics of the reactor. Due to the complexity of kinetic modeling, simple hydrodynamic models requiring a low computational power are usually chosen, which are derived from experimental observations. However, closure models can also be applied, where simplifications are used for solving the complex equations governing the motion of the fluid and solid phases in the fluidized bed. These two types of models are described in this section.

Closure Models

Closure models can be used to determine the hydrodynamic characteristics of the reactor. In these methods, the interaction of the gas and solid particles is studied through their governing equations of motion. Simplifications are applied to use mean values to represent point variables, which leads to two main methods of modeling: the two-fluid and the discrete element method.

In the Two-fluid method, an Eulerian-Eulerian approach is adopted, where the particle and gas phases are both considered to behave like interpenetrating continuum media. This method is widely used in fluidized bed modeling, and its equations are described in different publications [84]. It is noted that commercial softwares modeling two phase flow, such as Fluent and CFX, can be applied to solve these equations and model a system with this method.

In the discrete element method, a Lagrangian-Eulerian approach is used, where the trajectory of each particle is traced individually in a continuous fluid. The governing equations of this method are the Navier-Stokes equation for the fluid phase, which is treated as a continuum, and Newton's equation for each particle [85]. Due to the high computational power required by this method, only two dimensional modeling with a limited number of particles is practical. Since this method is computationally expensive, it is used for the study of fluidized bed individually, and usually cannot be combined with other phenomena such as chemical reactions.

Closure models have not been used to model the hydrodynamics of the process of decomposition of methane with carbon catalysts.

Empirical Models

Several empirical correlations have been developed to model the hydrodynamics of fluidized bed reactors. These models were derived and developed since 1960s. Several experiments with different conditions were conducted to determine these correlations. In these models, the velocities limiting each flow regime, as well as the expansion and voidage of the bed can be determined with the properties of the flow and catalyst, and operating conditions [86-89]. Fig. 2-12 presents an example of these empirical models. It is observed that this figure can be used to determine the limiting velocities of each regime and the boundaries between different particle groups as a function of a dimensionless diameter, d_p^*, and velocity, u^*, defined as follow:

$$d_p^* = d_p\left(\frac{g\rho_g\left(\rho_p - \rho_g\right)}{\mu^2}\right)^{1/3} \quad \textbf{(2-3)}$$

$$u^* = u\left(\frac{\rho_g^2}{g\mu\left(\rho_p - \rho_g\right)}\right)^{1/3} \quad \textbf{(2-4)}$$

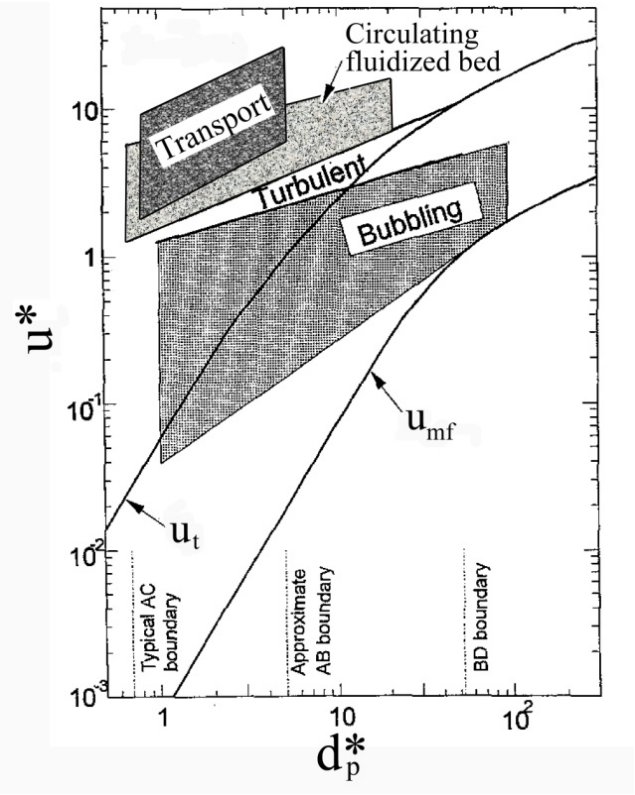

Fig. 2-12: Limits of fluidization regimes as a function of dimensionless diameter and velocity (Reprinted from [90]**, with permission from Elsevier).**

In these equations, d_p is the diameter of the particles, g is the acceleration of gravity, ρ_p and ρ_g are the densities of the particles and gas, respectively, μ is the viscosity of the gas and u the velocity of the gas.

The main advantage of the empirical methods is the simple and fast estimation of the required variables without extensive computational effort. However, since the correlations are developed with experiments in different conditions, the model to be used for each individual case should be carefully selected.

The fluidized bed reactor was used in two models developed for the thermal decomposition of methane over carbon [25, 26]. In the work of Muradov *et al.* [26] the hydrodynamic characteristics were determined with empirical equations, while experimental measurements were used by Dunker *et al.* [25]. The empirical correlations provide the required accuracy without adding to the complexity of the model, and will be used in this

study. A sensitivity analysis on the effect of the errors of the characteristics caused by these models confirmed their accuracy for the objective pursued.

2.4. Summary and Conclusions

Technologies of hydrogen production from fossil fuels were presented in this chapter. A comparison of the benefits and disadvantages of these technologies shows that the decomposition of methane is an appropriate method for hydrogen production. One of the main features of this process is the elimination of greenhouse gas emissions.

A catalyst is usually used to lower the high temperature required to decompose methane. Transition metals such as Ni, Fe, and Co were initially applied as the catalysts of this process. However, these catalysts deactivate rapidly and their regeneration produces a substantial amount of carbon dioxide. In order to overcome this problem, carbon was proposed as an alternative catalyst. Carbon has a lower initial activity compared to metal catalysts; however, it deactivates slowly and can be used for a longer period. Also, with carbon catalysts, handling of the carbon by-product does not produce any significant amount of CO_2. Activated carbon and carbon black are two types of amorphous carbon that can be effectively employed as catalysts for this reaction. Each of these types of carbon has a benefit: activated carbon has a high initial activity, while carbon blacks remain active for a much longer period.

The effect of the properties of carbon catalysts on their activity was investigated. The results show that the specific surface area and number of active sites are the main catalyst properties affecting the performance of the decomposition of methane. The number of surface sites quantifies the amount of high energy sites on the surface of the catalyst. This value is a function of the structural order and amount of defects, and is different for various types of carbon. It is noted that no method has been developed to adequately quantify the value of this parameter in literature.

The appropriate reactor for this process was determined to be a fluidized bed. This reactor eliminates the problem of clogging observed in fixed beds, and allows for a continuous process. It also provides a high contact area between the gas and catalyst, and improves the reaction rate. The optimal regime for the fluidized bed in this process is the

particulate regime, which produces a homogeneous gas-solid mixture. Since the carbon catalysts are classified as Geldart's group A particles, operation in this regime is possible, and has therefore been selected in this study.

In order to obtain an optimum design for the process and plan for its efficient operation, the effect of different operating parameters and catalyst properties on the performance of this reactor should be investigated. This aim can be achieved by modeling the process. To obtain a complete representation of the process, the governing equations of the reactor, the kinetics of the chemical reaction, and the hydrodynamic model of the bed should be coupled. The well stirred reactor was selected as an appropriate model for the reactor to attain the purpose of this study. Also, the hydrodynamics can be modeled within the required accuracy with empirical models. However, a more complex model is required for the kinetics to represent the effect of the catalyst properties. Most of the models available in literature use a global equation to represent this process with experimental constants specific to each catalyst. Therefore, investigation on the effect of the properties of the catalyst is not feasible with this method. Also, this model cannot be generalized for different types of carbon without performing experiments. On the other hand, the catalyst properties can be included in the detailed kinetic model. This model uses a reaction mechanism to describe the behavior of the process. Two different mechanisms have been proposed to model the effect of carbon catalysts in the decomposition of methane. One mechanism considers the adsorption of methane followed by a series of surface stepwise dissociation, while the other is based on the H-abstraction/C_2H_2-addition reaction sequence. After a thorough comparison, the second method was determined to be suitable for the current study. Consequently, the model of Dunker *et al.* [25], which uses this reaction mechanism, is the most appropriate kinetic model available in literature for the objective of this study. However, this model has some important drawbacks. The major problem is that the only catalyst property that was included in this model to account for the difference between the activities of various carbon types is the surface area. According to the earlier discussions the number of active sites should also be considered in the model. Experimental studies show that considering the surface area alone to represent the difference in the activity of various catalysts can result in large errors. It is also noted that this model cannot be used as a standalone application, since it is reliant on experimental measurements for obtaining the hydrodynamic characteristics of the fluidized

bed. Considering the problems of the existing model, it is concluded that the main effort in this study should be focused on developing a detailed kinetic model which considers the two important properties of carbon catalysts, namely the specific surface area and the number of active sites. Accordingly, a method should be developed to find the number of active sites for different types of carbon, since this value has not been quantified in available literature. Also, a hydrodynamic model should be coupled to eliminate the need to experiment. These goals will be pursued in the development of the model in the following chapter.

Chapter 3
Modeling of the Decomposition of Methane with Carbon Catalyst

The decomposition of methane is modeled to study the effect of different factors on the performance of this process. It is therefore important to select the main factors that affect the performance and are of interest in this investigation. Several studies have demonstrated the considerable effect of operating parameters such as temperature and gas flow rate. Also, the properties of the catalyst have a crucial role on the amount of hydrogen production. Although only carbon catalysts are investigated in this study, the different types of carbon available for this application have very distinct properties. Several experimental studies have demonstrated the extent of the effect of different properties of carbon catalysts on the amount of hydrogen produced [14, 18, 26, 34, 35, 37, 38, 40, 41, 58-62, 64, 65, 77, 91-93]. These findings emphasise the importance of including the catalyst properties in this model.

While the process of decomposition of methane with carbon catalysts has been the subject of multiple experimental studies, its modeling is limited. As discussed in earlier chapters, the majority of models used for this process apply a simplified power law to determine the rate of the reaction [28, 30-32, 94]. However, according to the objective of this study and the factors under consideration, a detailed model should be used. Considering that the available detailed model has a number of inaccuracies, the aim in this chapter is to develop a more accurate model. For this purpose, the kinetic model is emphasized and a simple well-stirred model with uniform and constant temperature is considered for the

reactor. The hydrogen production from the interaction of gas phase species and the effect of the surface of catalyst particles are separately obtained, and are then coupled to determine the overall performance of the process. The effect of the interaction of gas phase species, or the homogeneous decomposition of methane, is first modeled with a detailed reaction mechanism and the results are validated with available experimental data. Afterwards, the effect of the carbon catalyst is added by considering several surface reactions and deriving their reaction rates. The original conditions of the catalyst at the beginning of the process are considered in the model, and the initial amount of hydrogen production is obtained. In this phase, the nucleation and coagulation are considered negligible, and the effect of the catalyst is represented with surface reactions. The results of the complete model are compared to experimental data for validation. Also, the hydrodynamics of the fluidized bed is modeled with empirical correlations to decrease the dependence of the model to experiment.

3.1. Model Description

The detailed kinetic modeling of the process of decomposition of methane is performed by using a series of elementary reactions for describing the interaction of the gas species in a gas-phase reaction mechanism and adding the effect of the catalyst with a surface reaction mechanism. The development of these mechanisms is discussed in the following sections. The reactor considered for the process is a continuous fluidized bed with particulate fluidization and constant temperature. The composition of the exhaust mixture from this reactor is therefore determined using the time-dependent continuity equation for each gas species in an isothermal well-stirred reactor as follows [95]:

$$\frac{dY_k}{dt} = \frac{1}{\tau}(Y_{k,in} - Y_k) + \frac{\dot{\omega}_k MW_k}{\rho_g} \qquad k = 1, ..., K \qquad \textbf{(3-1)}$$

In this equation, Y_k Y_k and $Y_{k,in}$ are the mass fractions of the k^{th} species at the exit and inlet of the reactor, respectively. Also, τ is the residence time of the gas in the reactor, ρ_g is the density, and MW_k the molecular weight of the k^{th} species. The variable $\dot{\omega}_k$ represents the molar production rate of the k^{th} species. This value involves the production rates from the interaction of gas-phase species with each other, and the additional production rate due to the

presence of the catalyst particles. $\dot{\omega}_k$ is calculated using the elementary reactions in the gas-phase and surface mechanisms, which are discussed in the following sections.

The combination of continuity equations of all the species in the reactor forms a system of initial value ordinary differential equations (ODE). This set of equations is solved with a variable coefficient ODE solver developed by the Lawrence Livermore National Laboratory, DVODE [96], and determines the composition of the exhaust mixture in different times. It is observed from the continuity equation that the composition of the exhaust mixture depends on the residence time, while the temperature and pressure also affect this value through the species molar production rate and density.

3.2. Modeling Hydrogen Production from the Homogeneous Decomposition of Methane [95]

It is observed from Equation (3-1) that one of the basic parts in modeling the thermocatalytic decomposition of methane is the model of the homogeneous decomposition of methane. This model is also valuable in studying the thermal decomposition of methane as an individual process, such as in solar reactors. A simplified first-order rate kinetic expression is generally used in predicting the hydrogen production from this process [19, 20, 33]. However, in the current study, it is necessary to use a detailed kinetic model due to the requisite to combine such model with the effect of the catalyst for the thermocatalytic process. While the detailed modeling of the thermal decomposition of methane as a distinct process for hydrogen production is very limited in literature, such model has been studied in multiple cases for the decomposition of light hydrocarbons as part of the fuel combustion [83, 97-99]. Due to the nature of the combustion reactions, the mechanisms of decomposition in these studies were developed in conjunction with the oxidation of hydrocarbons, and in different conditions compared to hydrogen production. Consequently, although mechanisms of the process of decomposition are included in combustion models, the accuracy of their application for the thermal decomposition of methane for hydrogen production should be investigated and necessary modifications should be applied to obtain proper results for their new purpose.

In order to find an appropriate reaction mechanism to represent the thermal decomposition of methane, a method similar to that presented by Hughes *et al.* [100] for

combustion is used. A base mechanism is first selected and sensitivity analysis is performed on its elementary reactions to determine the important reactions in the conditions thought. The different rate constants of these reactions available from literature are investigated to find the ones that are uncertain and can therefore be changed. The mechanism is then modified by changing the uncertain rates of important elementary reactions in reasonable limits and evaluating their effect on the results. An appropriate mechanism is then obtained by comparing the result with experimental data and selecting the rates which cause the least difference. It is noted that no attempt was made to add elementary reactions to the selected mechanism, or to modify the thermodynamic properties of the species.

3.2.1. Selection of a Base Mechanism

As stated earlier, there are no reaction mechanisms in literature for modeling the thermal decomposition of methane as a distinct process. However, the pyrolysis of light hydrocarbons has been studied along with the oxidation as part of the combustion process. Indeed, the decomposition of methane can be regarded as a part of combustion reaction mechanisms, and can be modeled by modifying such mechanisms. Many reaction mechanisms have been developed to model the combustion of hydrocarbons in different research centers. In this study, in order to find an appropriate base mechanism, some of the major reaction mechanisms applied for modeling the combustion of hydrocarbons are used. The combustion mechanisms used in this study are those presented by Appel *et al.* [83], Hidaka *et al.* [101], Smith *et al.* [98], known as the GRI-Mech 3.0, Dagaut *et al.* [99], and Konnov [97], as well as the Leeds mechanism [100]. To incorporate the new application, the oxidation reactions and species containing oxygen atoms were removed from combustion mechanisms, leaving the reactions describing the pyrolysis of hydrocarbons. Since the pyrolysis reactions included in combustion mechanisms were developed in combination with oxidation and in different conditions compared to hydrogen production, it is expected that not all of the combustion mechanisms will yield correct results in modeling this process. The validity of using these reactions to describe the decomposition of methane should therefore be investigated by comparing the results with experimental data related to the thermal decomposition of methane. The comparison of the results obtained from the mentioned combustion mechanisms with experimental data available from literature are shown in Figs. 3-1 to 3-3. It

is noted that the results of the mechanism developed in this study are also plotted in these figures, while the details of these results will be discussed in subsequent sections.

Fig. 3-1 shows the results of the modified combustion mechanisms and the experimental data obtained by Back *et al.* [102] for hydrogen production from decomposition of methane at a low temperature of 1038 K in a time range of 1000 seconds, at a pressure of 0.58 atm. It is observed that the results of the Appel and Hidaka mechanisms are the closest to the experimental data, respectively. At time periods lower than 500 seconds, the Dagaut mechanism also provides a suitable result; however, as the time increases, a large overprediction is observed in the hydrogen yield obtained from this mechanism. The GRI-Mech 3.0 and Leeds mechanisms produce a large overprediction over the entire time range, while the Konnov mechanism completely deviates from experimental results.

In Fig. 3-2, the results of the mechanisms are compared with experimental data obtained by Murphy *et al.* [103] for a low residence time of around 10 seconds, with a mixture of helium and methane. In this case, the decomposition of methane is investigated for temperatures between 1275 and 1450 K. It is observed from Fig. 3-2(A) that the value of

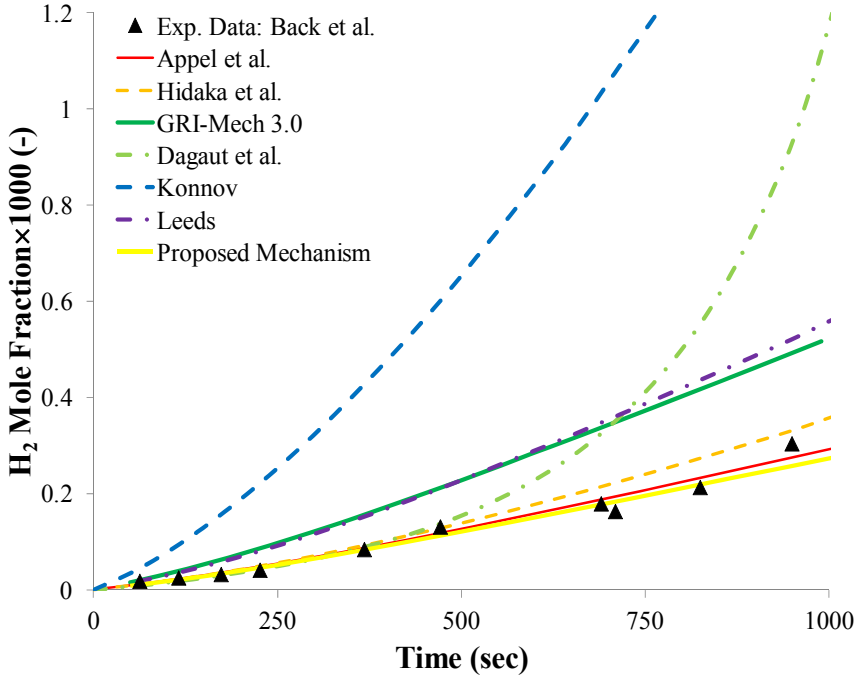

Fig. 3-1: Hydrogen yield from methane decomposition at 1038 K, 0.58 atm using different modified combustion mechanisms, and comparison with experimental data from Back *et al.* [102].

outlet methane predicted by all mechanisms is very close to the experimental data, except the values obtained from the Konnov and Dagaut mechanisms, both of which produce a large underprediction over this temperature range. Fig. 3-2(B) shows the methane conversion to hydrogen obtained with different mechanisms, which is the percentage of methane converted to hydrogen compared to its initial value. Methane conversion, X_{CH4}, is calculated with the mole fraction of hydrogen produced, x_{H2}, using the following equation:

$$X_{CH4} = \frac{x_{H2}}{(2 - x_{H2})(p_{in,CH4}/p_{in})} \quad \textbf{(3-2)}$$

In this equation, the ratio $p_{in,CH4}/p_{in}$ represents the partial pressure of methane in the inlet mixture. There is no experimental data available to validate the amount of hydrogen produced from different mechanisms. However, this graph shows that the methane conversion obtained from the Appel, Hidaka, GRI-MECH 3.0, and Leeds mechanisms are nearly the same. Since the amount of methane consumption obtained from all of these mechanisms is very close to experimental data, the amount of hydrogen production they provide is also considered to be a sound prediction, and can be used as a base of comparison for the new reaction mechanism. On the other hand, the Konnov and Dagaut mechanisms which lead to an error in obtaining the value of methane in the outlet flow produce an overprediction for hydrogen.

Fig. 3-3 shows the comparison of the simulation results and experimental data obtained by Shah *et al.* [104] in a large residence time of more than 200 seconds, for temperatures between 1150 and 1450 K. This graph shows that at temperatures lower than 1275 K, the Leeds, GRI-Mech 3.0, Appel, and Hidaka mechanisms are close to the experimental data, respectively, while the two other mechanisms overpredict hydrogen production. Between 1275 and 1350 K, the Hidaka and Appel mechanisms agree reasonably well with experiment, the results of the Leeds and GRI-Mech 3.0 mechanisms are lower, and the prediction of the other mechanisms are higher than experimental data. At higher temperatures, the results obtained from the Leeds and GRI-Mech 3.0 mechanisms are considerably lower than experiment, while the other four mechanisms are relatively close to these data. Calculations of the total difference between results of reaction mechanisms and these experimental data

over the whole temperature range show that the Appel mechanism produces the closest results.

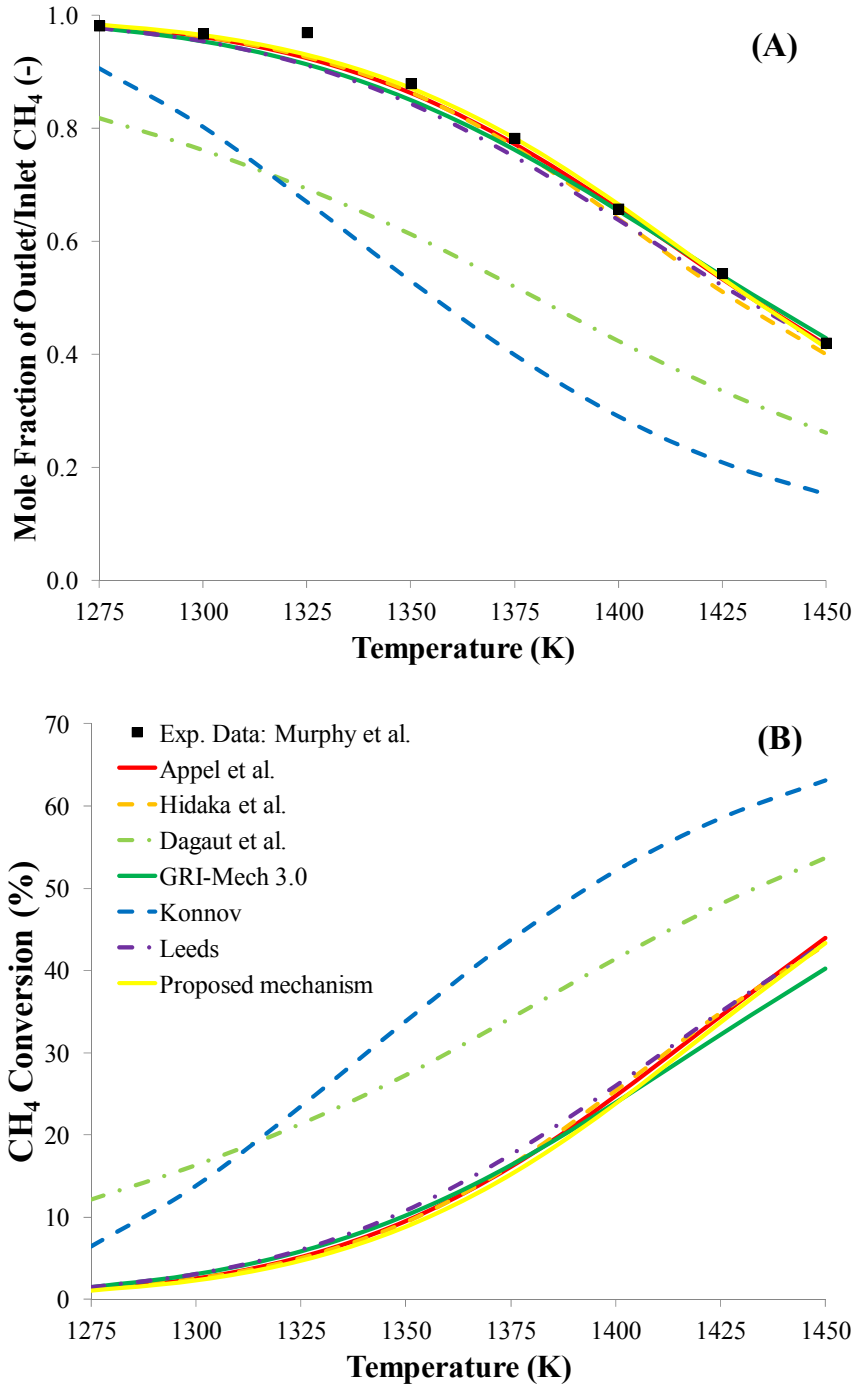

Fig. 3-2: Results of modified combustion mechanisms and experimental data from Murphy *et al.* [103] for decomposition of methane in 90% helium, with a residence time of 8.5 seconds. (A) mole fraction of outlet to inlet methane, and (B) methane conversion to hydrogen.

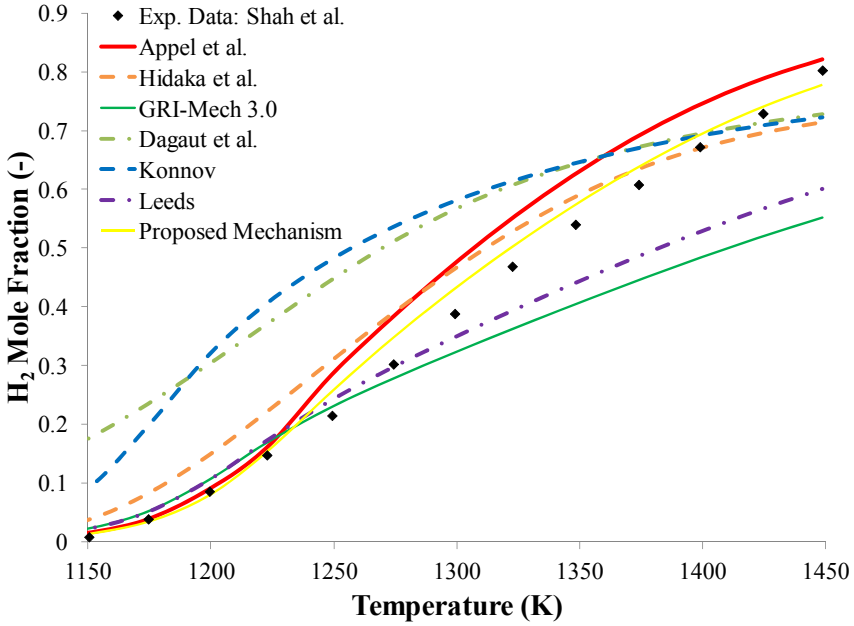

Fig. 3-3: Comparison of the hydrogen yield from decomposition of methane obtained from different mechanisms with experimental data from Shah *et al.* [104] in a residence time of 230 seconds.

This comparison shows that the Appel and Hidaka mechanisms are the closest to experimental data available, while the former mechanism has the least overall difference with experimental data. The hydrocarbon decomposition part of the Appel mechanism is therefore the most suitable mechanism investigated over the temperature and time range studied considering the available information and is selected as the base mechanism for the decomposition of methane. This mechanism includes the reactions of C_1 and C_2 species from the GRI-Mech 1.2 mechanism [105], where the bonds between the atoms of methane and ethane are broken and the gases are decomposed to smaller molecules and radicals, such as H, H_2, CH and other combinations of carbon and hydrogen. The main reactants and the resulting products are then combined in a set of reactions to form larger linear hydrocarbons up to C_6, comprising the precursors of aromatic species. The next step is the formation of the first aromatic ring, which is a six-membered ring of benzene or phenyl radical, and is mainly produced from the recombination of propargyl radicals, as well as the reaction of n-C_4H_3 or n-C_4H_5 with acetylene. These single-ring molecules grow to polycyclic aromatic hydrocarbons (PAHs) through the H abstraction-C_2H_2 addition mechanism. It is noted that pyrene, which consists of four fused benzene rings, is the largest PAH species considered in

this mechanism. The solid carbon particles are produced by the coalescence of two PAH molecules and the formation of dimers, which is not considered in this chapter.

It is also noted that the thermodynamic data associated with this mechanism are based on the NASA-Lewis Thermodynamic Database [106], and are in the form of polynomials.

The Appel mechanism produces a good representation of the experiment at low residence times in the range of temperature investigated. When the residence time increases, the results of the model are close at low temperatures, while the difference between the model and experiment increase at higher temperatures. Nevertheless, this mechanism can create a difference as high as 35%, which should be reduced for a more accurate representation of the decomposition of methane, which is discussed in the following sections.

3.2.2. Sensitivity Analysis

In order to modify the base mechanism for more accurate results, the main elementary reaction affecting hydrogen production should be first determined with sensitivity analysis. The largest difference between experimental data and the results from the model with this mechanism are observed in the conditions of experiments performed by Shah *et al.* [104] at temperatures between 1250 and 1425 K. Therefore, the sensitivity analysis is performed in these conditions, and the first-order sensitivity coefficient of hydrogen mole fraction is obtained for each elementary reaction using the Senkin program [107] and is then normalized over the time period. The normalized sensitivity of the 10 most effective reactions at temperatures of 1250, 1300, 1350 and 1400 K are shown in Fig. 3-4(A) to 3-4(D).

It is observed from Fig. 3-4 that at a temperature of 1250 K, reaction R1 has by far the highest effect on hydrogen production, followed by reaction R2. Although the sensitivity to R1 and R2 reduces with temperature, they remain the dominant reactions at 1300 K, and the latter is among the three most important reactions at 1400 K. On the other hand, the considerable decrease of sensitivity to R1 causes this reaction to become the fourth reaction at 1350 K and fall out of the ranking at 1400 K. Reactions R3 and R4 also have a high effect at 1250 K and follow R1 and R2 at this temperature, but lose their relative importance at higher temperatures, become the bottom 2 reactions at 1350 K, and fall out of the ranking at 1400 K. It is observed that, in contrast to the previous reactions, the importance of R8 and R9

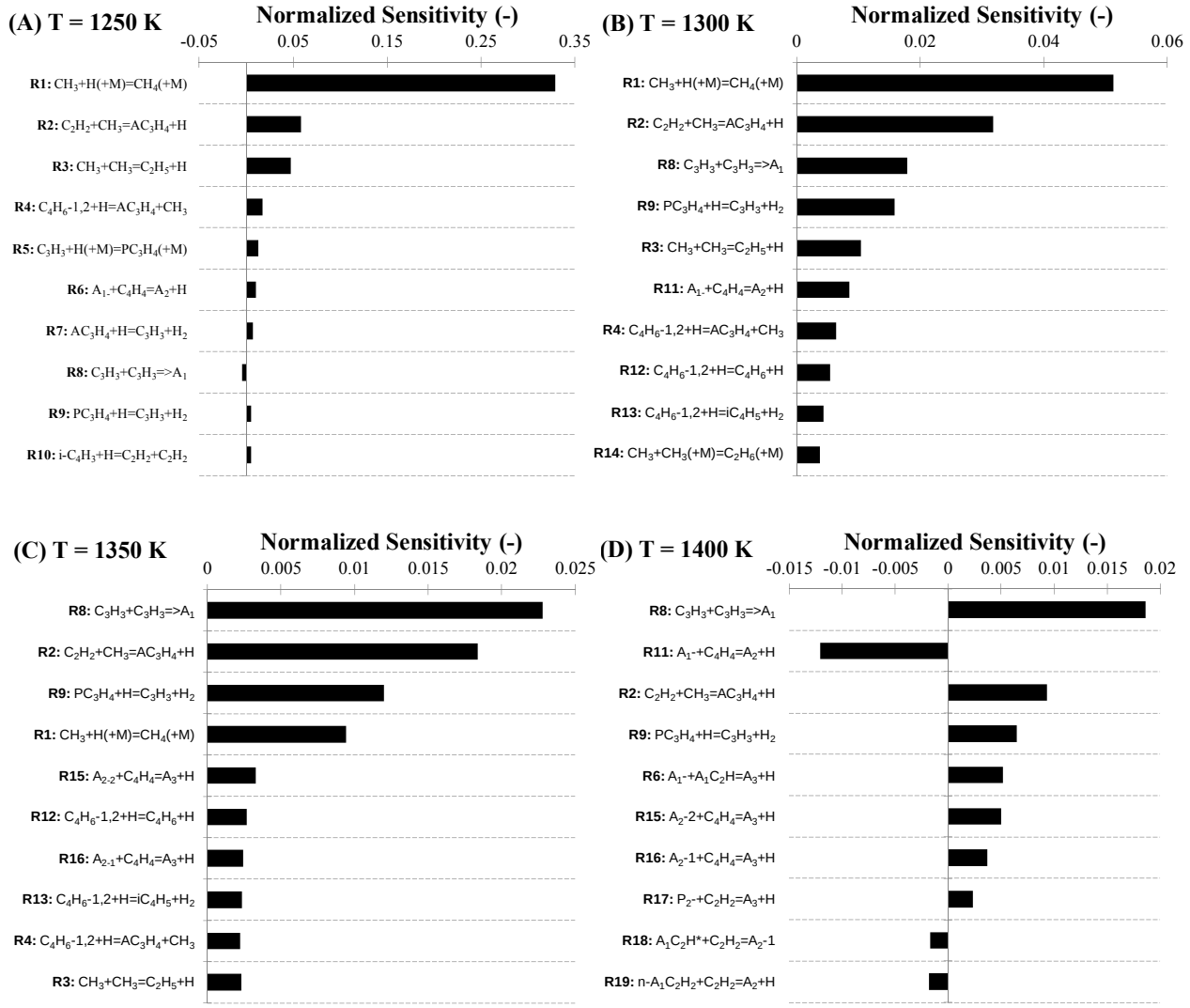

Fig. 3-4: Normalized sensitivity of hydrogen production for the 10 most effective reactions of the Appel mechanism for the decomposition of methane in the conditions of experiments presented by Shah *et al.* [104] at (A) 1250 K, (B) 1300 K, (C) 1350 K, and (D) 1400 K.

increases with temperature. Although these reactions are in the bottom three reactions at 1250 K, they follow R1 and R2 at 1300 K, and R8 becomes the leading reaction at temperatures higher than 1350 K. Reaction R9 also has a high effect at elevated temperatures and follows R2 at 1350 and 1400 K. Consequently, reactions R2 and R9 are the second and third effective reactions at 1350 K, while R11 precedes them at 1400 K, where it is ranked second with a negative sensitivity. It is also noted that although reaction R15 does not have a significant effect at temperatures lower than 1300 K, this reaction takes the fifth and sixth place at 1350 and 1400 K, respectively.

3.2.3. Analysis of Reaction Rates

After determining the main reactions in the conditions of interest, it should be determined if the rate constant of these reactions is well established and is to be kept constant, or it can be changed to improve the mechanism. This evaluation can be performed for each elementary reaction by comparing the rate obtained from different available sources; a considerable difference in the reaction rate shows the feasibility of altering the rate constants to improve the mechanism [100, 108]. The rate constants of the reactions in various mechanisms are listed in Table 3-1.

The mechanisms included in this table are those used in the comparison performed in section 3.2.1, and additional mechanisms mainly taken from the NIST kinetic database [109]. This database is an online directory that provides detailed chemical kinetic data used in a high number of models.

In order to evaluate the difference of the coefficients presented in Table 3-1 and the Appel mechanism, the reaction rate obtained from each of the mechanisms available are plotted in Figs. 3-5 through 3-12, between 1200 K and 1450 K, for reactions with more than 2 various sets of rate coefficients. The difference between the rate of a reaction and its equivalent in the original mechanism is considered to be significant if it is larger than a factor of 2 at any temperature in the range studied. In this case, the use of this rate is assessed as an alternative in the development of the new mechanism.

Fig. 3-5 shows that a wide range of values can be obtained for the rate of reaction R1 by modifying its rate constants. This value can vary from 0.25 to 3.5 times the rate of the Appel mechanism, by using the rate constants of Sheen *et al.* [110] and Glaude *et al.* [111], respectively.

It is observed from Fig. 3-6 that the lowest rate of reaction R2 is that of the Appel mechanism, followed closely by the GRI-Mech 3.0. The highest rate of this reaction is obtained from the coefficients provided by Gupta *et al.* [112] with a value as high as about 8 times its minimum value over the temperature range.

Table 3-1: Most sensitive reactions in hydrogen production and their rate coefficients in the form $AT^n \exp(-E_a/RT)$, in cm, mol, cal, and K units*.

		Mechanisms used in Section 3.2.1				Additional Mechanisms			
No.	Reaction	A	N	E_a	Reference	A	n	E_a	Reference
R1	$CH_3+H(+M)\rightleftarrows CH_4(+M)$	1.27×10^{16}	-0.6	383	[83, 101]	3.18×10^{15}	-0.63	383	[110]
		1.39×10^{16}	-0.53	536	[98]	2.14×10^{15}	-0.4	0	[113]
		1.69×10^{14}	0	0	[100]				
	k_0	2.48×10^{33}	-4.76	2440	[83]	6.19×10^{32}	-4.76	2440	[110]
		1.42×10^{33}	-4.76	2440	[101]	3.31×10^{30}	-4	2108	[113]
		2.62×10^{33}	-4.76	2440	[98]				
		1.41×10^{24}	-1.8	0	[100]				
R2	$C_2H_2+CH_3\rightleftarrows AC_3H_4+H$	5.72×10^{20}	-2.4	31500	[83]	5.14×109	0.86	22153	[110]
		6.74×10^{19}	-2.08	31590	[98]	1.44×10^{24}	-3.24	30357	[112]
R3	$CH_3+CH_3\rightleftarrows H+C_2H_5$	4.99×10^{12}	0.1	10600	[83, 97]	1.41×10^{13}	0.1	10600	[110]
		1.5×10^{12}	0.1	10600	[101]	1.32×10^{17}	-1.29	16106.2	[112]
		6.84×10^{12}	0.1	10600	[98]	8.00×10^{15}	0	26510	[114]
		3.01×10^{13}	0	13513	[99]				
R4	$C_4H_6(1,2)+H\rightleftarrows AC_3H_4+CH_3$	8.00×10^{13}	0.0	1000	[83]				[110,
						2.00×10^{13}	0	2000	115]
						6.00×10^{12}	0	2100	[111]
R5	$C_3H_3+H(+M)\rightleftarrows PC_3H_4(+M)$	3.00×10^{13}	0.0	0.0	[83]	1.66×10^{15}	-0.37	0.0	[115]
	k_0	0.14×10^{32}	-5.00	-6000	[83]	8.78×10^{45}	-8.9	7974	[115]
R6	$A_1-+A_1C_2H=A_3+H$	1.10×10^{23}	-2.9	15890	[83]	9.55×10^{11}	0	4308	[115]
R7	$AC_3H_4+H\rightleftarrows C_3H_3+H_2$	5.75×10^{7}	1.9	7530	[83]	3.36×10^{7}	6	1692	[113]
		1.00×10^{14}	0.0	15009	[99]	5.89×10^{8}	1.5	3594	[112]
		2.00×10^{7}	2.0	5000					[110,
					[97]	1.30×10^{6}	2	5500	115]
						1.00×10^{12}	0	1500	[114]
R8	$C_3H_3+C_3H_3\rightarrow A_1$	5.00×10^{12}	0.0	0.0	[83]	2.00×10^{12}	0	0	[110]
		3.00×10^{11}	0	0	[97, 101]	1.63×10^{44}	-9.20	27574	[112]
						4.96×10^{52}	-11.74	35181.7	
						5.56×10^{20}	-2.54	1692	[115]
R9	$PC_3H_4+H\rightleftarrows C_3H_3+H_2$	1.15×10^{8}	1.9	7530	[83]	4.42×10^{8}	1.5	4253	[112]
		1.00×10^{12}	0	1500	[99]	1.70×10^{5}	2.5	2500	[111]
		1.30×10^{6}	2	5500	[97]	2.00×10^{7}	2	5000	[116]
R10	$i\text{-}C_4H_3+H\rightleftarrows C_2H_2+C_2H_2$	2.80×10^{23}	-2.55	10780	[83]				
R11	$A_1-+C_4H_4\rightleftarrows A_2+H$	3.30×10^{33}	-5.7	25500	[83]				
R12	$C_4H_6(1,2)+H\rightleftarrows C_4H_6+H$	2.00×10^{13}	0	4000	[83]				
R13	$C_4H_6(1,2)+H\rightleftarrows i\text{-}C_4H_5+H_2$	1.70×10^{5}	2.5	2490	[83]	4.42×10^{8}	1.5	4072	[112]
R14	$2CH_3(+M)\rightleftarrows C_2H_6(+M)$	2.12×10^{16}	-1.0	620	[83, 101]	4.24×10^{16}	-0.97	620	[110]
		6.77×10^{16}	-1.18	654	[98]	3.60×10^{13}	0	0	[111]
		9.21×10^{16}	-1.20	636	[99]	9.03×10^{16}	-1.18	654	[114]
		3.60×10^{13}	0	0	[100]				
	k_0	1.77×10^{50}	-9.67	6220	[83]	3.54×10^{50}	-9.67	6220	[110]
		2.12×10^{50}	-9.7	6220	[101]	1.30×10^{41}	-7.00	3000	[111]
		3.40×10^{41}	-7.03	2760	[98]	3.18×10^{41}	-7.03	2760	[114]
		1.14×10^{36}	-5.25	1705	[99]				
		3.63×10^{41}	-7.00	11.56	[100]				
R15	$A_2\text{-}2+C_4H_4\rightleftarrows A_3+H$	3.30×10^{33}	-5.7	25500	[83]				
R16	$A_2\text{-}1+C_4H_4\rightleftarrows A_3+H$	3.30×10^{33}	-5.7	25500	[83]				
R17	$P_2-+C_2H_2\rightleftarrows A_3+H$	4.60×10^{6}	2.0	7300	[83]				
R18	$A_1C_2H^*+C_2H_2\rightleftarrows A_2\text{-}1$	2.20×10^{62}	-14.6	33100	[83]				
R19	$n\text{-}A_1C_2H_2+C_2H_2\rightleftarrows A_2+H$	1.60×10^{16}	-1.3	5400	[83]	5.55×10^{25}	-3.91	13093	[112]

*** The species nomenclature is the same as in reference** [83]**. Accordingly, AC_3H_4 denotes allene, PC_3H_4 propyne, A_1 benzene, A_1- phenyl, A_2 naphthalene, etc.**

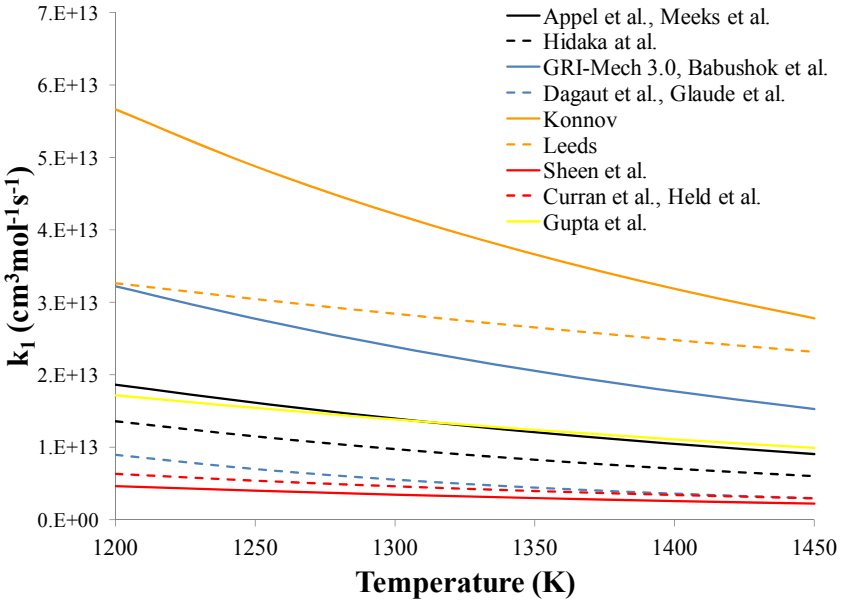

Fig. 3-5: Rate coefficients for reaction R1 between 1200 and 1450 K, at atmospheric pressure.

According to Fig. 3-7, the rate of reaction R3 obtained from the Appel mechanism is very close to that of the Dagaut mechanism. The values obtained from the GRI-Mech 3.0, Held *et al.* [114], and Sheen *et al.* [110] for the rate of this reaction are larger than that of the Appel mechanism, and can increase it up to 3 times, while the rates from Gupta *et al.* [112] and Hidaka mechanism are about 3 to 5 times smaller than this value.

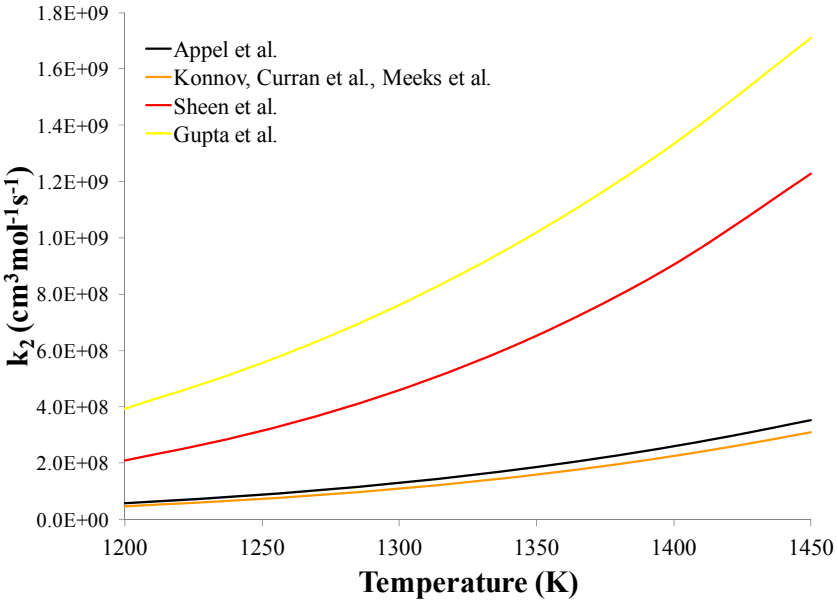

Fig. 3-6: Rate coefficients for reaction R2 between 1200 and 1450 K.

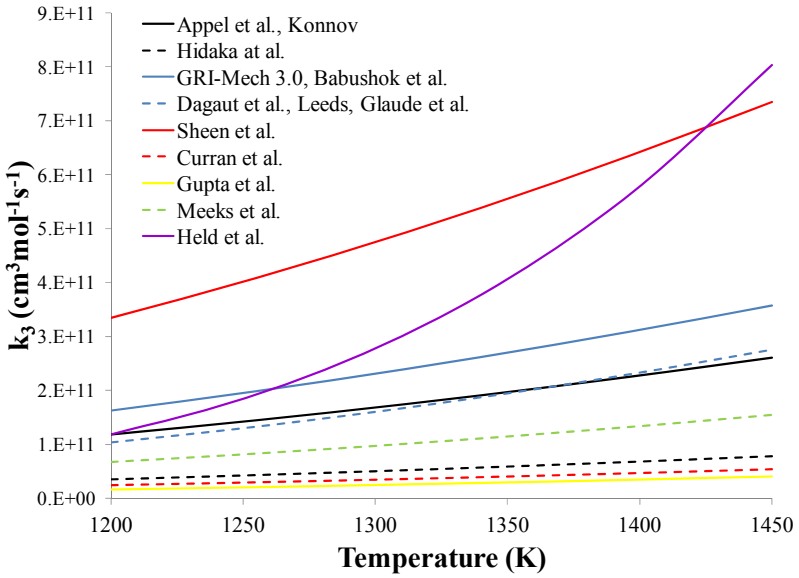

Fig. 3-7: Rate coefficients for reaction R3 between 1200 and 1450 K.

It is observed from Fig. 3-8 that the rate of reaction R4 can decrease significantly by using the mechanism of Gupta *et al.* [112]. Fig. 3-9 shows that k_7 increases by using Gupta *et al.* [112] or Konnov mechanisms, with the former having a rate of about 3 times that of the Appel mechanism. All other coefficients provided for this reaction in Table 3-1 produce a smaller value, with a minimum rate of around 10 times smaller.

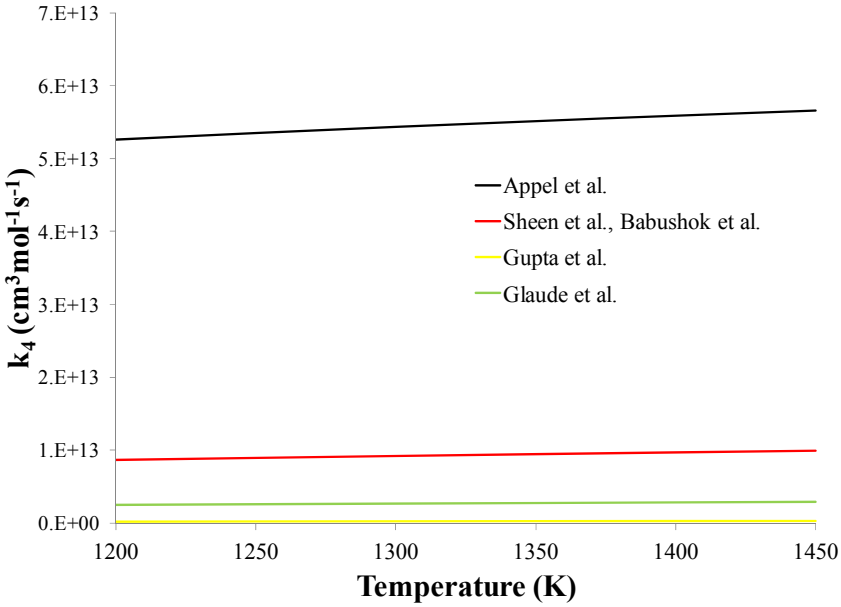

Fig. 3-8: Rate coefficients for reaction R4 between 1200 and 1450 K.

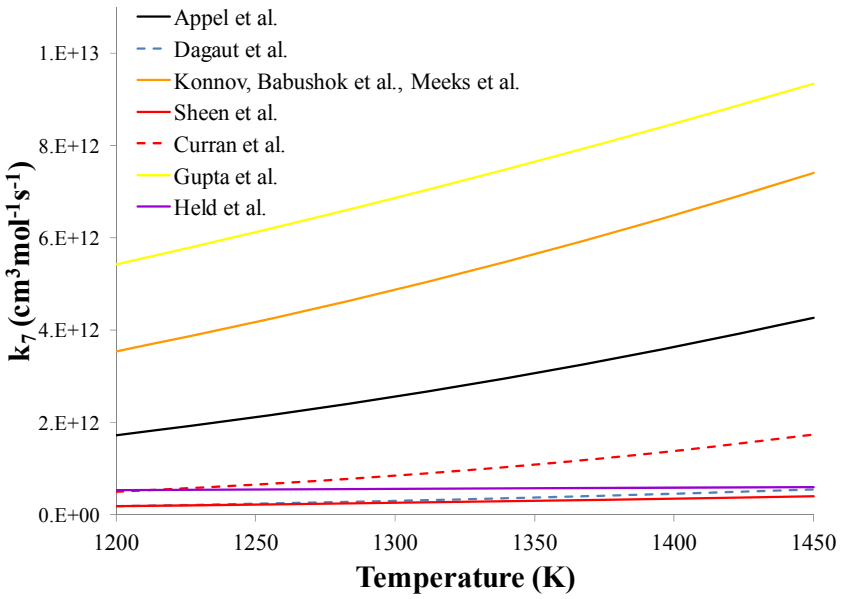

Fig. 3-9: Rate coefficients for reaction R7 between 1200 and 1450 K.

The rate of reaction R8 does not change with temperature, as shown in Fig. 3-10, except for the coefficients provided by Babushok *et al.* [115], where it decreases with temperature. The highest k_8 is obtained from the Appel mechanism, and the smallest with the coefficients of Gupta *et al.* [112], which is 45 times lower.

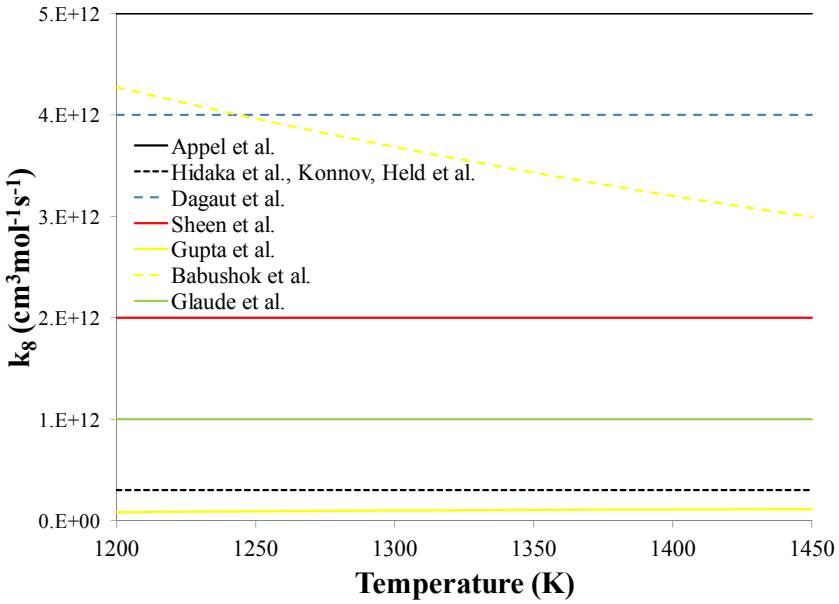

Fig. 3-10: Rate coefficients for reaction R8 between 1200 and 1450 K.

Fig. 3-11 shows that k_9 of the Appel mechanism is the highest followed by that of the Konnov mechanism. The rates obtained by Gupta *et al.* [112] and Glaude *et al.* [111] coefficients come next. The value of k_9 from the mechanisms of Sheen *et al.* [110] and Dagaut are relatively low, with the former having the smallest value which is up to 10% smaller than that of the Appel mechanism.

Although several sets of coefficients are available for reaction R14, Fig. 3-12 shows that the rate obtained from all of these mechanisms are very close, except for the mechanisms of Sheen *et al.* [110] and Leeds, which produce a noticeably larger rate, with the latter being 3 to 4 times higher than the Appel mechanism.

For reaction R10, the rates calculated from the Appel and Hidaka mechanism are almost identical. The results also show that the coefficients recommended by Gupta *et al.* [112] for reactions R13 and R19 cause a minor increase in the rates, while they increase k_{12} up to 2.5 times compared to the Appel mechanism. The rate obtained from Babushok *et al.* [115] is slightly lower than the Appel mechanism for reaction R6, and up to around 2 and 5 times higher for reactions R5 and R17, respectively. The effect of reactions R11, R15, R16, and R18 was not investigated due to the lack of information about these elementary reactions in the mechanisms studied.

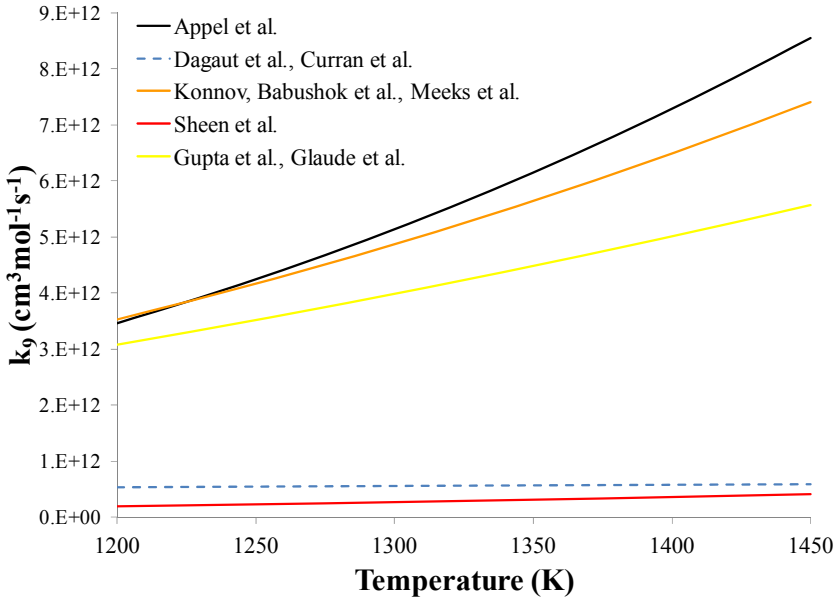

Fig. 3-11: Rate coefficients for reaction R9 between 1200 and 1450 K.

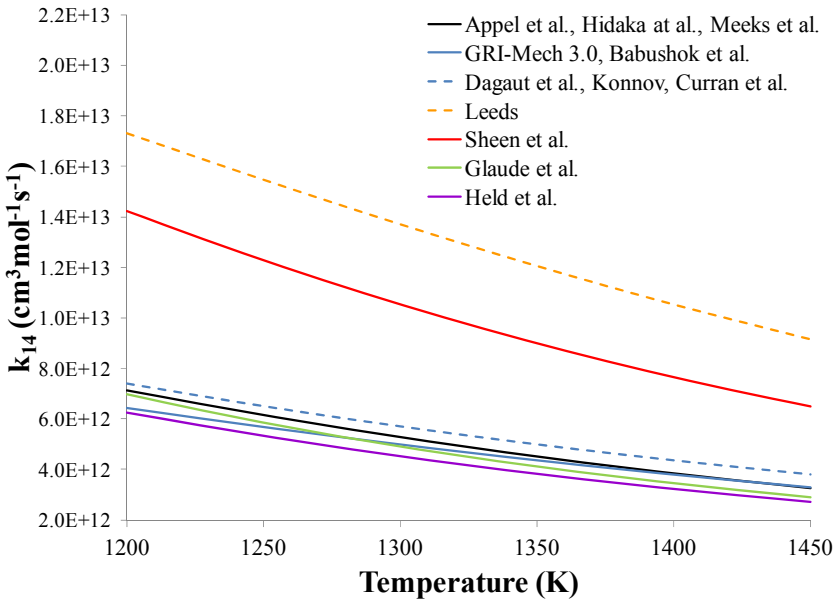

Fig. 3-12: Rate coefficients for reaction R14 between 1200 and 1450 K.

3.2.4. Modification of Mechanism and Comparison with Experiment

After determining the main reactions and the ones that have uncertain rate coefficients, the effect of replacing these values in the Appel mechanism with the parameters available in other studies is investigated. This study shows that changes in the rate constants of reaction R1 with reaction rate coefficients from Table 3-1 has a prominent effect on the amount of hydrogen produced. Some of the values provided in Table 3-1 for this reaction can reduce the high difference between simulation results and experimental data observed in Fig. 3-3 to a negligible value. However, since reaction R1 is the highest sensitivity reaction in a wide range of temperatures and times, variations of its rate constants also cause the results in other conditions to deviate from experiment. In the new mechanism, the optimal results were obtained with the rate coefficients of the Hidaka mechanism for this reaction. Since the third body reaction of methyl and hydrogen radicals to methane is also included in the Hidaka mechanism, this reaction was added to the new mechanism along with the constants of reaction R1. Replacing the rate coefficients of the reaction of benzene formation from Propargyl radicals, reaction R8 using available data has the second highest effect on the results. This reaction was changed to duplicate reactions with the rate constants proposed by Gupta *et al.* [112]. In addition, the rate coefficients of hydrogen abstraction reactions from propyne and allene with hydrogen radical, R9 and R7, were modified to those used by Sheen

et al. [110] and Dagaut, respectively. The rate of reaction R4 was also changed by using the coefficients provided by Glaude *et al.* [111]. It is noted that the reaction of combination of methyl radicals into ethyl and hydrogen radicals, reaction R3, also has a considerable importance in reducing the error in high residence times. However, due to its effect on the results in other conditions the rate coefficients of this reaction was not modified.

The results of the new mechanism are compared with experimental data and other mechanisms in Figs. 3-1 to 3-3. These figures show that the new mechanism yields the most accurate representation of experiment. When this mechanism is used to model the decomposition process, the maximum and average differences between experimental data obtained by Shah *et al.* [104] and simulation results are reduced by 15% and around 7.5%, respectively, while the adequate prediction of the model for other experimental cases remains nearly unchanged.

The validity of the kinetic model was also investigated by comparing its results at chemical equilibrium with the values obtained by using the Gibbs minimization method. In the latter method, the set of species expected to be present in the products of the process are first specified, and the composition of these species that minimizes the Gibbs energy of the product mixture is determined considering the conservation of mass and elements. The equilibrium values from the kinetic model are obtained by increasing the residence time of the process until the mole fractions of the products are constant. The comparison of equilibrium data from these two methods is shown in Fig. 3-13. It can be observed that the results of the two models are very close.

The results of hydrogen production from the new mechanism were also compared to the experimental data of Lee *et al.* [41], in a residence time of around 40 seconds, and a temperature of 1220 to 1320 K. In these conditions, a good agreement is observed between the model and experiment, and the error in predicting the amount of hydrogen is decreased by at least 7% compared to the Appel mechanism. The new mechanism was also used to find the values of some species other than hydrogen and methane, such as acetylene, ethylene, and ethane. The results show that, in conditions of the work of Back *et al.* [102], these values are almost similar to the Appel mechanism and close to experimental results. Also, at a low residence time of around 10 seconds, in the temperature range of the experiments of Murphy

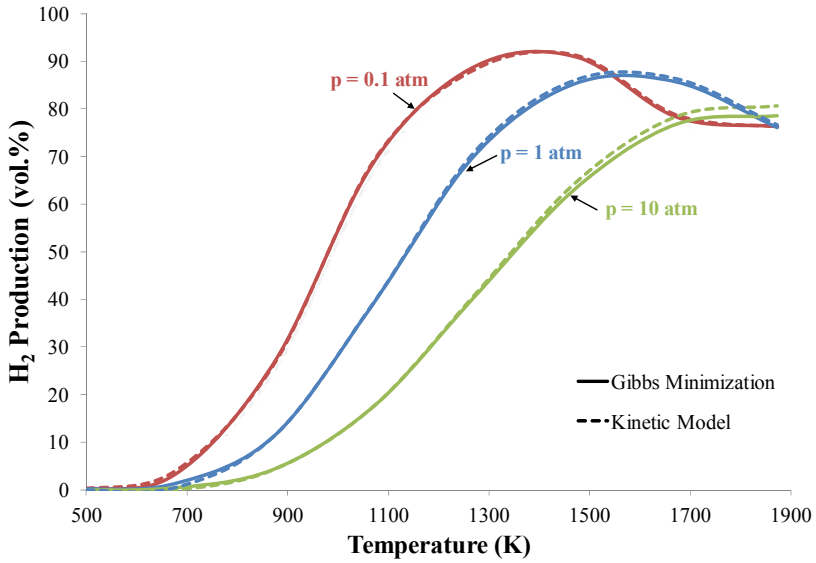

Fig. 3-13: Comparison of hydrogen production at equilibrium obtained from the model and with the Gibbs minimization method.

et al. [103], the amount of ethylene and acetylene obtained with the new mechanism is in the same range as the results of other combustion mechanisms.

It can be concluded that the mechanism developed has an acceptable accuracy considering the available data and can be used to predict the amount of hydrogen produced from thermal decomposition of methane.

3.3. Model of Hydrogen Production from the Interaction of the Gas and Catalyst Surface

After finding the production rate of species from the homogeneous decomposition of methane, the effect of the catalyst should be added to complete the solution of Equation (3-1). For this purpose, a surface reaction mechanism is selected for the detailed kinetic model. The equations of reaction rates of surface reactions are derived while including the main properties of carbon catalysts. Two different methods are applied to find the reaction rates and the most suitable method is determined with comparison with experimental data. Modeling of the distribution of solid particles is also discussed, and the hydrodynamics of the fluidized bed reactor is modeled to reduce the dependency of the model to experimental data.

3.3.1. Selection of the Surface Reactions

In the detailed kinetic model of the thermocatalytic decomposition of methane, a surface reaction mechanism is used to model the hydrogen production from the surface of catalyst particles in Equation (3-1). As explained in section 2.3.2, the mechanism initially proposed by Dunker *et al.* [25, 117] is used in this study, which consists of the following surface reactions:

$$C_s - H + H \rightleftarrows C_s\bullet + H_2 \quad \text{(SR1)}$$

$$C_s\bullet + H \rightarrow C_s - H \quad \text{(SR2)}$$

$$C_s\bullet + C_2H_2 \rightarrow C_s - H + H \quad \text{(SR3)}$$

$$C_s\bullet + C_2H_6 \rightleftarrows C_s - H + C_2H_5 \quad \text{(SR4)}$$

$$CH_4 (+C_s - H) \rightleftarrows CH_3 + H(+C_s - H) \quad \text{(SR5)}$$

$$C_2H_4 (+C_s - H) \rightleftarrows C_2H_2 + H_2 (+C_s - H) \quad \text{(SR6)}$$

$$C_2H_6 (+C_s - H) \rightleftarrows CH_3 + CH_3 (+C_s - H) \quad \text{(SR7)}$$

$$C_2H_5 (+C_s - H) \rightleftarrows C_2H_4 + H(+C_s - H) \quad \text{(SR8)}$$

In this mechanism, the surface sites on the carbon catalyst are considered to be in the form of carbon radical, $C_s\bullet$, and carbon atoms saturated with hydrogen, $C_s - H$. The first three reactions were directly taken from the surface growth mechanism in the soot formation model of Appel *et al.* [83], and the remaining reactions were added by Dunker *et al.* [25]. A Sensitivity analysis was performed on the gas-phase mechanism developed in the previous section to investigate the possibility of improving the surface mechanism presented by adding surface reactions similar to important gas-phase reactions in the conditions under consideration. This investigation shows that reactions SR5 to SR8 are the most important reactions found using this method, and considering reactions that follow them does not improve the results.

3.3.2. Rate of Surface Reactions

After selecting the surface reactions to be used in the kinetic model, their rates should be determined. Two methods have been suggested to find the rate of these reactions. In the first method, the rate coefficients are calculated by analogy with similar gas-phase reactions,

while in the second method, the rate of each reaction is determined with the kinetic theory [118, 119]. In previous models, the rate obtained from these methods is derived by considering two properties of the catalyst particles: the surface area and the number of surface sites. Since the later is nearly constant in different types of carbon, the only catalyst property affecting the hydrogen yield obtained with these models is the surface area.

Experimental studies show that although particles with larger surface areas usually have a higher activity, this parameter cannot justify the trend of changes in the rate of hydrogen production from different types of carbon [37, 39, 40, 60, 61, 120]. Some of these studies suggest that this difference can be explained by considering the number of active sites on the surface of the catalysts [37-39, 41, 61, 65]. This value has been found to be associated with the crystallinity and the number of defects on the surface of carbon particles. However, no experimental method has been found to quantify this value, nor has it been applied in existing models. In this section, the equations used to find the rate for the kinetic model are developed with the number of active surface sites, and this value is estimated by combining the model with experimental data.

The equation for obtaining the rate of the i^{th} reaction, r_i, with the first method, using analogy with similar gas-phase reactions, takes the following form when the number of active surface sites is considered:

$$r_i = k_i C_i \frac{\chi_{as} A_s}{N_A} \tag{3-3}$$

where k_i is the per-site rate coefficient obtained from gas-phase reactions, A_s is the total surface area of the particles per volume, and N_A is Avogadro's number. Depending on whether the forward or reverse rate is calculated, C_i and χ_{as} are the molar concentration of the gaseous species and the number density of the active surface sites in the reactants or products, respectively. At this point, a factor f_s is defined as follows:

$$f_s = \frac{\chi_{as}}{\chi_{os}} \tag{3-4}$$

where χ_{os} is the number density of surface sites on ordered carbon, or graphene sections of the catalyst. Accordingly, f_s can be defined as the ratio of number density of active sites on the catalyst to that of surface sites on ordered carbon. It is noted that the number density of $C_s - H$ surface sites on the graphene sections is estimated by considering one site in a rectangular area with one side being half-width of the benzene ring, 1.23 Å, and the other the distance between PAH layers, 3.51 Å [121]. Since these values are nearly the same for different kind of carbon in this study, χ_{os} is equal to 2.3×10^{15} cm^{-2} in all cases. The number density of $C_s\bullet$ is calculated with a steady state assumption for this radical as follows:

$$\chi_{C_s\bullet} = \frac{k_1[H] + k_{-4}[C_2H_5]}{k_{-1}[H_2] + k_2[H] + k_3[C_2H_2] + k_4[C_2H_6]}\chi_{C_s-H} \qquad \textbf{(3-5)}$$

In the second method, the rate of reactions is determined with the following equation derived using the kinetic theory.

$$r_i = f_s\gamma_i C_i A_s\sqrt{\frac{k_B T}{2\pi m_i}} \qquad \textbf{(3-6)}$$

In this equation, γ_i is the collision efficiency of the i^{th} reaction, m_i is the mass of the reactant, k_B is the Boltzmann constant, and T is the temperature. It is noted that the derivation of the rate of reaction from kinetic theory and the definition of f_s have lead to the inclusion of this factor in Equation (3-6). The reverse rate of these reactions is calculated using the equilibrium constant. The collision efficiency of each reaction and the factor f_s are determined in the following sections.

The most appropriate of the methods previously described should be used to determine the rate of surface reactions. The results obtained from the analogy with gas phase reactions are more accurate when the required information is available. Equation (3-3) is therefore used for reactions SR1 to SR4. However, due to the nature of the fall-off reactions SR5 to SR8, this method cannot be applied without applying changes to the current form of the surface reactions. Consequently, Equation (3-3) is not the obvious choice to find the rate of these reactions. The results obtained from using both methods of kinetic theory and analogy

with gas-phase reactions for reactions SR5 to SR8 are compared in the following sections to determine the suitable one.

Kinetic Theory [122]

To use Equation (3-6) for reactions SR5 to SR8, the value of the collision efficiencies, and the initial value of f_s should first be specified. The experimental data of Dunker *et al.* [117] are used for this purpose. In these experiments, methane was decomposed in a fluidized bed reactor of carbon particles. 14 experiments were performed in a temperature range of 1080 to 1260 K and residence time between 4 and 9 seconds, with three different commercial carbon black catalysts of Black Pearls 120 (BP120), Black Pearls 2000 (BP2000), and Vulcan XC-72 (XC72). The amount of hydrogen production was measured in different times of the run in each case.

Experiments show that carbon blacks catalysts have a high initial activity at the beginning of the experiments which decreases with time, until a quasi-steady state is reached with a rather constant amount of hydrogen production [35, 36, 38, 57]. The value of collision efficiencies are determined by using the data at the quasi-steady condition. Experimental studies have shown that the initial activity of catalysts and their specific surface area are not proportional [34, 37, 40, 41, 61] and lead to the conclusion that the number density of active sites of various catalysts differs. In other studies, comparison of the activity of the catalyst at quasi-steady state and the surface area of the fresh catalyst shows a linear trend until the activity reaches a maximum and stays constant [38, 41, 65] as demonstrated in Fig. 2-6. It is noted that the latter comparisons were made between different conditions, whereas comparing the parameters at the same condition leads to more valuable conclusions. In this study, experimental data of Lazaro *et al.* [35] and Dunker *et al.* [117] were used in Fig. 3-14 to show that the trend of variations of the activity and specific surface area becomes completely linear when both of these values are considered at the quasi-steady state condition. The difference of trends observed between the cases where the reaction rate is compared with the initial and quasi-steady state surface area can be explained considering the different fraction of pores in each catalyst. Carbons with higher specific surface areas, such as BP2000, have generally larger fraction of pores which are rapidly blocked by the

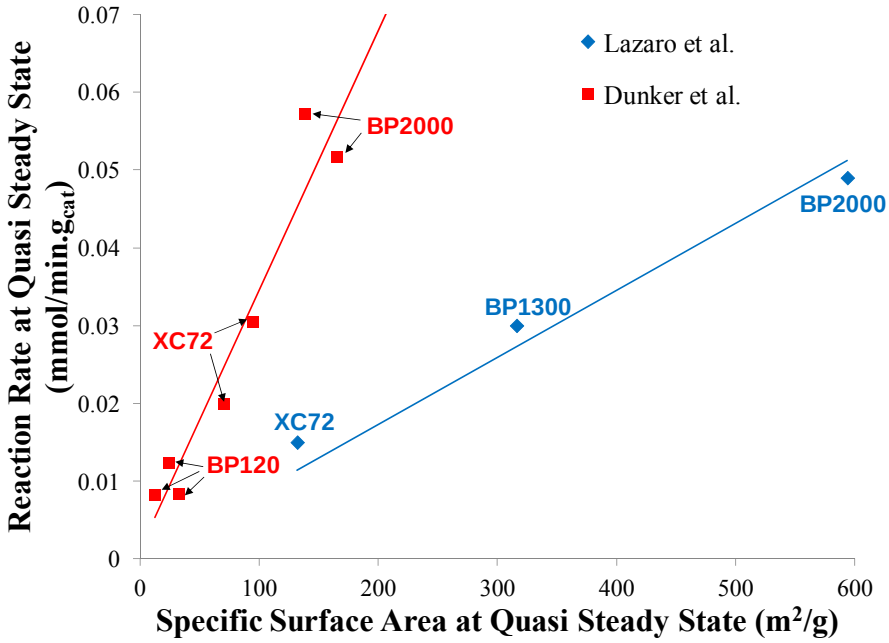

Fig. 3-14: Variations of reaction rate versus specific surface area at quasi-steady state condition.

deposited carbon, causing a larger decrease in specific surface area relative to catalysts with lower initial surfaces areas.

The linear trend observed in Fig. 3-14 implies that the number density of active sites of different carbon blacks converges to an identical value at the quasi-steady state condition. In this study, this value is considered equivalent to soot. According to the equations describing soot formation f_s is set equal to one at the quasi-steady state condition, and the collision efficiency can be determined using experimental data in this condition. The ratio of collision efficiencies of reactions SR5 to SR8 and the corresponding gas-phase reactions are assumed equivalent, and the collision efficiencies of these reactions are found to be $9\pm1\times10^{-11}$, $5\pm0.5\times10^{-09}$, $1.35\pm0.15\times10^{-06}$, and 0.41 ± 0.05, respectively. It is noted that applying reaction probabilities in the specified ranges yields in similar amounts of hydrogen. The results of the model with these collision efficiencies, at quasi-steady conditions closely follow experimental values as shown in Fig. 3-15.

The initial value of the factor f_s for each catalyst can now be determined using experimental data at the start of each run. The amount of hydrogen production obtained from the model with f_s equal to one, which implies a number density of surface sites equal to soot

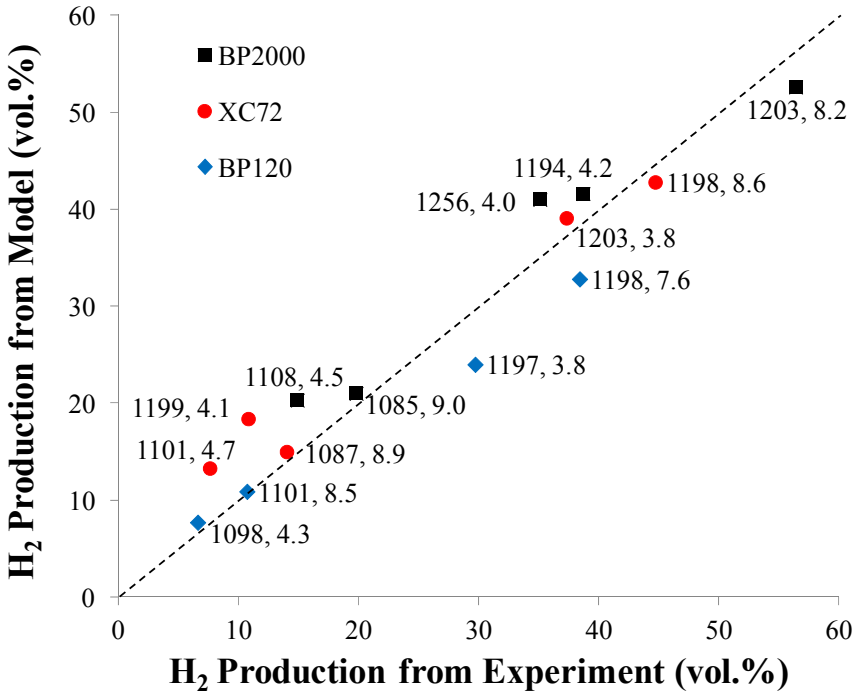

Fig. 3-15: Volumetric percentage of hydrogen production obtained from model compared to experimental values at quasi-steady state conditions. The values in the labels show the temperature in Kelvin and residence time in seconds.

particles, is compared with experimental results in Fig. 3-16. It is observed that by using soot properties, the values of hydrogen obtained from the model are significantly lower than experimental values. This can be explained by the fact that carbon catalysts are more active than soot particles and have a higher number of active surface sites, which should be considered in the model. This justifies the use of the factor f_s in the calculation of reaction rates. This factor can be determined by adjusting the results of the model with experimental data for each of the catalysts.

This investigation shows that the initial number of active surface sites per unit mass of the catalyst for BP120, XC72, and BP2000 is 7×10^{17}, 1×10^{18}, and 2×10^{19} g^{-1}, respectively. This is in agreement with experimental studies which show that BP2000 has a higher degree of disorder and more defects than XC72 [34]. The results obtained by introducing the values obtained for f_s in the model are presented in Fig. 3-17, and are in reasonable agreement with experimental data.

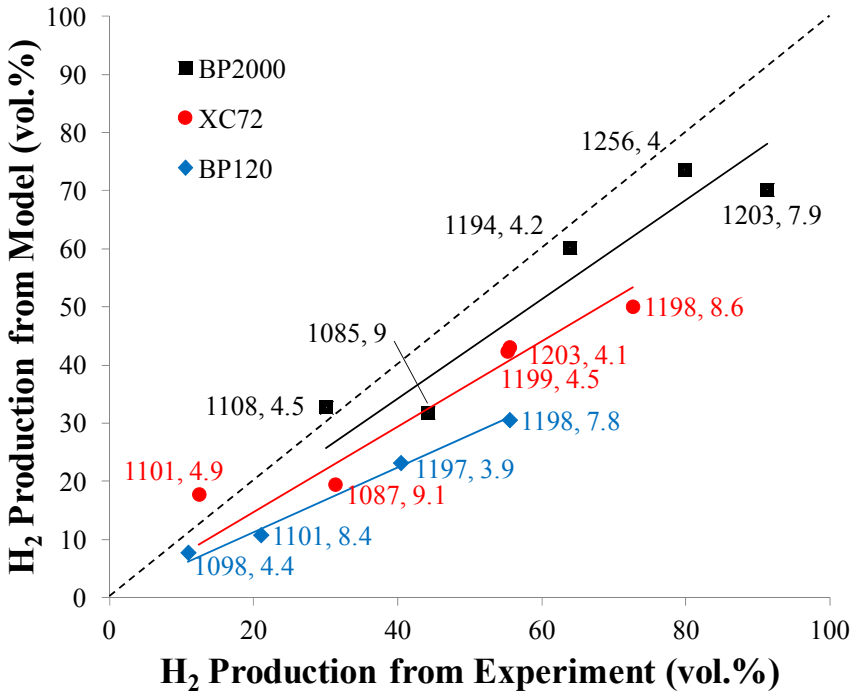

Fig. 3-16: Initial percentage of hydrogen production obtained from experiments compared to model with number density of surface sites equal to that of soot. The values in the labels show the temperature in Kelvin and residence time in seconds.

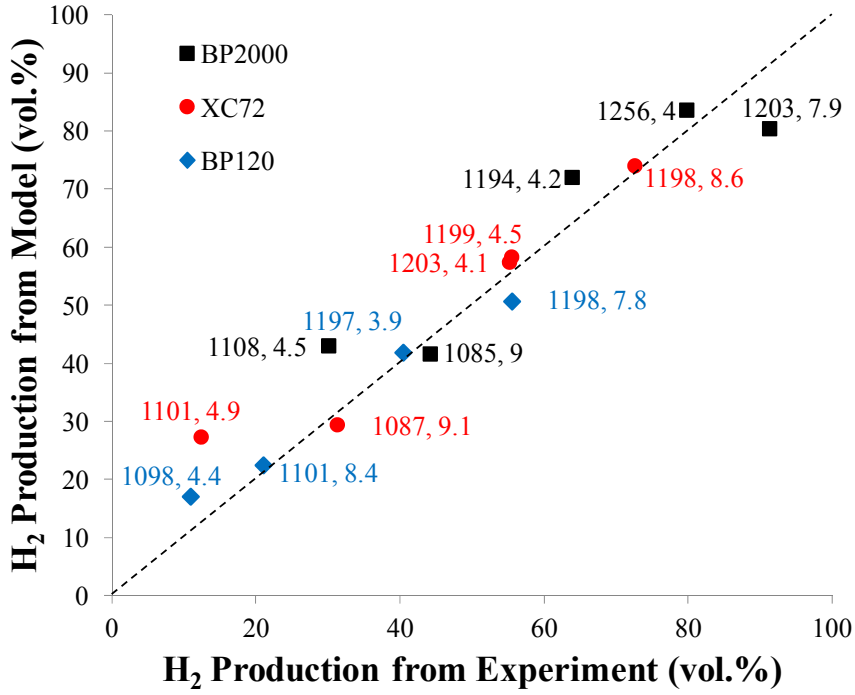

Fig. 3-17: Initial percentage of hydrogen production obtained from experiments compared to model with adjusted number density of surface sites. The values in the labels show the temperature in Kelvin and residence time in seconds.

Overall, it can be concluded from Figs. 3-15 and 3-17 that the values obtained from the model can reasonably predict the amount of hydrogen production.

Analogy with Gas-Phase Reactions

In the method of analogy with gas-phase reactions, Equation (3-3) is used to find the rate of the reactions with the per-site rate coefficient being determined with data from similar gas-phase reactions. Although this method is more accurate than the kinetic method to obtain reaction rates, the calculation procedure cannot be applied to fall-off reactions like reactions SR5 to SR8. In this section, this method is used by assuming these reactions are third body reactions. This assumption implies that when the catalyst is added to the reactor, it affects the process through surface reactions, as opposed to having a partial participation depending on other factors when fall-off reactions are considered. This assumption is plausible and describes the role of the catalyst in a more acceptable way than the original set of surface reactions. The new form of surface reactions along with their rate coefficients obtained from similar gas phase reactions in the mechanism of Appel *et al.* [83] are presented in Table 3-2.

After finding the rate coefficients of surface reactions, Equation (3-3) is used to find the rate of these reactions. In contrast with the kinetic theory method where two parameters of collision efficiency and f_s were determined with experimental data to calculate the rate of surface reactions, in this method, only f_s should be specified. This parameter is determined

Table 3-2: Surface reactions representing the effect of carbon catalysts in methane decomposition and their rate coefficients obtained from analogy with gas-phase reactions in the form $AT^n \exp(-E_a/RT)$, in cm, mol, cal, and K units.

Surface Reaction		A	n	E_a
SR1:	$C_s - H + H \rightleftarrows C_s\bullet + H_2$	4.17×10^{13}	0.0	13000
SR2:	$C_s\bullet + H \rightarrow C_s - H$	$2.\times10^{13}$	0.0	0
SR3:	$C_s\bullet + C_2H_2 \rightarrow C_s - H + H$	8.0×10^{7}	1.56	3800
SR4:	$C_s\bullet + C_2H_6 \rightleftarrows C_s - H + C_2H_5$	2.07×10^{11}	0.0	3600
SR5':	$CH_3 + H + C_s - H \rightleftarrows CH_4 + C_s - H$	2.48×10^{33}	-4.76	1980
SR6':	$C_2H_4 + C_s - H \rightleftarrows C_2H_2 + H_2 + C_s - H$	7.00×10^{50}	-9.31	81000
SR7':	$CH_3 + CH_3 + C_s - H \rightleftarrows C_2H_6 + C_s - H$	1.77×10^{50}	-9.67	5053
SR8':	$C_2H_4 + H + C_s - H \rightleftarrows C_2H_5 + C_s - H$	1.20×10^{42}	-7.62	5663

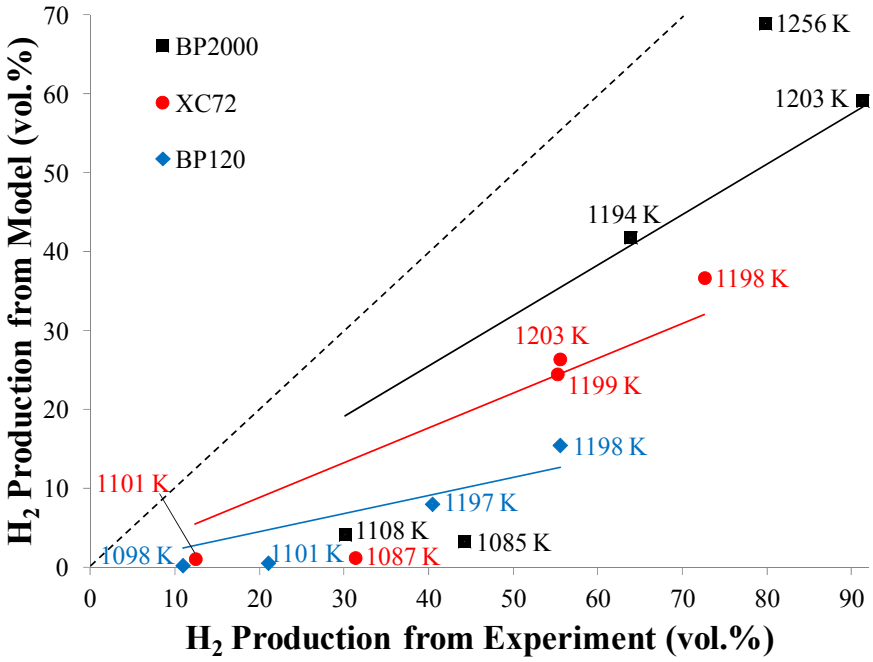

Fig. 3-18: Initial percentage of hydrogen production obtained from experiments compared to model with the coefficient f_s equal to one. The values in the labels show the temperature in Kelvin.

using the initial conditions in experiments of Dunker *et al.* [117] described in the previous subsection. A preliminary analysis is first performed on the results of the model with f_s equal to one. These results are compared with experiment in Fig. 3-18.

It can be observed that similar to the results of the kinetic theory, each catalyst has a unique slope. This confirms that the number of surface sites depends on the type of catalyst used. One important observation from this figure is that the difference between the results of the model and experiment are much larger at low temperatures relative to high temperatures.

In conclusion, the number of surface sites to be used in the model is a function of temperature, and its value varies inversely with temperature. This result is in accordance with the fact that the number of surface sites is linked to the degree of disorder of carbon, which is negatively affected by temperature. The variations of the number of surface sites determined by the model with temperature are illustrated in Fig. 3-19. These results are used to determine correlations representing the factor f_s as a function of temperature for each catalyst used in the mentioned experiments as follows:

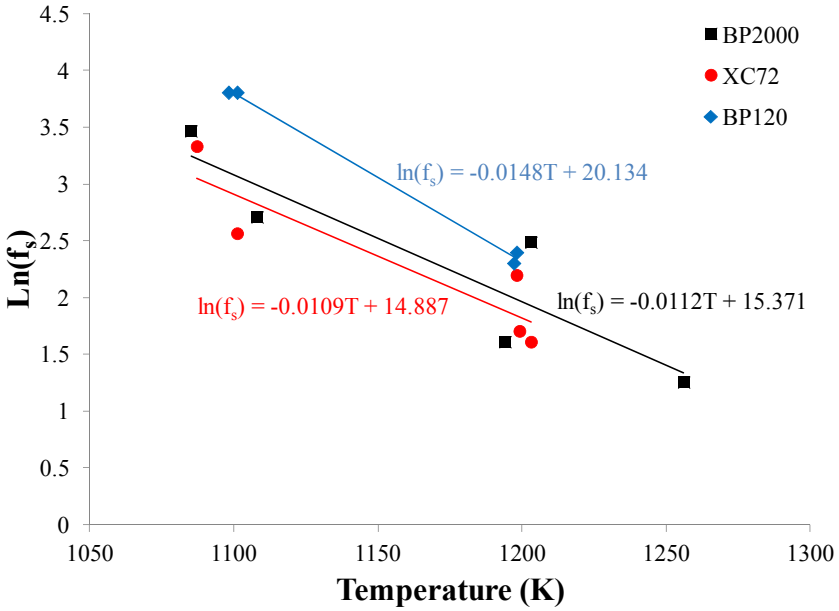

Fig. 3-19: Variations of factor f_s with temperature for catalysts BP2000, XC72, and BP120.

$$f_{s,BP2000} = 4.7\times10^{6}\exp(-0.0112T)$$

$$f_{s,BP120} = 5.5\times10^{8}\exp(-0.0148T) \qquad \textbf{(3-7)}$$

$$f_{s,XC72} = 2.9\times10^{6}\exp(-0.0109T)$$

Fig. 3-20 shows the results of using the above correlations in the model. This figure shows that the results of this model are in good agreement with experimental data.

In Fig. 3-21, the results obtained by using the kinetic theory and analogy with gas phase reactions are compared with experiment. This figure shows that the later method yields in more accurate result. In comparing these methods, it should also be noted that fewer assumptions are used when analogy with gas phase reactions is used to calculate the reaction rate. As a result, this method is more appropriate and is therefore selected in this study.

Further validation is performed by comparing the model results in conditions used by Lee *et al.* [41] and their experimental data. These experiments were conducted with BP2000 as catalyst in a flow of methane with a flow rate of 25 cm^3(STP)/min and in a temperature range from 1023 K to 1323 K. The results presented in Fig. 3-22 show the good agreement of the model with experiment.

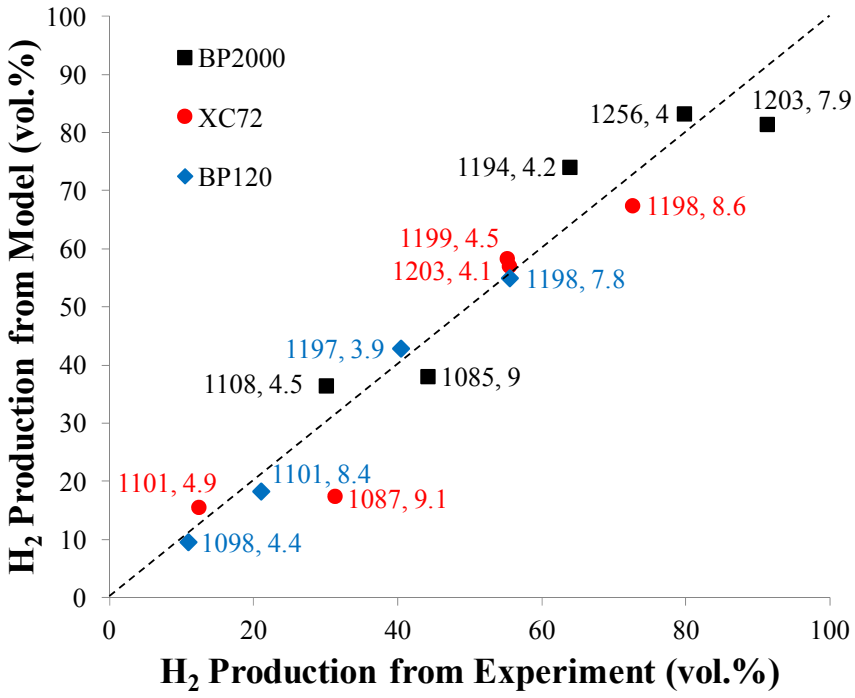

Fig. 3-20: Initial percentage of hydrogen production obtained from experiments compared to model with adjusted number density of surface sites. The values in the labels show the temperature in Kelvin and residence time in seconds.

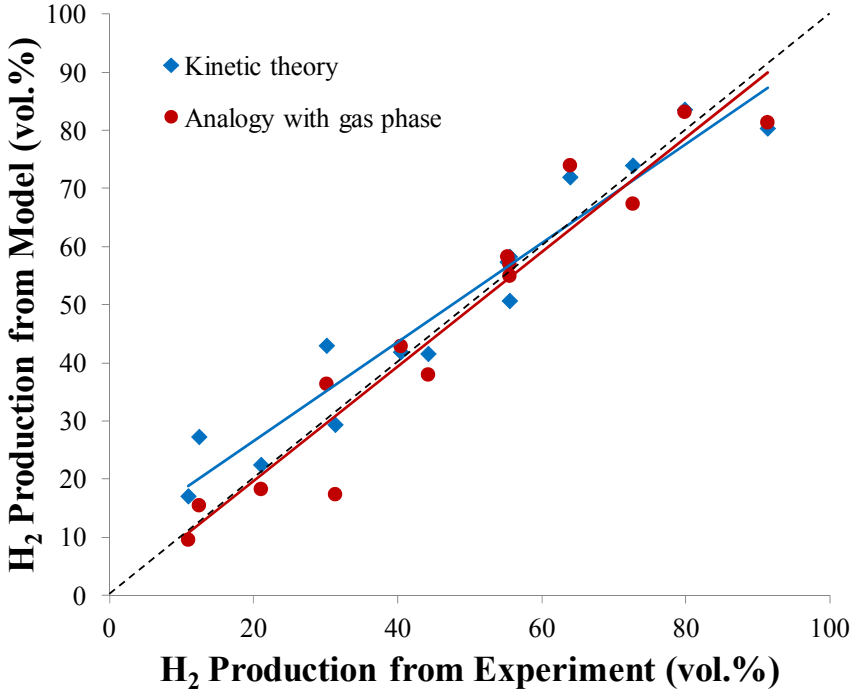

Fig. 3-21: Comparison of results obtained from the model using the two methods of kinetic theory and analogy with gas phase reactions for finding reaction rates with experiment.

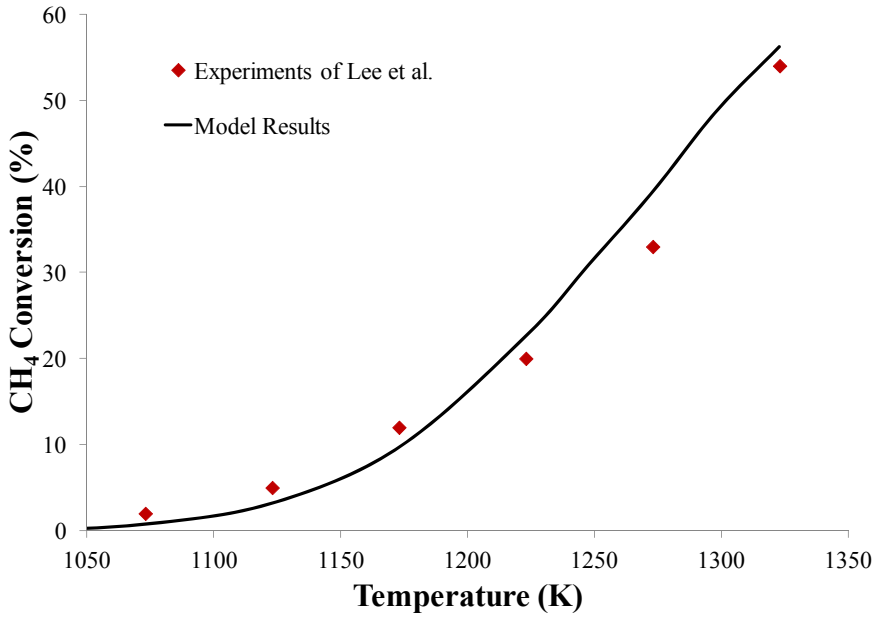

Fig. 3-22: Results of the model with the method of analogy with gas phase compared to experimental data performed by Lee *et al.* [41].

3.3.3. Variations of Particle Distribution

The dependence of the model on the variations of particle distribution and carbon formation is observed with the presence of the term A_s in the calculations of the rate of surface reactions. During the process, this value changes with the variations in particle distribution due to physical and chemical phenomena. To obtain an accurate value for hydrogen production through time and model the transient decomposition of methane, a method should be used to determine these variations over time.

The method that has been proposed for finding the variations of the distribution of carbon particle is the method of moments developed by Frenklach [123]. This method has been widely used for modeling soot formation due to its computational efficiency. The base of this model is the application of moments of the particles to describe the distribution of particles:

$$M_r = \sum_{i=1}^{\infty} i^r N_i \qquad r = 0, 1, \ldots, 5 \qquad \textbf{(3-8)}$$

In this equation, M_r is the r^{th} moment, i is the number of carbon atoms and N_i the number density of size i particles. As noted in this equation, the use of the first 6 moments is sufficient to obtain suitable results.

The phenomena that are likely to affect the distribution of the carbon particles in this process are: (1) the nucleation of polyaromathic hydrocarbons into solid particles, (2) the coagulation of particles through collision and formation of larger particles, and (3) the growth of the solid particles through surface reactions. The models of these phenomena with the method of moments along with their derivation are extensively explained in literature [119, 123]. According to the results of Dunker *et al.* [25] coagulation does not occur in the conditions under consideration for the thermocatalytic decomposition of methane. Therefore, only the nucleation and surface growth on the catalyst particles should be considered in modeling this process. Experimental investigations on surface growth of carbon catalysts reveal that the size of the pores in the catalyst and their distribution are the determining parameters in the variations of particle distribution due to surface growth [39, 58, 59, 61, 93]. Consequently, to model the changes in the variable A_s with time due to this phenomenon, either a model should be used that considers these factors, or correlations should be derived to represent these changes with time for different catalysts. Since the model in the method of moments does not include these important factors, it cannot represent the surface variations of each catalyst correctly and is not suitable for this study. Also, a correlation for the reduction in the surface of carbon black catalysts has been obtained by Muradov [39]. However, it fails to soundly model the variations in the surface of catalyst particles in different experimental conditions available in literature. In conclusion, the transient model of the decomposition of methane cannot be obtained with the current knowledge about surface area variations with surface growth. The model is therefore used to study the initial behavior of the process, or any other time where the surface area of the catalyst is known. Consequently, the time frame used for solving Equation (3-1) is in the range of the residence time of the reactor. Since this value is relatively small, it is assumed that nucleation and surface reactions do not affect the value of A_s. This assumption has been confirmed in experimental studies by comparing the activation energy of the decomposition of methane over different types of carbon and those of carbon nuclei generation and crystallite growth.

These investigations show that the activation energy of the process is closer to that of the carbon crystallite growth, and the rate of this phenomenon is much higher than the nucleation of carbon particles. It was concluded that the growth of carbon on the catalyst is the major controlling step in this process [39, 40]. This assumption was further verified by including the nucleation in the model with the method of moments, and investigating its effect with multiple input conditions. The results show that the effect of nucleation in the time frame investigated is negligible.

Since the model is used to study the initial behavior of the process, A_s can be determined using the properties of the catalyst and experimental data, with the following equation:

$$A_s = S_{BET} \frac{1-\varepsilon}{\varepsilon} \rho_p \quad \textbf{(3-9)}$$

where ε is the void fraction of the reactor, and S_{BET} and ρ_p are the specific surface area and the apparent density of the catalyst, respectively. The properties of the catalyst are usually available from the provider but they can also be measured experimentally. While S_{BET} is obtained with the BET equation from the N_2 adsorption–desorption isotherms, ρ_p can be determined by Hg porosimetry or dibutylphthalate (DBP) adsorption by using the pore size. The void fraction of the reactor is either obtained by performing some measurements on the actual set of experiments, or with a model of the fluidized bed as explained in the next section.

3.3.4. Modeling the Hydrodynamics of Fluidized Bed

The reactor considered in this study for the thermocatalytic decomposition of methane is a fluidized bed operating in a particulate regime. Some of the characteristics of fluidization are used in modeling this process either as variables in the applied equations or for determining the limits where it is applicable. Experimental methods have been proposed to determine these values. However, the objective of this study is to model the process without performing experiments. It is crucial for the inputs of the model to be determined with minimal or, if possible, no experimental data. In this section, the appropriate correlations to determine the

required characteristics of the bed with the properties of the catalyst particles and the flow are obtained to reduce the dependence of the overall model on experiments.

Void Fraction

The void fraction of the fluidized bed is required to calculate the volume of the gas in the reactor, and is used in the calculations of the residence time and the rate of the surface reactions. The equation proposed by Richardson and Zachi [124] is the most popular model for finding the void fraction in a fluidized bed:

$$\varepsilon^n = \frac{u}{u_t'} \tag{3-10}$$

In this equation, u is the velocity of the fluid, and u_t' is the velocity that creates a void fraction equal to unity. The exponent n depends on the properties of the reactor, and can be either a constant value or a function of the characteristics of the bed and particles. Equation (3-10) was originally proposed for liquid-solid systems. However, its application was extended to gas-solid beds with a method developed by Geldart and Wong [89], which will be used in this study. The difference between this method and the original model of Richardson and Zachi is in the values of n and u_t'.

In the original model for liquid-solid beds, the exponent n has a constant value of 4.65, while the following equation was suggested by Geldart and Wong [89] for finding this value in gas-solid systems:

$$n = 4.65\left(\frac{HR}{1.11}\right)^{4.16} \tag{3-11}$$

where HR is the Hausner ratio, which is defined as the highest to lowest bulk densities of the catalyst in a fixed bed. The highest bulk density is that of a tapped fixed bed of catalyst, and the lowest density is that of loosely packed bed. To find these densities without performing experiments, the equations for the tapped voidage and the loosely packed voidage developed by Hoffman *et al.* [125] are used as follows:

$$\rho_{loosely-packed} = 0.584\rho_p\phi_p^{0.862}\left(1-\exp(-142\rho_p d_p)\right) \quad \textbf{(3-12)}$$

$$\rho_{tapped} = 0.68\rho_p\phi_p^{0.848}\left(1-\exp\left(-371\rho_p d_p\right)\right) \quad \textbf{(3-13)}$$

where $\rho_{loosely-packed}$ and ρ_{tapped} are the bulk densities of a loosely packed and tapped fixed bed of particles, respectively. Also, ϕ_p and d_p are the sphericity and diameter of the catalyst particles, respectively.

Another disparity between the model for the expansion of liquid-solid beds and gas-solid beds is the method of determining u_t'. In liquid-solid reactors, this value is equal to the terminal velocity, u_t, which is obtained with the Stokes equation as follows:

$$u_t = \frac{d_p^2 g\left(\rho_p - \rho_g\right)}{18\mu} \quad \textbf{(3-14)}$$

where g is the acceleration of gravity and μ is the viscosity of the gas. In gas-solid beds the following equation is applied to find u_t':

$$\frac{n}{4.65} = 1.26\left(\frac{u_t'}{u_t}\right)^{0.132} \quad \textbf{(3-15)}$$

The values of n and u_t' from Equations (3-11) and (3-15), respectively, are combined with Equation (3-10) to derive the void fraction of the bed.

Minimum Fluidization and Minimum Bubbling Velocities

To operate the fluidized bed reactor in a homogeneous phase, the velocity of the flow should be higher than the minimum fluidization velocity to exit the fixed state, and lower than the minimum bubbling velocity to avoid the formation of bubbles. These two velocities should therefore be obtained before performing additional calculations to ensure that the conditions under investigation in a simulation create particulate fluidization. Several correlations have been suggested to find the minimum fluidization velocity. In this study, some of these

correlations are presented and the results are compared with experimental data to find the suitable equation for the process under consideration.

The general equation used to determine the minimum fluidization velocity is derived by considering the fact that at the onset of fluidization the drag force caused by the gas flow, which is proportional to the pressure drop in the reactor, is equal to the weight of the particles. When the famous Ergun equation [126] for fixed beds is used to represent the pressure drop at incipient fluidization, this equation takes the following form:

$$\frac{1.75}{\phi_p \varepsilon_{mf}^3} \mathrm{Re}_{mf}^2 + \frac{150(1-\varepsilon_{mf})}{\phi_p^2 \varepsilon_{mf}^3} \mathrm{Re}_{mf} = \mathrm{Ar} \qquad \textbf{(3-16)}$$

where ε_{mf} and Re_{mf} are the void fraction and Reynolds number at minimum fluidization, respectively, and Ar is Archimedes number. Re_{mf} and Ar are defined as follow:

$$\mathrm{Re}_{mf} = \frac{d_p u_{mf} \rho_g}{\mu} \qquad \textbf{(3-17)}$$

$$\mathrm{Ar} = \frac{d_p^3 g \rho_g (\rho_p - \rho_g)}{\mu^2} \qquad \textbf{(3-18)}$$

where u_{mf} is the velocity at minimum fluidization. Several studies were performed to simplify Equation (3-16) and replace the terms containing sphericity and void fraction with experimental values that would yield acceptable results for different materials and flows. One form of equation resulting from these studies is as follows:

$$\mathrm{Re}_{mf}^2 + K_1 \mathrm{Re}_{mf} = K_2 \mathrm{Ar}$$

or $$\qquad \textbf{(3-19)}$$

$$\mathrm{Re}_{mf} = \sqrt{(K_1/2)^2 + K_2 \mathrm{Ar}} - K_1/2$$

where K_1 and K_2 are constant coefficients obtained by experiment. Several studies have been performed to determine these parameters [127-134], some of which are presented in Table

3-3. Equation (3-19) with the coefficients obtained by Wen and Yu [127] is one of the most accepted correlations for obtaining the minimum fluidization velocity.

Another correlation that is widely used to find the minimum fluidization velocity is the one proposed by Leva [87]. This equation was also developed by using the Ergun equation at the onset of fluidization. However, the first term in Equation (3-16) was considered negligible by assuming a low Reynolds number at the start of fluidization. Also, in contrast to the previous method where the term including the void fraction and sphericity was replaced by a constant value, Leva used experimental data to find this expression as a function of the Reynolds number. This equation can be rearranged to take the following form:

$$Re_{mf} = K_3 Ar^{K_4} \tag{3-20}$$

where K_3 and K_4 are constant parameters as observed in Table 3-3. This form of equation has been used in many studies with different values suggested for the coefficients K_3 and K_4 [135-138]. While Equation (3-21) with the constants suggested by Leva is one of the most widely used methods to find the minimum fluidization velocity, some more recent coefficients proposed for this method are also presented in Table 3-3.

Another method considered to find the minimum fluidization is the one developed by Xu *et al.* [139] in a more recent study. In this method, a correlation has been suggested for the minimum fluidization velocity where the effect of cohesiveness between the particles has been added to Equation (3-16):

Table 3-3: Values of coefficients K1, K2, K3, and K4 suggested by different authors for Equations (3-19) and (3-20).

Authors and References	$K_1/2$	K_2	K_3	K_4
Wen and Yu [127]	33.7	0.0408		
Grace [128]	27.2	0.0408		
Zhiping *et al.* [130]	22.1	0.0354		
Leva [87]			0.00108	0.94
Gauthier *et al.* [136]			0.0022	0.818
Subramani *et al.* [135]			0.00066	1

$$Re_{mf}^2 + \frac{85.71(1-\varepsilon_{mf})}{\phi_p} Re_{mf} = 0.57\varepsilon_{mf}^3 \phi_p Ar + 4.79\times10^{-9} \frac{\varepsilon_{mf}^{0.52}\phi_p d_p \rho_g}{L_0 \mu^2} \quad \textbf{(3-21)}$$

where L_0 is the height of the bed. The last term in this equation models the effect of the cohesiveness between particles.

The minimum fluidization velocity for the conditions of experiments performed by Dunker *et al.* [117] were obtained with Equations (3-16) and (3-19) to (3-21), with the constants presented in Table 3-3. The results are compared with the actual gas velocity in these experiments in Fig. 3-23. Since the experiments were performed in fluidized conditions, the velocity in all of the tests is higher than the minimum fluidization velocity. Therefore, the only equations that are suitable to be used for this reactor are those proposed by Wen and Yu [127], Leva [87], Subramani *et al.* [135]. In this study, the equation proposed by Leva [87] is used. Another observation from this figure is that the results obtained from Equation (3-16) with the complete form of the Ergun equation and the correlation proposed by Xu *et al.* [139] in Equation (3-21) are very close, which shows that the effect of cohesiveness between the particles is negligible in these conditions.

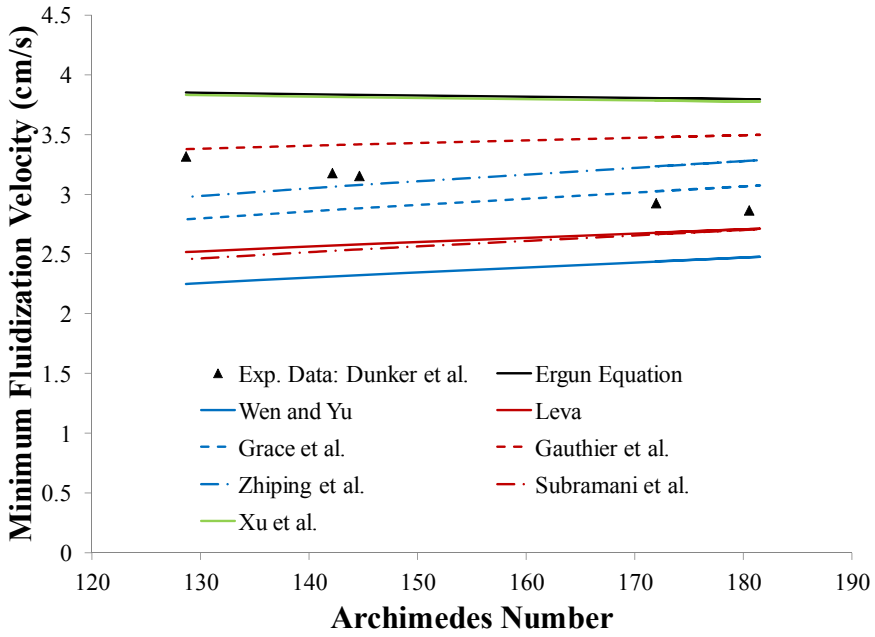

Fig. 3-23: Comparison of the minimum fluidization velocity obtained with different correlations and experiments of Dunker *et al.* [25].

For a particulate fluidization, the velocity of the gas should be smaller than the minimum bubbling velocity, which is calculated with the equation proposed by Abrahamsen and Geldart [140]:

$$u_{mb} = 2.07\exp(0.716F_{45})\frac{d_p\rho_g^{0.06}}{\mu^{0.347}} \quad \textbf{(3-22)}$$

where F_{45} is the mass fraction of particles with a diameter of less than 45 μm. This correlation is the most common method used to find the minimum bubbling velocity [141].

3.4. Summary

In this chapter, a detailed kinetic model was developed for the thermocatalytic decomposition of methane in a fluidized bed of carbon particles. The amount of hydrogen from the process was obtained by combining the production from the interaction of gas-phase species with each other, and the additional production due to the presence of the catalyst particles.

The kinetics of the homogeneous decomposition of methane, which represents the interaction of gas phase species, was modeled using a detailed reaction mechanism obtained with several combustion mechanisms. The most suitable mechanism was first selected as a base with available experimental data. Sensitivity analysis was then performed to determine the reactions having the highest effect in conditions under consideration. In the next step, the uncertain reactions were determined, and their appropriate rate constants were selected. As a result, a new mechanism with a higher accuracy was obtained. This mechanism can predict the amount of the main products of decomposition of methane reasonably well, and decreases the difference between experimental data and simulation results up to 15%.

After obtaining a suitable model for the homogeneous decomposition of methane, the effect of the catalyst was added with a surface reactions mechanism. The primary form of this mechanism comprises some reactions from a model for soot formation, and additional reactions added to reflect the distinction of the process of decomposition of methane. Further investigation resulted in the modification of a number of existing surface reactions to a more suitable form that represents the presence of the catalyst more accurately. The rates of the surface reactions were determined with two methods of analogy with gas phase reactions and

the kinetic method. Comparison of these two methods revealed that the former yields more accurate results with fewer simplifying assumptions and was therefore selected to be used in this model. The number of active sites on the surface of the catalyst was implemented in the model to account for the distinct activity of different catalysts that cannot be explained by considering the surface area alone. A method was presented to estimate the number density of these sites with the proposed model and experimental data. The initial value of this parameter was estimated for several carbon black catalysts using available experimental data. It is noted that due to the lack of experimental and theoretical information on the changes of the surface structure of carbon catalysts in a transient process, the developed model is only applicable to study the initial activity of the catalyst.

The hydrodynamics of the fluidized bed was also modeled to eliminate the dependency of the required inputs to experiments. For this purpose, the void fraction of the bed and the limits of the particulate regime were determined with available correlations.

The model presented in this chapter can be used to study the effect of different operating parameters, such as temperature, and different properties of the catalyst, such as the number of active sites, on the hydrogen yield from the process. This purpose is described in the next chapter.

Chapter 4
Results and Discussion

The model developed in the previous chapter is used to determine the effect of different factors on the performance of the decomposition of methane in a particulate fluidized bed. Considering that the aim of using this process is the production of hydrogen, the performance can be represented with either the percentage of hydrogen in the products or the methane conversion. In this study, methane conversion is more convenient for a consistent comparison between different effects. Generally, the changes observed in methane conversion are due to the combination of the variations of the reaction kinetics, and the hydrodynamic characteristics of the fluidized bed. The former occurs when a variable affects the rate of the reactions, while the latter is caused by changes in the minimum fluidization velocity and void fraction. The different factors that affect the conversion and are studied in this chapter are the temperature, fluidization state, and inlet gas composition as well as the properties of the catalyst, namely the particle size, particle pore volume, number of active sites, and the percentage of fine particles. A nominal value is attributed to each of these factors, and the variations in conversion caused by the changes of each factor in a certain range are investigated, while the other factors remain constant. The nominal values are those of a fluidized bed reactor operating at the onset of fluidization with a residence time of around 3 seconds. The inlet gas is pure methane at atmospheric pressure, and the temperature of the bed is 1250 K. The catalyst used in this reactor is the carbon black BP2000. As explained in the previous chapter, investigation is only performed on the initial activity of the catalyst.

Consequently, the number of active sites is calculated with Equation (3-7), and the specific surface area is 1337 cm^2/g [57, 62, 77]. The size of the catalyst particles is also an important factor. Although the primary particles of BP2000 are 15 nm, they aggregate into larger spherical particles of 0.5 to 1 mm [62, 142]. Therefore, an average diameter of 0.75 mm is used for these particles, which was obtained with the experimental data of Dunker *et al.* [117] and the fluidization regime charts of Kunii *et al.* [86]. The apparent density of 0.24 g/cm^3 is used, which has been obtained with Hg Porosimetry [35]. It is also noted that in cases where a mixture of methane and argon is used as the inlet gas, the viscosity of methane is determined with the equation and coefficients of Todd *et al.* [143] and the viscosity of Argon is derived with the method of Lemmon *et al.* [144].

In the following sections, the results of the investigation on the effect of different operating conditions and catalyst properties on methane conversion are presented. Most of the factors considered in this study affect the amount of residence time. Considering this fact and that the residence time is one of the main parameters contributing to the variations of conversion, the first section is dedicated to the effect of this factor as an individual variable, without any changes in other factors. This study is useful in explaining the trend of changes in the subsequent sections. It is noted that the variations of residence time with other factors are mostly due to the changes of the minimum fluidization velocity. Since the bed is operated at the particulate regime, the velocity should be controlled to maintain this assumption. This can be performed by applying changes to the inlet flow rate, and the size of the reactor. Several combinations of changes of these variables can result in the required regime. These combinations can be classified into different cases. The variations of residence times with the main factor are different in each of the cases, and consequently the conversion is affected too. In this study, the variations of conversion with each of the main factors are investigated in a number of these cases. The simultaneous effect of two factors in the most important case is then discussed. The conclusion derived from these results is discussed in the last section.

4.1. Residence Time

Residence time represents the average time that the inlet gas spends in the bed of catalyst. Many factors can affect the amount of this variable. In this section, the reactor is assumed to operate at the onset of fluidization, and other parameters such as the mass of the catalyst, the

volumetric flow rate of the inlet gas, and the size of the reactor regulate the residence time. Using a high residence time results in an increase in methane conversion as can be observed in Fig. 4-1, which is in accordance with the definition of this parameter. However, this figure also shows that the increase in conversion is higher at low residence times. At 1250 K, the increase in conversion obtained by increasing the residence time from 1 to 50 seconds is around 35%, 70% of which can be obtained in 10 seconds. The effect of different parameter on the variations of methane conversion with residence time is discussed in this section. It is noted that the properties of the catalyst are constant and the velocity at the onset of fluidization is employed unless stated otherwise.

Temperature

Variations of methane conversion with residence time at different temperatures are shown in Fig. 4-1. Methane conversion changes considerably with residence time at lower temperatures. However, this change reduces as the temperature increases, which is due to the proximity of the conversion at high temperatures with the equilibrium value. Changing the residence time from 1 second to 50 seconds increases the conversion 56% at 1100 K, and 19% at 1400 K. As a result, when lower temperatures are used changes in residence times,

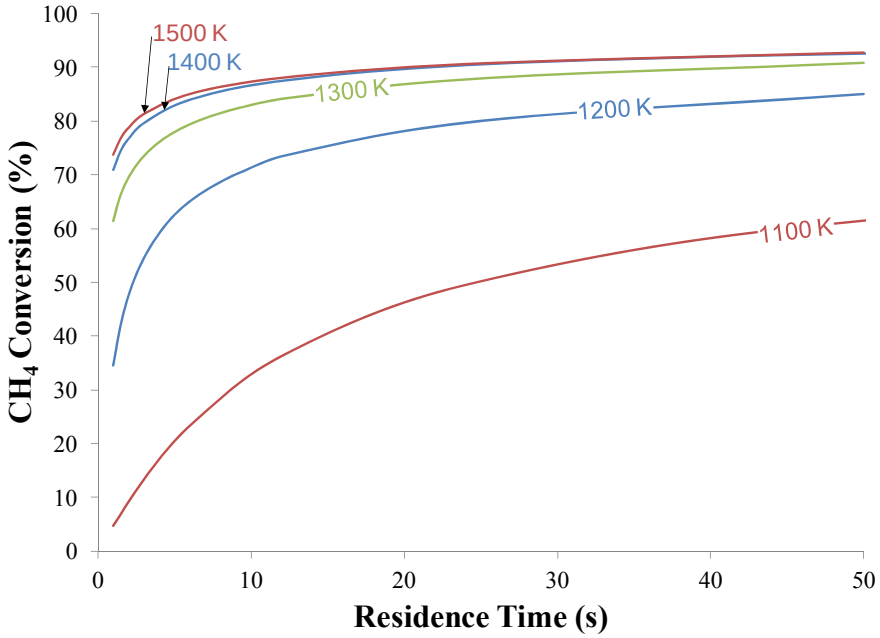

Fig. 4-1: Effect of temperature on the variations of methane conversion with residence time.

especially lower ones has a high impact on the conversion, while at higher temperatures the changes are much smaller.

Velocity

Increasing the velocity from minimum fluidization to minimum bubbling while maintaining the residence time constant does not affect the trend of variations and negligibly reduces the conversion by less than 1%. Changing the velocity from minimum fluidization to minimum bubbling conditions increases the residence time required to produce 80% and 90% conversion only around 1 and 3 seconds, respectively, which emphasises the small effect of velocity on the trend and amount of variation in conversion with residence time.

Gas Composition

The effect of decreasing the partial pressure of methane by adding the inert gas of argon and changing the feed gas composition is illustrated in Fig. 4-2. It is observed that when a conversion of less than 70% is intended, changing the gas composition does not have an appreciable effect on the residence time required. However, the residence time for producing higher amounts of conversion is considerably decreased when argon is added to the feed gas,

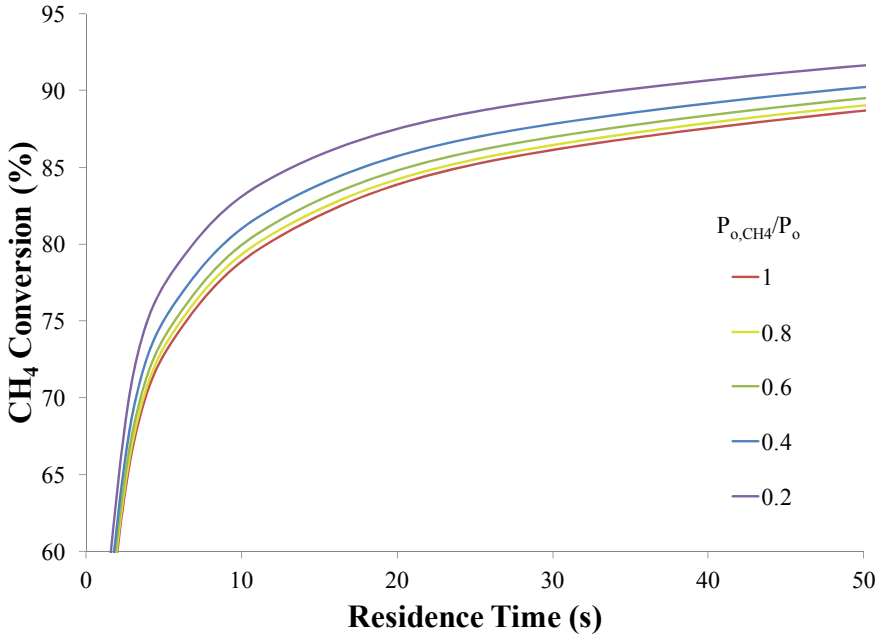

Fig. 4-2: Effect of feed gas composition on the variations of methane conversion with residence time.

and the difference between the residence time required with different feed gas compositions becomes larger as higher values are aimed for the conversion. These results are similar to those obtained by Ozalp *et al.* [31]. For example, the decrease of residence time required to obtain a conversion of 80% when 20% of the flow is comprised of methane is 5 seconds and this value increases to more than 30 seconds for a conversion of 90%.

Catalyst Size

Fig. 4-3 shows the variation of conversion with residence time with different catalyst particle sizes. It is observed that the rate of conversion change is similar for different sizes at high residence time. On the other hand, when lower residence times are used, the change of conversion occurs with higher rates for larger particles. As a result, the residence time required to produce a specific conversion considerably increases when smaller particles are used, especially when the aimed conversion is higher than 60%. For example, the residence time required to produce 80% conversion decreases by 15 seconds when the particle diameter is increased from 0.02 to 0.075 cm. It is also noted that using catalysts with particles diameters equal to or larger than 0.075 cm results in very close conversion values. The trend observed in Fig. 4-3 is due to the changes of void fraction explained in section 4.5.

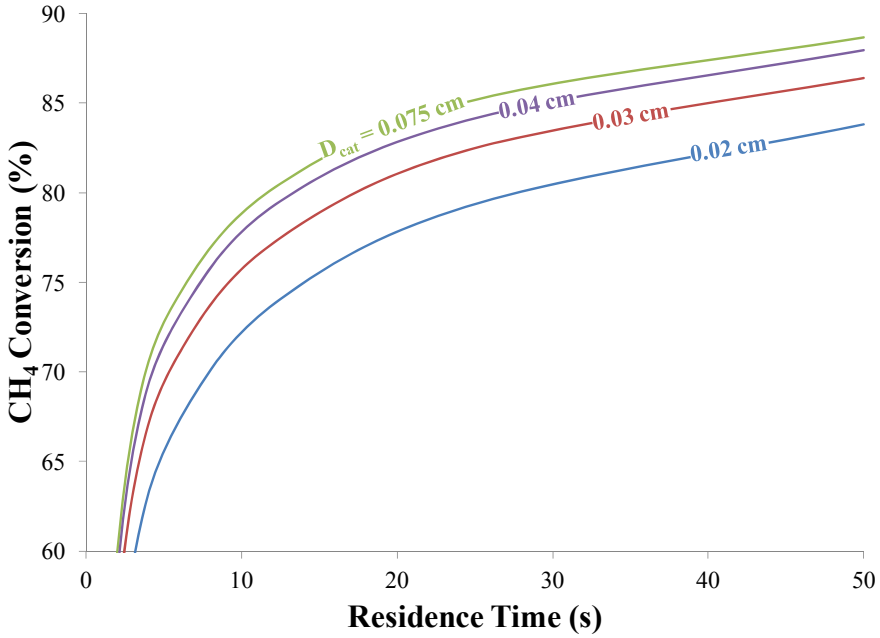

Fig. 4-3: Effect of particle size on the variations of methane conversion with residence time.

Pore volume

The changes of conversion with residence time when particles with different pore volumes are used are shown in Fig. 4-4. It is observed that the residence time required to obtain a certain amount of conversion increases with the pore volume. The trend observed in this figure is due to the additional mass of catalyst required in a reactor with constant residence time when the pore volume is decreased. This will be discussed further in section 4.6. As an example, a bed of particles with the smallest pore volume used in this investigation can produce a conversion of 80% with a residence time of 7 seconds, while a residence time of more than 20 seconds provides this conversion with the highest pore volume.

Number of Active Sites

The effect of the number of active surface sites on the changes of conversion with residence is observed in Fig. 4-5. This figure shows that although the trend of variation of conversion is very similar with all the specific surface areas, the rate of increase of conversion in short residence times is higher when a catalyst with a small number of active sites is used. Consequently, the residence time required to achieve a specific conversion is considerably

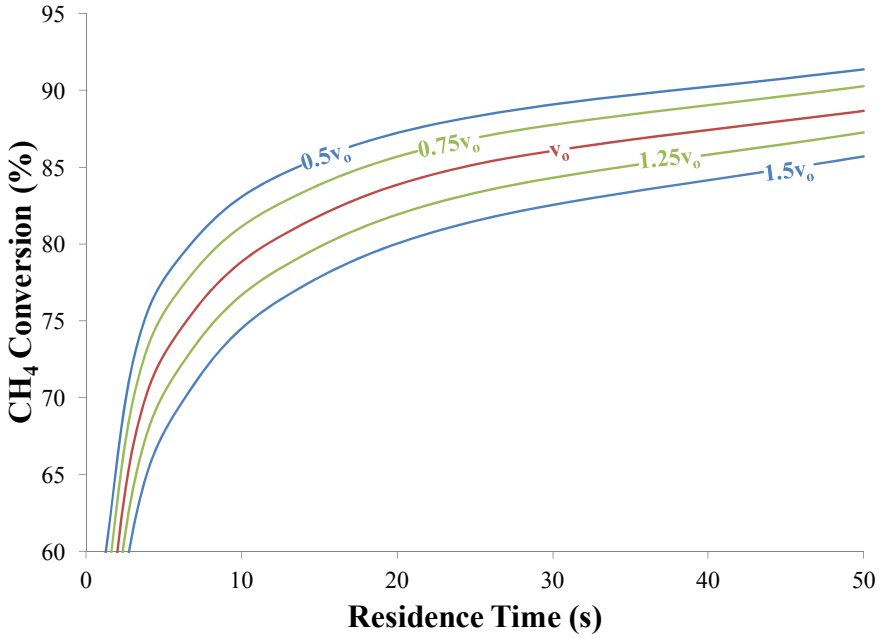

Fig. 4-4: Effect of particle pore volume on the variations of methane conversion with residence time.

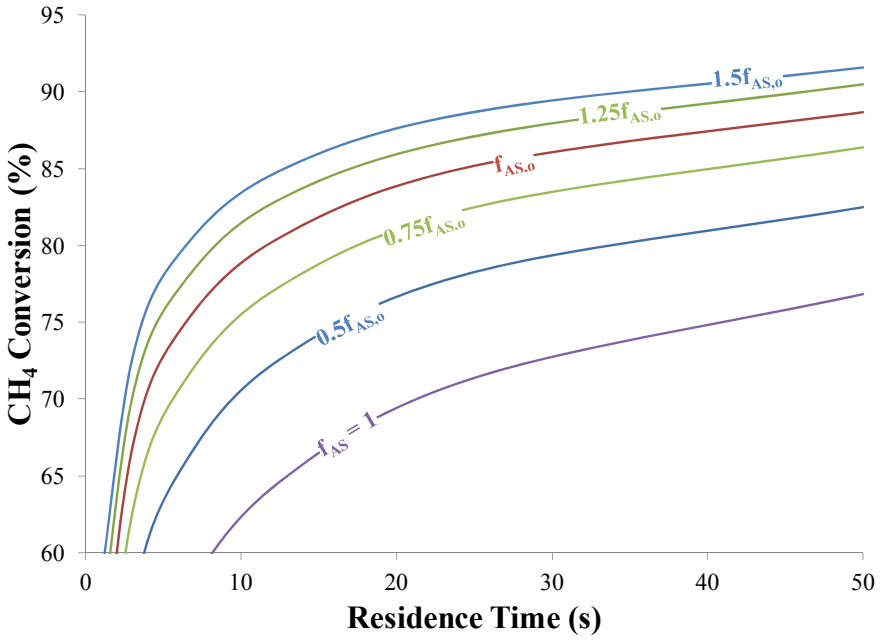

Fig. 4-5: Effect of the number density of active sites of catalyst on the variations of methane conversion with residence time.

smaller with a large number of active sites. For example, the residence time necessary for converting 80% of the inlet methane decreases around 25 seconds when the number of active sites of the original catalyst is increased by 50%. The trend observed is due to the increase the probability of surface reactions with the number of surface sites.

Fine Particles

The variations of conversion with residence time with different amounts of fines in the catalyst bed are presented in Fig. 4-6. It is observed from this figure that the rate of conversion change relative to low residence times decreases with the percentage of fines. On the other hand, at larger residence time this rate remains closely the same. This causes the residence time required to produce a specific conversion to increase with the addition of fines, especially when a large conversion is aimed. As a sample, when a conversion of 80% is required, the residence time should be increased around 20 seconds when 20% of fines are present in the catalyst bed. This trend will be explained in section 4.8.

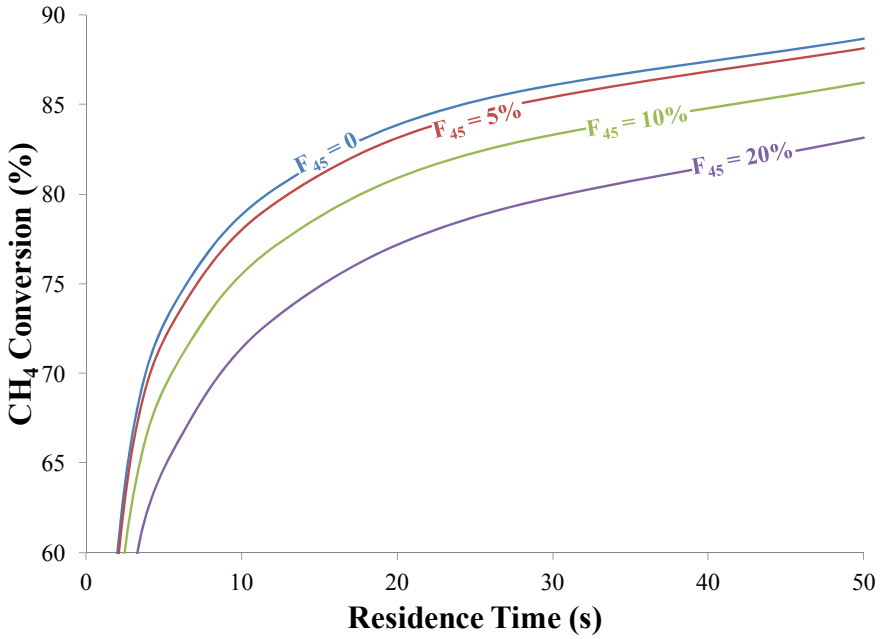

Fig. 4-6: Effect of the addition of fines on the variations of methane conversion with residence time.

4.2. Temperature

Changing the temperature affects the rate of gas phase and surface reactions, and therefore causes variations in the conversion of methane. In addition to the effect of temperature on the kinetics of the process, it also influences the minimum fluidization and minimum bubbling velocities, mainly due to its effect on the gas viscosity. Since the reactor is to operate in the particulate regime, and preferably at the onset of fluidization, the temperature affects the residence time, which causes further changes in the conversion. To regulate the velocity and satisfy the criteria of the regime, a variable reactor size or gas flow rate is used with a specific catalyst. Since the changes in these variables affect the extent of the variations of residence time with temperature, the degree of these changes should be specified before determining the effect of temperature on conversion. Four different cases are investigated for the variations of residence time with temperature considering the changes of these variables. In the first case, the effect of a constant residence time is investigated while the reactor operates at the onset of fluidization. In cases 2 and 3, a constant normal inlet flow rate is considered, which is obtained by either changing the reactor size and maintaining minimum fluidization conditions, or by allowing higher velocities in a specific reactor size,

respectively. The residence time in different temperatures is determined as follows for these two cases:

$$\tau_{T2} = \frac{\tau_{T1} T_1 (1-\varepsilon_1)}{T_2 (1-\varepsilon_2)} \quad \textbf{(4-1)}$$

In case 4, the inlet flow rate is changed to maintain the minimum fluidization velocity in a specific reactor, with a varying residence time calculated as follows:

$$\tau_{T2} = \frac{\tau_{T1} u_{mf1} T_1 (1-\varepsilon_{mf1})}{u_{mf2} T_2 (1-\varepsilon_{mf2})} \quad \textbf{(4-2)}$$

The variations of the methane conversion with temperature have been investigated in these four cases. The results show that the amount and the trend of variations of methane conversion are very close in all the cases, with up to 3% difference in the conditions used in this study. This is due to the fact that while the residence time in these cases differ somewhat, the resulting changes are negligible compared to those caused by the variations of temperature. Consequently, only the variations of conversion with a constant residence time will be investigated in this section.

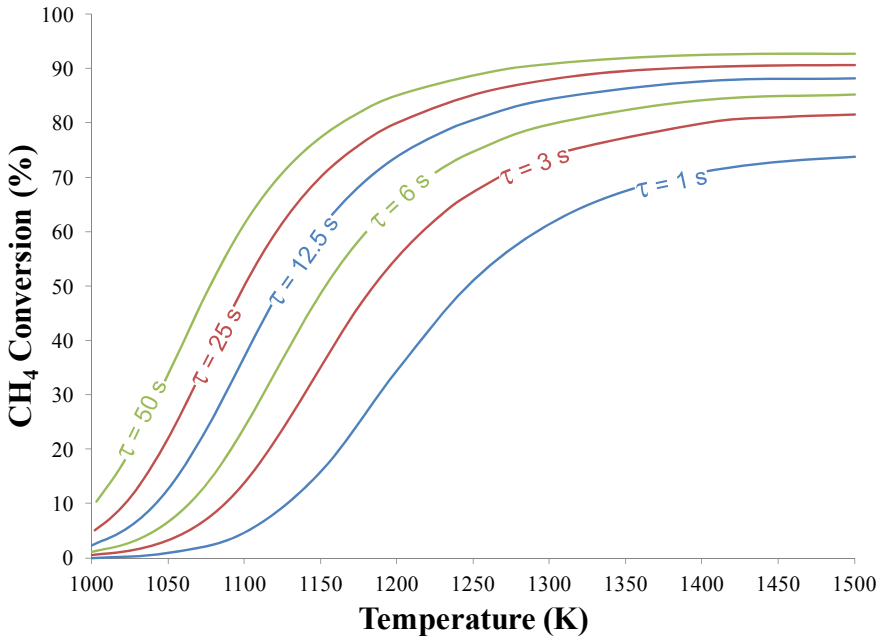

Fig. 4-7: Effect of residence time on the variations of methane conversion with temperature.

The general trend of variations of conversion with temperature can be observed in Fig. 4-7. Temperature has a small effect at lower and higher temperatures, while a significant change occurs in the conversion in a certain range of temperature. As an example, with a residence time of around 3 seconds, a 57% increase is observed in conversion between 1050 K and 1250 K. The effect of different factors on the extent of this change and the temperature at which it occurs follows.

Fig. 4-7 also shows the effect of temperature on methane conversion in different residence times. It is observed that the temperature range at which the methane conversion increases considerably and the amount of this increase are different for each residence time. As higher residence times are used, this range tends to move toward lower temperatures, and its value increases. The main change in methane conversion at a residence time of 1 second occurs between 1150 and 1350 K with a raise of 55%, while it increases 67% between 1000 and 1150 K at 50 seconds.

Velocity

The effect of increasing the velocity on the variations of conversion with temperature in a

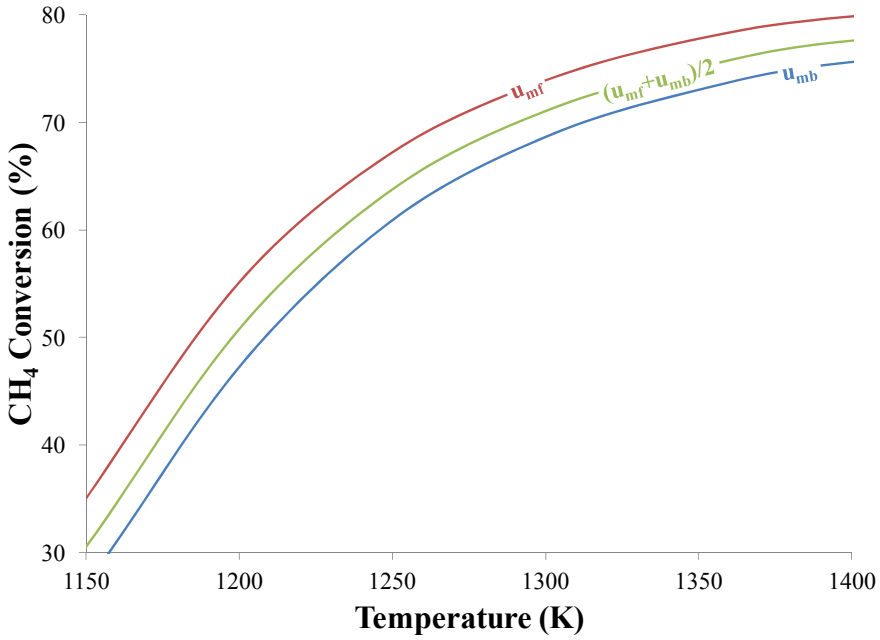

Fig. 4-8: Effect of velocity change with inlet flow rate on the variations of methane conversion with temperature.

specific reactor is investigated in Fig. 4-8. The velocity is changed from minimum fluidization to minimum bubbling conditions by increasing the inlet flow rate. This figure shows that the rate of change in conversion with temperature and its trend are not affected by the velocity. However, the high increase in conversion occurs at lower temperatures with lower velocities. for example, in order to obtain a conversion of 75% a temperature of 1400 K is required with the minimum bubbling velocity while with the minimum fluidization velocity, this conversion occurs at around 1310 K. Since the residence time is lower at the onset of fluidization, the increase in conversion in these conditions occur at a lower temperature than the conditions of minimum bubbling, as explained in the results of Fig. 4-7.

Gas Composition

The effect of the inlet gas composition on the variations of conversion with temperature is investigated by assuming that the residence time remains constant with temperature change, while the addition of argon is considered to affect the residence time with a change in inlet flow rate, as explained in section 4.4. It is observed from results shown in Fig. 4-9 that although the trend of the variations of conversion with temperature is roughly similar with different inlet gas compositions, decreasing the partial pressure of methane slightly increases

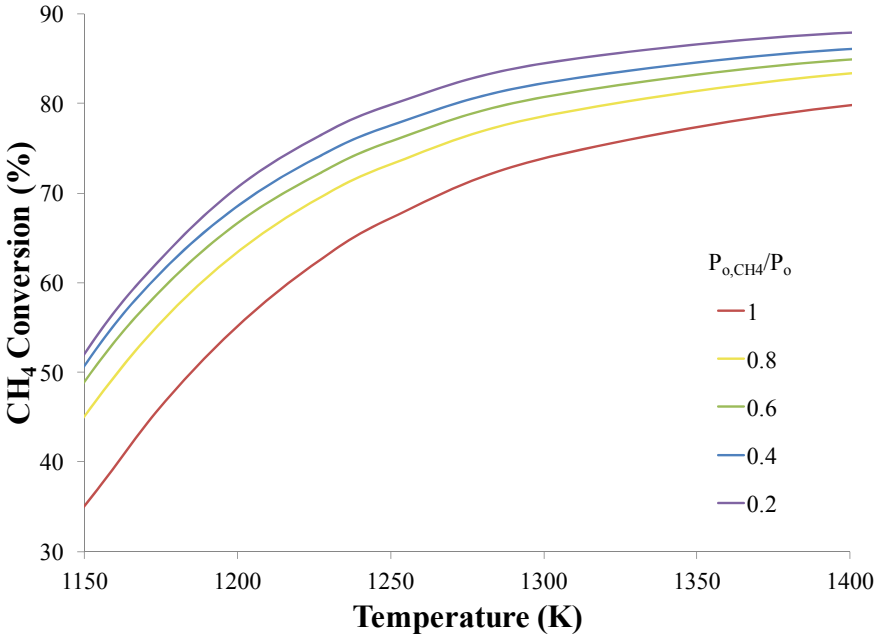

Fig. 4-9: Effect of inlet gas composition on the variations of methane conversion with temperature.

the rate of variations at lower temperatures. Therefore, the conversion approaches its maximum value at lower temperatures when argon is present. For example, 90% of the final conversion is achieved at around 1300 K when pure methane is used, and at 1250 K when the flow is composed of 80% argon.

Catalyst Size

Fig. 4-10 shows the variations of methane conversion with different catalyst sizes. It is observed that when smaller particles are used in the process, the sharp increase of methane conversion shifts toward lower temperatures. As a result, a much higher conversion is attained at lower temperatures when small particles are used. For example, when small particles of 0.025 cm diameter are used, 90% of the final conversion is reached at around 1200 K, while larger particles with a diameter of 0.125 cm reach this value at a temperature higher than 1300 K. This trend is due to the considerably high residence time of small particles, due to the reduction in minimum fluidization velocity, and the discussion following Fig. 4-7.

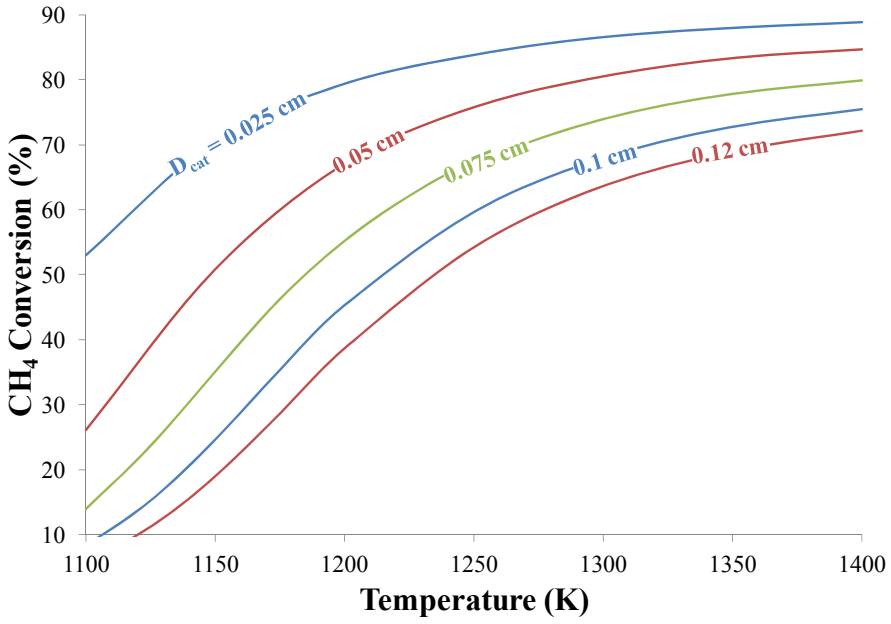

Fig. 4-10: Effect of particle size on the variations of methane conversion with temperature.

Pore volume

Fig. 4-11 shows the variations of conversion with temperature when different catalyst pore volumes are used. This figure shows that as the pore volume increases, the high rate of conversion change shifts towards lower temperatures. For example, when a particle with the lowest pore volume investigated in this study is used, 90% of the maximum conversion is obtained at a temperature of 1325 K, while a particle with the highest pore volume reaches this conversion at around 1275 K. Using particles with higher pore volume decreases the minimum fluidization velocity, and therefore increases the residence time. Therefore, according to results of Fig. 4-7, the highly porous particles to reach a higher conversion at a lower temperature. It is noted that the graph of the particle with the smallest pore volume stops at a temperature of 1200 K since bubbling occurs for this particle at lower temperatures.

Number of Active Sites

Fig. 4-12 shows the variations of conversion with temperature when particles with different number of active sites are used. It is observed that the trend of variations is similar with

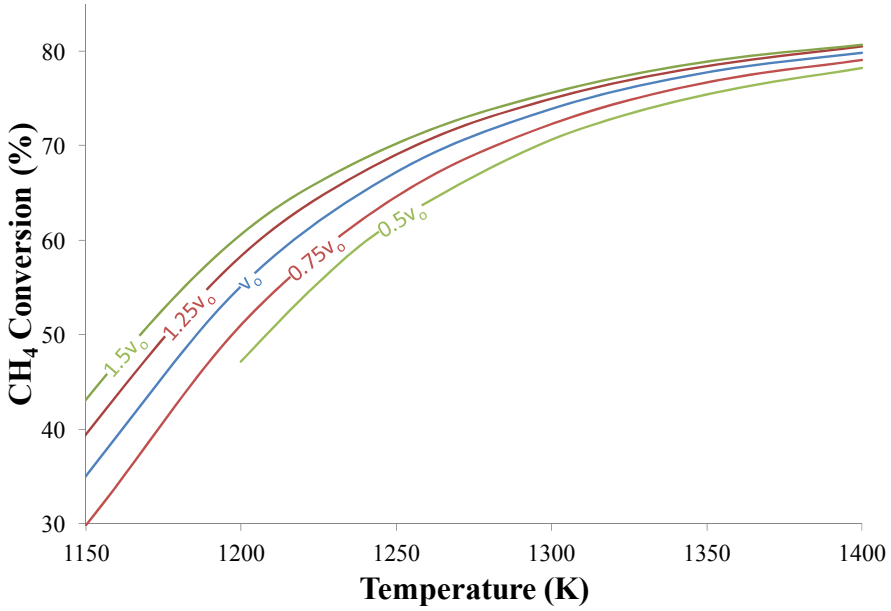

Fig. 4-11: Effect of particle pore volume on the variations of methane conversion with temperature.

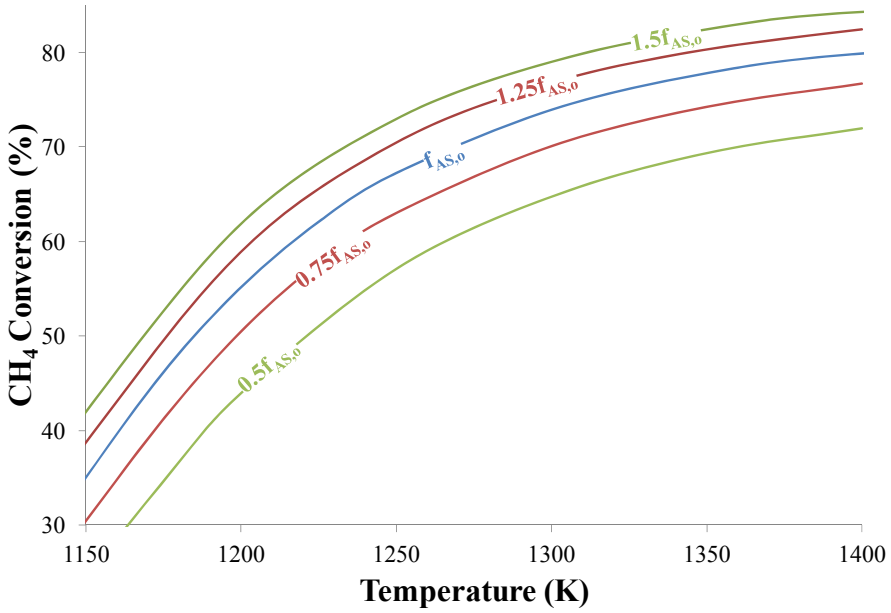

Fig. 4-12: Effect of number of active surface sites of particles on the variations of methane conversion with temperature.

different number of active sites. However, when a larger number of active sites are available, the major variation in conversion takes place at lower temperatures.

The temperature required to reach 90% of the final conversion decreases by 50 K when the number of surface sites is increased between the limits shown in Fig. 4-12. This is due to the higher reaction rate resulting from a high number of active sites.

Fine Particles

The changes of conversion with temperature when different amounts of fine particles of 45 μm are added to the bed are shown in Fig. 4-13. It is observed from this figure that similar to the use of small particles, the addition of fines causes the sharp increase of conversion to occur at lower temperature. At the conditions used in Fig. 4-13, 90% of the final value is originally obtained at 1275 K, while when 20% of fine particles of 45 μm are added, this temperature reduces to 1175 K. This is caused by the high residence time associated with larger amounts of fines, which results from the decrease of the minimum fluidization.

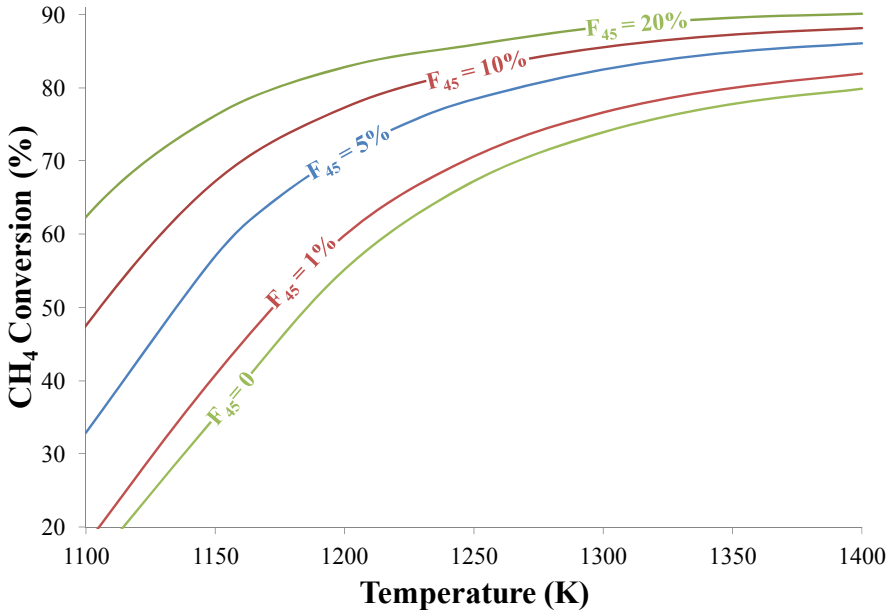

Fig. 4-13: Effect of the addition of fines on the variations of methane conversion with temperature.

4.3. Velocity

The effect of changing the velocity between the minimum fluidization and the minimum bubbling conditions is investigated in this section. Variations in the velocity can be generally made by changing either the geometry of the reactor or the gas flow rate. Since the variations of velocity affect the residence time, similar to the investigation performed on the effect of temperature, changes in residence time should be investigated prior to methane conversion. The cases investigated in this section are similar to those studies in section 4.2, with the exception of the case where the flow rate and reactor size are constant, since it results in a specific amount for the velocity and is not applicable here. In case 1, changing the velocity with a constant residence time does not cause any appreciable change in the conversion. Calculations show that the variation of the velocity in this limit only causes a very small increase in the void fraction. Since the kinetics of the process is not affected in any other way, the effect of this slight change of voidage on the conversion is negligible. When the properties and characteristics of the catalyst remain unchanged, variations of the reactor size with a constant flow rate, case 2, causes a varying residence time which is obtained as follows:

$$\tau_u = \frac{\tau_{mf}(1-\varepsilon_{mf})}{1-\varepsilon_u} \quad \textbf{(4-3)}$$

Since the changes in void fraction due to velocity change between the limits of minimum fluidization and bubbling are small, the variation of residence time in this case is generally insignificant. Consequently, the conversion obtained in cases 1 and 2 are very close and approximately unaffected by the change in velocity.

On the other hand, in the last case where the flow rate is altered, the changes in residence time are more prominent and can be calculated with the following equation.

$$\tau_u = \frac{\tau_{mf} u_{mf}(1-\varepsilon_{mf})}{u(1-\varepsilon)} \quad \textbf{(4-4)}$$

This equation shows that, since changes in the void fraction are generally much smaller than the velocity, in most cases, the residence time is almost inversely proportional to the velocity. Therefore an increase in the flow rate and velocity would cause the residence time to decrease, which in turn noticeably reduces methane conversion, as observed in Fig. 4-14. Although the largest changes in conversion occur while using a variable inlet flow rate, these variations are very small in the nominal conditions. Nonetheless, the effect of different operating variables and catalyst properties on this value in case 4 is presented in this section to investigate if these factors can change the significance of the variations.

Temperature

It is observed in Fig. 4-8 that increasing the temperature reduces the relative amount of the decrease of conversion with velocity. An increase in temperature from 1150 to 1350 K reduces the amount of decrease from 22 to 6% point. It is noted that the minimum fluidization and minimum bubbling velocities only slightly decrease when higher temperatures are used. Since the variations of void fraction are also negligible, according to Equation (4-4), the total change in residence time is almost constant at different temperature. As discussed in section 4.1, residence time has a smaller effect on conversion at higher temperatures, which explains the trend observed.

Gas Composition

Fig. 4-14 shows the impact of using different mixtures of methane and argon as the inlet gas. While increasing the velocity form minimum fluidization to minimum bubbling reduces the conversion only by 9% point with a flow of pure methane, mixing the feed gas with 20% argon causes a 14% point decrease. It is noted that increasing the argon content from 20% to 80% only increases the reduction in conversion by 2%. This trend of increase in the reduction can mainly be attributed to the expansion of the limits of fluidization and the difference between the two limiting velocities due to the decrease in Archimedes number. This difference between the limiting velocities considerably increases when a small amount of argon is added to the inlet gas, while it becomes almost constant with larger amounts of argon. This phenomenon occurs due to the trend of changes in the viscosity of the inlet gas with the addition of argon, which has a high viscosity relative to methane. It is also mentioned that the change of feed gas composition considerably changes the minimum fluidization and minimum bubbling velocities with small amounts of argon, while these velocities become approximately constant with larger amounts of the inert gas.

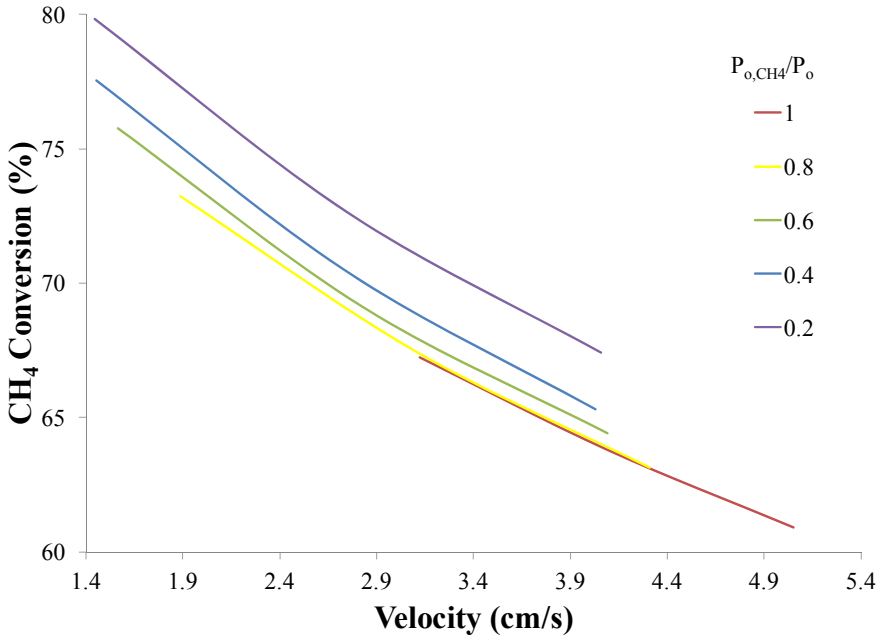

Fig. 4-14: Effect of feed gas composition on the variations of methane conversion with velocity.

Catalyst Size

Variations of the catalyst size significantly affect the minimum fluidization and minimum bubbling velocities, as observed in Fig. 4-15. Small diameters are associated with lower fluidization, and therefore have a higher residence time. Fig. 4-3 shows that changes in conversion are more considerable at low residence times when similar changes are applied. However, the difference between the minimum bubbling and minimum fluidization velocities is much higher for small particles, and results in a very large change in residence time according to Equation (4-4). Consequently, as observed in Fig. 4-15, the decrease in conversion with velocity is higher for small particles, with a maximum decrease of 14% point for the smallest particle considered in this study.

Pore volume

The pore volume of the catalyst particle affects its apparent density, and therefore changes the minimum fluidization velocity. However, Equation (3-22) and experimental studies [145] show that these changes do not affect the minimum bubbling velocity. Therefore, using particles with higher pore volume increases the difference between the velocities at the onset

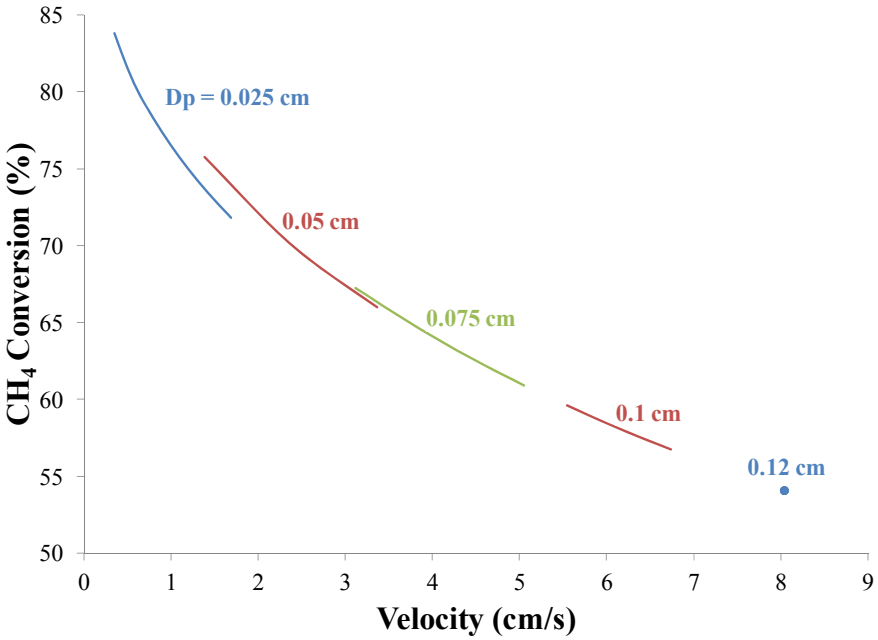

Fig. 4-15: Effect of the particle size on the variations of methane conversion with velocity.

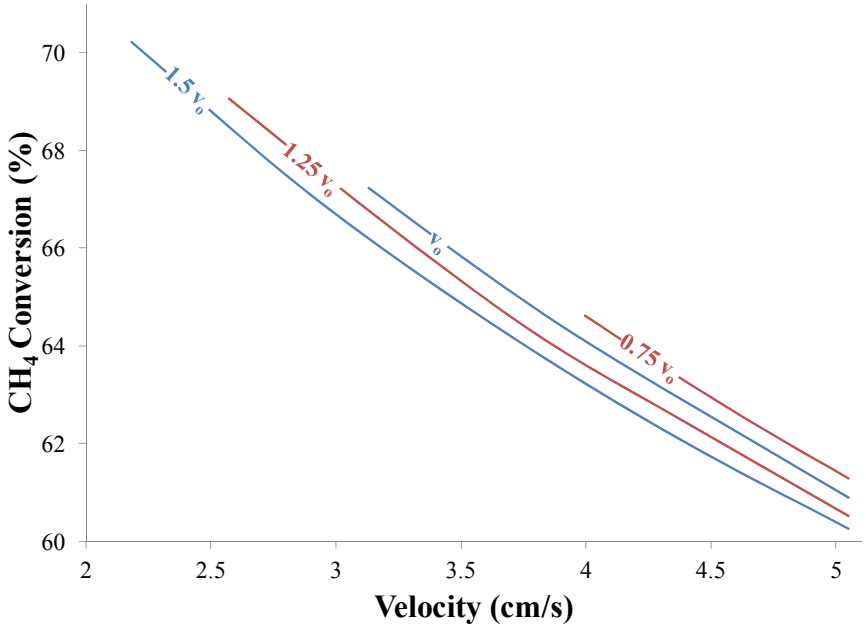

Fig. 4-16: Effect of particle pore volume on the variations of methane conversion with velocity.

of fluidization and bubbling, as observed in Fig. 4-16. The changes of conversion in a specific pore volume are mainly due to changes of residence time with velocity. Since the variations of void fraction are small, the residence time is inversely proportional with the velocity. Consequently, increasing the pore volume of the particle causes larger changes in the conversion, as illustrated in Fig. 4-16. This figure also shows that the rate of change of conversion with velocity is almost the same with different pore volumes.

Number of Active Sites

Fig. 4-17 shows the variations of conversion with velocity when catalyst particles with different number of active sites are used. It is observed that the decrease of conversion caused by a rise in velocity is slightly reduced when the particles have a larger number of active sites. The change of conversion from minimum fluidization to minimum bubbling velocity is around 12% point when half of the nominal number of active sites are considered, and decreases to 8% point when the nominal value is increased by 50%. It is noted that the variation of the number of active sites alone does not affect the dynamics of the particles; therefore, the void fraction, residence time and velocities at minimum fluidization and minimum bubbling conditions remain unchanged.

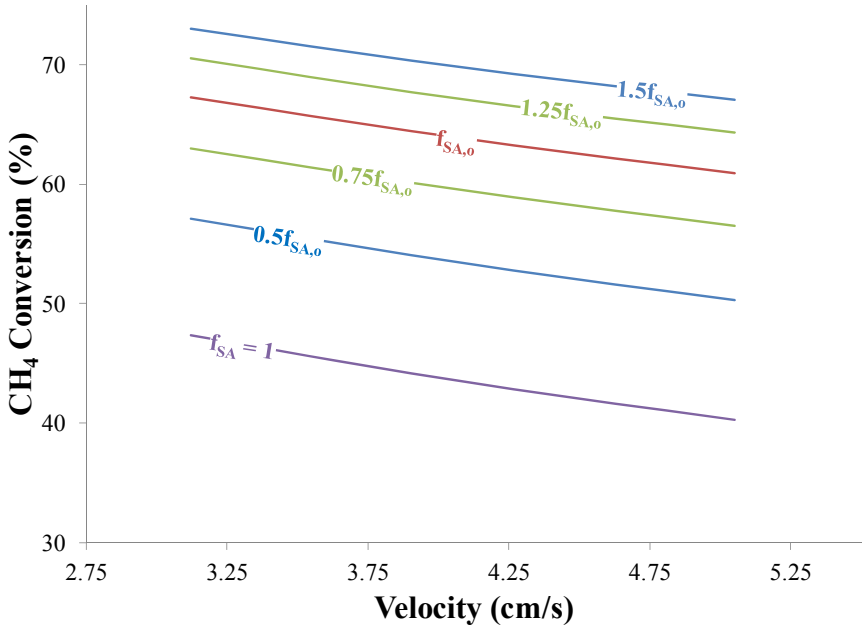

Fig. 4-17: Effect of number density of active surface sites of the particle on the variations of methane conversion with velocity.

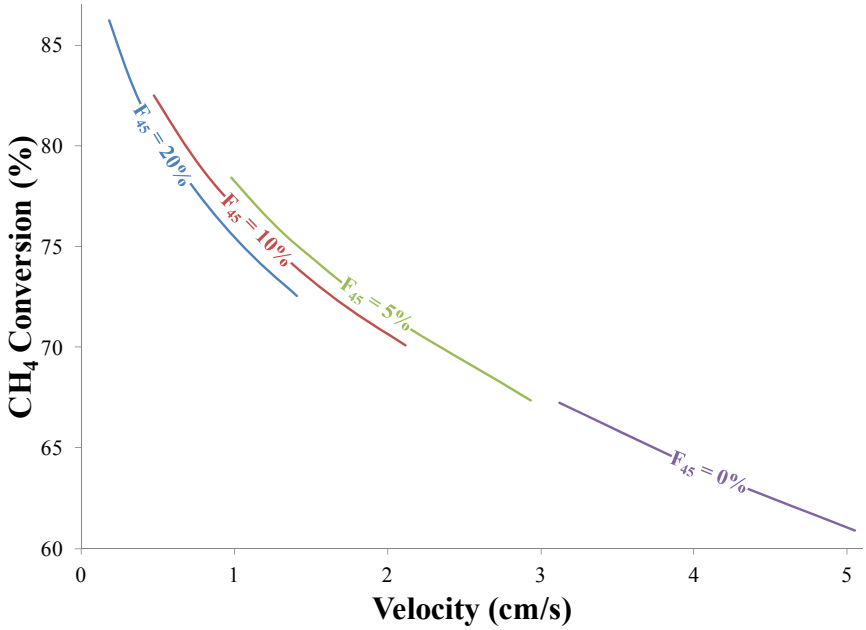

Fig. 4-18: Effect of the addition of fines on the variations of methane conversion with velocity.

Fine Particles

Fig. 4-18 shows the changes of conversion with velocity when different amounts of fine particles are present in the bed. It is observed that the variations of conversion are significantly higher when larger amounts of fines are used. For example, a velocity between the minimum fluidization and minimum bubbling conditions changes the conversion by 9% at nominal conditions, while this amount increases to 16% with 20% fines. Calculations show that the ratio of the minimum bubbling to minimum fluidization velocities is much higher when fines are added to the bed. According to Equation (4-4), the residence time also experiences larger changes, causing higher variations in the conversion.

4.4. Inlet Gas Composition

Observation on the reaction of methane decomposition reveals that, according to LeChatelier's principle, decreasing the pressure improves methane conversion. Since the effect of adding or increasing the amount of an inert gas in a reacting mixture is similar to decreasing the pressure of the reaction [146], the effect of adding argon to the feed gas is investigated in this section. It is noted that the additional cost of separation of argon from the outlet gas should be considered in the evaluation of this factor. In addition to decreasing the partial pressure of methane, the composition of the feed gas also affects the behavior of the fluidized bed. When argon is added to the inlet stream of a certain reactor with specific operating parameter, its relative high viscosity compared to methane causes a decrease in the fluidization velocity and therefore affects the conversion. In this section, the effect of adding different percentages of argon to the inlet methane gas is investigated. The properties of the catalyst are considered to be independent of the gas compositions; however, the minimum fluidization and minimum bubbling velocities considerably vary due to changes in the gas viscosity, and affect the residence time. The four cases discussed in section 4.2 for the variations of residence time are considered.

In case 1, where the residence time is constant, introducing argon causes an increase in methane conversion, due to its effect on the kinetics of the process. It can also be concluded from the results of Fig. 4-2 that using higher residence times reduces these variations. The

increase in conversion with a residence time of 1 second is around 10% point, while this value reduces to 5% point with a residence time of 50 seconds.

In cases 2 and 3, the inlet flow rate is constant and the variable residence time is calculated as follows:

$$\tau_{comp2} = \frac{\tau_{compl}(1-\varepsilon_1)}{1-\varepsilon_2} \quad \textbf{(4-5)}$$

Calculations show that in case 2, where minimum fluidization conditions are sustained, the change of void fraction is negligible and the residence time remains almost constant. Therefore, the amount of methane conversion with different inlet gas composition is the same in cases 1 and 2. In case 3, where the inlet flow rate and reactor size are kept constant, the addition of argon will decrease the minimum fluidization velocity and the velocity used will therefore be higher than the minimum fluidization condition. As a result, the void fraction and residence time slightly increase, and variations of methane conversion are somewhat lower than the two previous cases.

In case 4, the inlet flow rate is changed to maintain the minimum fluidization velocity in a certain reactor, with a variable residence time calculated as follows:

$$\tau_{comp2} = \frac{\tau_{compl} u_{mf1}(1-\varepsilon_{mf1})}{u_{mf2}(1-\varepsilon_{mf2})} \quad \textbf{(4-6)}$$

As noted earlier, changes in void fraction with the inlet gas composition are negligible. Therefore, since the minimum fluidization decreases with the insertion of argon, a much higher residence time is obtained. In this case, the effect of velocity change on the conversion is the result of the combination of the increase in residence time and the effect of the decrease of methane partial pressure on the kinetics of the reaction. In the nominal conditions, the addition of 90% argon to the inlet gas in case 4 increases the methane conversion by 15%.

It can be concluded that the addition of argon positively affects methane conversion in all cases, with case 4 having the highest impact. In this section, the effect of different parameters on the variations of conversion with the insertion of up to 90% argon in the inlet flow is investigated for this case.

Temperature

The effect of temperature on the variations of methane conversion with insertion of argon to the inlet flow can be observed from Fig. 4-9. This Figure shows that methane conversion increases by adding argon to the inlet flow at all temperatures. However, the effect of lower temperatures is more prominent. At a low temperature of 1150 K, the addition of 90% argon increases the conversion by around 50% point, while at a higher temperature of 1350 K this increase is only 15% point. Calculations show that changing the temperature does not affect the void fraction, and has a negligible effect on the changes of minimum fluidization with inlet gas composition. Therefore, the residence time with a specific amount of argon in the inlet gas is approximately unaffected by temperature change and the residence time change in different temperatures is approximately similar. The trend observed in Fig. 4-9 can be explained by the fact that the variations of residence time at low temperature have a larger effect on the conversion. It is also observed that the rate of conversion increase at each temperature is higher when small amount of argon is added.

Velocity

The changes of methane conversion with feed gas composition at different velocities can be observed from Fig. 4-14. The minimum fluidization velocity is more dependent on the viscosity of the flow than the minimum bubbling velocity. Since argon has a high viscosity compared to methane, the viscosity of the flow instantly increases with the addition of small amounts of argon, and as the amount of argon is increased, the rate of increase of viscosity reduces until the viscosity of argon is finally reached. Therefore, adding small amounts of argon to the feed gas considerably decreases the minimum fluidization velocity, while it has a smaller effect on the minimum bubbling velocity. These changes in the minimum fluidization and bubbling velocities create an equivalent increase in residence time, which in turn causes an augmentation in the conversion. It is observed that at minimum fluidization, the insertion of small amounts of argon considerably affects the conversion; however at higher velocities this effect is less prominent. As an example, in the case studied in Fig. 4-14, inserting 90% argon in the feed flow increases the conversion at onset of fluidization and bubbling by 9 and 3.5% point, respectively. Since the variations of the minimum and bubbling velocities become less prominent when large amounts of argon are added to the

feed gas, the increase of conversion in these conditions is mainly caused due to the effect of the change of methane partial pressure on the kinetics. As a result, the rate of change of conversion in these conditions is similar for all the velocity range.

Catalyst Size

The variations of methane conversion with the feed gas composition using different particle diameters are shown in Fig. 4-19. As discussed earlier, the increase in residence time caused by the insertion of argon results in higher conversions. Also, the residence time increases when using small particles, due to the decrease in minimum fluidization velocity. According to the results of Fig. 4-3, the changes in conversion with residence time are much faster at low residence times. Therefore, a higher increase in conversion occurs when larger particles are used, which is observed in Fig. 4-19. With a catalyst size of 0.12 cm the addition of 90% argon creates a conversion change of more than 30% point, while using a smaller particle with a diameter of 0.025 cm causes a 9% point change.

Pore volume

The change of conversion with the addition of argon to the inlet gas when particles with different pore volumes are used is shown in Fig. 4-20. Observation can be made that the

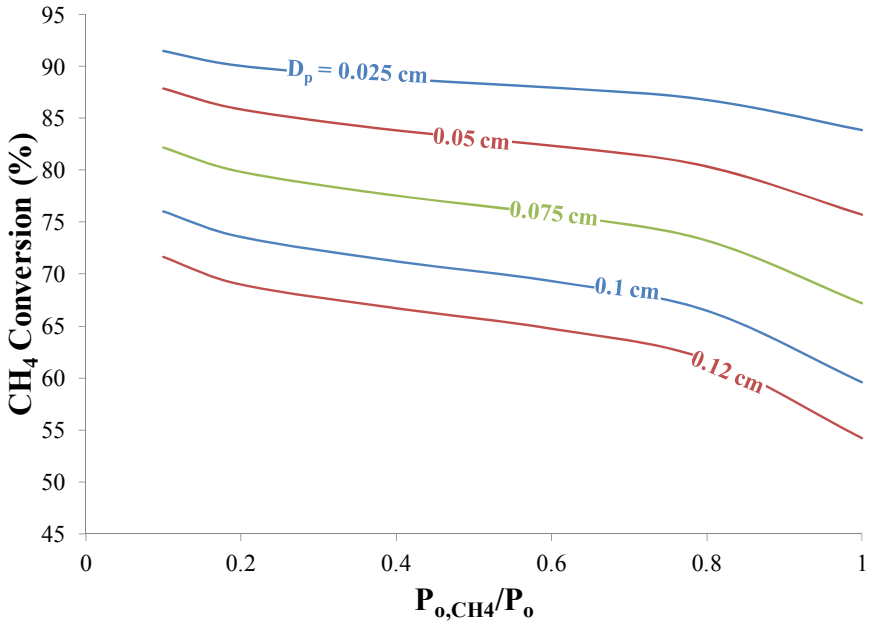

Fig. 4-19: Effect of particle size on the variations of methane conversion with insertion of argon.

effect of the feed gas composition is reduced when particles with higher pore volumes are used. The change in conversion due to replacing 90% of the feed gas with argon is around 28% point when half of the nominal pore volume is used, while this value decreases to 18% point when the pore volume is increased by 50%. The increase in conversion with the addition of argon is due to the combined effect of decrease of methane partial pressure and increase of residence time. While the use of larger pore volumes does not affect the former, it lowers the minimum fluidization velocity, which results in a larger residence time. According to Fig. 4-4, the variations of conversion are more prominent with smaller residence times which explains the trend observed in Fig. 4-20.

Number of Active Sites

The change of conversion with feed gas composition when catalyst particles with different number of active sites are used is shown in Fig. 4-21. It is observed that using larger specific surface areas lowers the increase of conversion due to the addition of argon. The increase of conversion due to the inclusion of 90% argon in the inlet gas is 25% point when half of the active sites in the nominal case are used, and rises to 19% point when this value is increase by 50%.

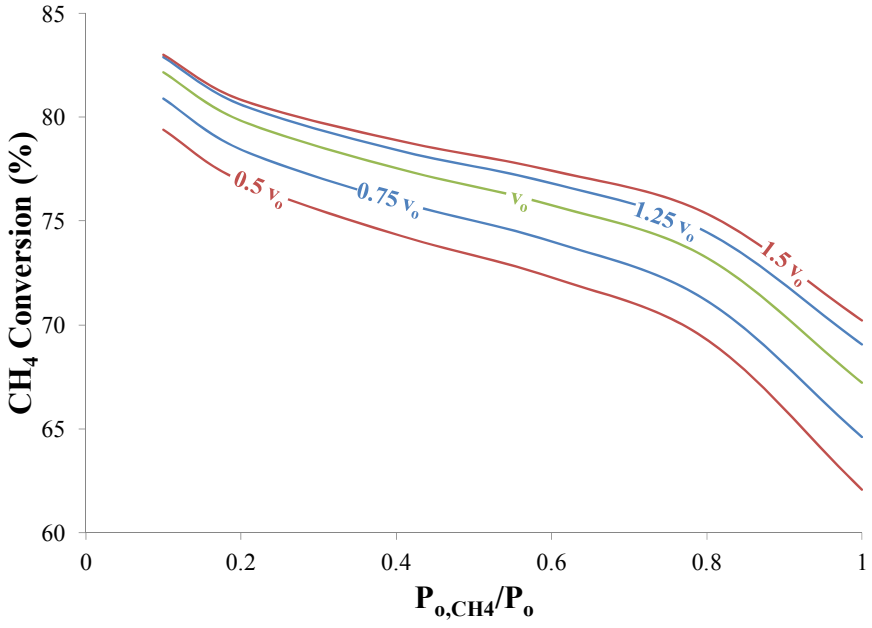

Fig. 4-20: Effect of particle pore volume on the variations of methane conversion with insertion of argon.

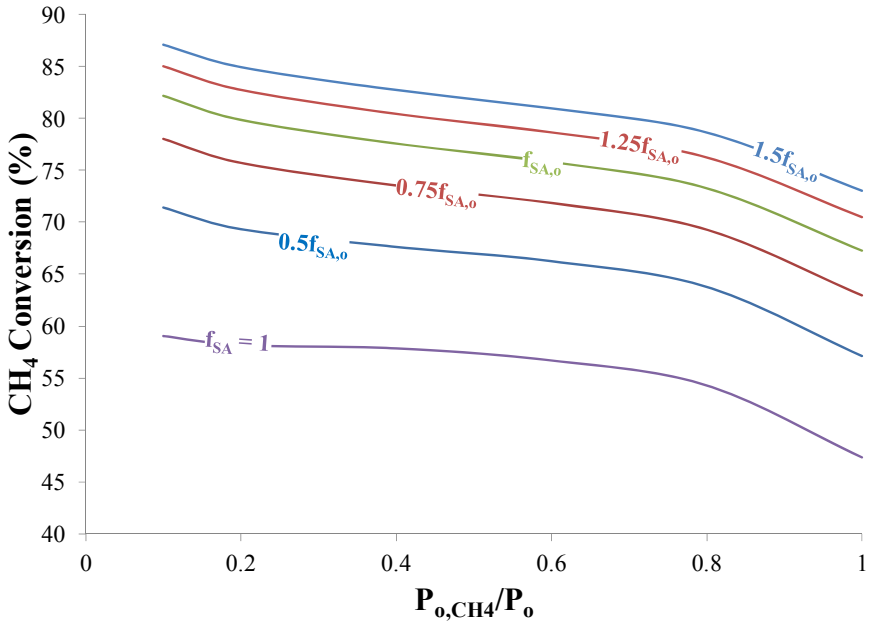

Fig. 4-21: Effect of the number of active sites of the particle on the variations of methane conversion with insertion of argon.

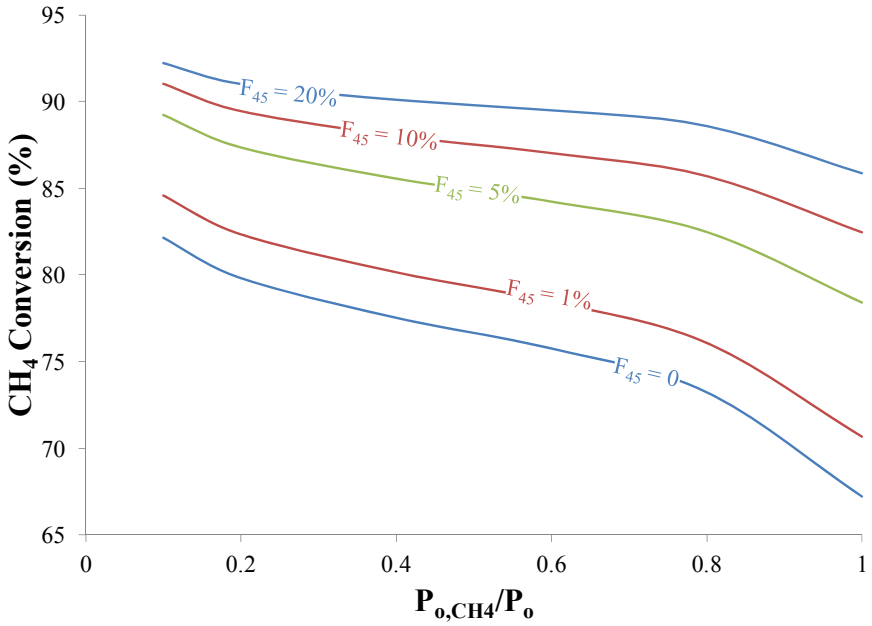

Fig. 4-22: Effect of the addition of fines on the variations of methane conversion with inlet feed composition.

Fine Particles

The changes of conversion with the inlet gas composition when different amounts of fines are used in the bed are presented in Fig. 4-22. This figure shows that the increase of conversion with the addition of argon is more prominent when the amount of fines added to the bed is smaller. The increase of conversion with 80% of argon in the feed gas is originally 22% point, while this value decreases to 7% point when 20% of fines are present in the bed. Calculations show that the relative increase in residence time of a bed with a specific amount of fines remains unchanged when argon is added to the feed gas. Since the residence time increases when fines are added to the bed, according to Fig. 4-6 the changes in conversion decrease, as observed in Fig. 4-22.

4.5. Catalyst size

The size of the particles is an important factor for the hydrodynamics of the fluidized bed, and affects the minimum fluidization velocity and voidage. Smaller particles reach the onset of fluidization at lower velocities, and their homogenous fluidization is extended over a wider range of velocities. However, particles smaller than a certain limit, which are classified as Geldart's group C particles, have a very high interparticular force and are difficult to fluidize. Also, homogeneous fluidization does not occur with large particles classified as Geldart's group B particles, and bubbles form as soon as the fluidization state is reached. Geldart's group A particles, which have diameters between the limits of Group C and B particles, experience a homogeneous fluidization regime, which is generally ideal for catalytic processes. In this section the effect of changing the size of the BP2000 particle on the conversion is investigated. The high and low limits for the particle diameter are selected as to remain in group A boundaries, so that homogeneous fluidization is observed in the reactor. It is assumed that the properties of the catalyst do not change with size. Since the particle size affects the velocity, the residence time is also affected, and its variations are investigated with the 4 cases discussed in previous sections. The varying residence time in each case is calculated with equations similar to those in section 4.4. The results of the investigation show that the decrease in particle size causes a decrease in minimum fluidization velocity and voidage. The decrease of the void fraction increases the ratio of

surface sites to gas in the reactor, and the probability of surface reactions, and creates a larger effect on conversion changes. In case 1, where the residence time is constant, this decrease in void fractions result in a small drop in conversion, as observed in Fig. 4-3. This figure also shows that the rate of reduction of conversion with respect to the particle size decreases at higher residence times. Increasing the residence time from 1 to 50 seconds changes the conversion reduction from 15 to 6% point.

In case 2, in addition the effect on the void fraction, the decrease of particle size also results in an increase in residence time, which eliminates the effect of the voidage, resulting in an almost constant conversion. Since the minimum fluidization and bubbling velocities vary extensively with the particle size, a constant velocity cannot be employed which would maintain particulate fluidization conditions for all the particle sizes in this study. Therefore, case 3 is not applicable. In case 4, due to the large change of minimum fluidization velocity with particle size, residence time changes considerably and causes large variations in conversion. The change of the particle diameter from 0.12 to 0.025 cm increases the conversion by 30%.

The effect of different parameters on the variations of conversion due to a change of diameter from 0.12 to 0.025 cm in case 4 is investigated in this section. It is noted that the properties of the catalyst, such as specific surface area and number density of active sites are considered to be unaffected by the change in the size of the catalyst.

Temperature

Fig. 4-10 shows that increasing the temperature decreases the reduction in conversion due to the use of large size particles. Increasing the particle diameter from 0.025 to 0.12 cm causes a decrease of 75% point at 1150 K, which is reduced to 20% point at 1400 K. Although the particle size considerably affects the residence time due to the change in minimum fluidization velocity, the residence time with a specific particle size is approximately unaffected by temperature. Therefore, the total residence time change at each temperature is the same and the difference between the conversion decrease at each temperature is the result of the effect of temperature on conversion change with residence time discussed in section 4.1.

Velocity

The changes of conversion with particle size at a specific state, such as the onset of fluidization or higher velocities up to bubbling can be observed in Fig. 4-15. With a specified particle size, the residence time at minimum fluidization conditions is the highest, since it is inversely proportional with velocity, and it therefore causes a relatively high conversion. Also, with the largest particle size considered, which is the limit between Geldart's group A and B particles, the minimum fluidization and bubbling velocities are equal. Consequently the rate of decrease of conversion with particle diameter is the highest at the onset of fluidization. In the range studied in Fig. 4-15, the decrease in conversion at minimum fluidization velocity is 35% point compared to 25% point observed with the minimum bubbling velocity.

Gas Composition

It is observed from Fig. 4-19 that adding argon to the inlet methane flow not only increases methane conversion, but it also reduces the difference between hydrogen production from large and small catalyst particles. The difference in methane conversion obtained from pure methane when the particles of size changes from 0.125 to 0.025 cm is 37% point, while adding 80% argon to the flow changes this value to 25% point. The increase of conversion with smaller particles is due to the decrease in minimum fluidization velocity which increases the residence time. The change in minimum fluidization velocity and the resulting variations of residence time between the two size limits are similar for different feed compositions. However, the residence times are smaller with lower amounts of argon. By observing Fig. 4-3 it is obvious that the same change in residence time has a higher impact at lower residence time, which justifies the trend of variations observed in Fig. 4-19.

Pore volume

Fig. 4-23 shows the changes of conversion with the particle size when catalyst particles with different pore volumes are used. It is observed that particles with smaller pore volumes cause a larger increase in the conversion. While the smallest pore volume in this study causes an increase of 78% point in conversion with the decrease in particle size in Fig. 4-23, this change is 41% with the largest pore volume. This is due to the high residence time obtained

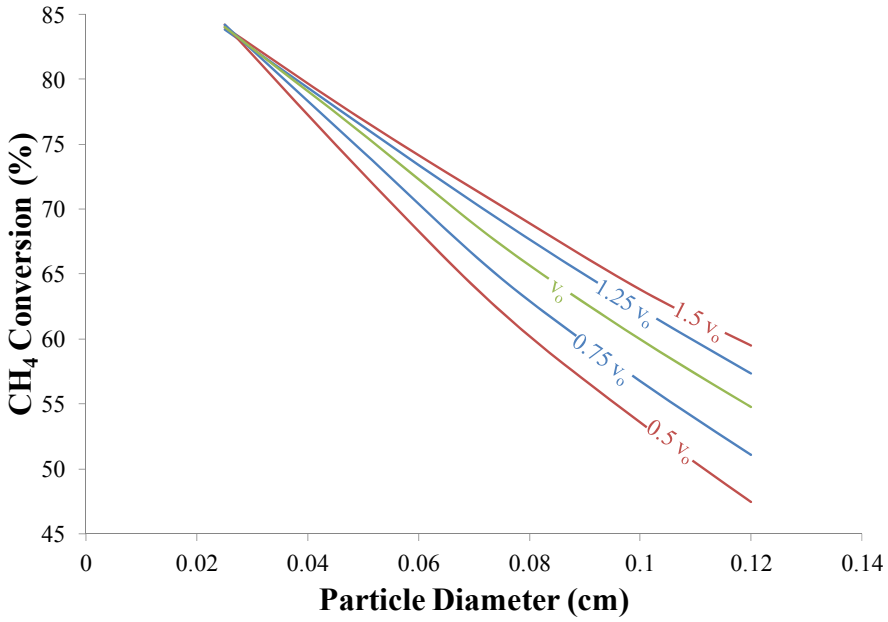

Fig. 4-23: Effect of particle pore volume on the variations of methane conversion with particle size.

when particles with large pore volumes are used, which variations cause a smaller effect on conversion as observed in Fig. 4-3.

Number of Active Sites

Fig. 4-24 shows the variation of conversion with particle size when the catalyst has different number of active sites. It is observed that as the number of active sites increases the effect of particle size on conversion will decrease. With the largest number of active sites used in these calculations, the decrease of conversion in the range of particle size studied is 44% point, while a catalyst with a third of this value causes an 80% point increase. Since the number of active sites does not affect the characteristics of fluidization, this effect is due to the kinetics of the reaction and the changes in the rate of the reaction.

Fine Particles

Fig. 4-25 shows the changes of conversion with particle diameter when different amounts of fines are added to the bed. It is observed that the addition of fines considerably decreases the difference between the conversion of small and large catalyst particles. The nominal increase

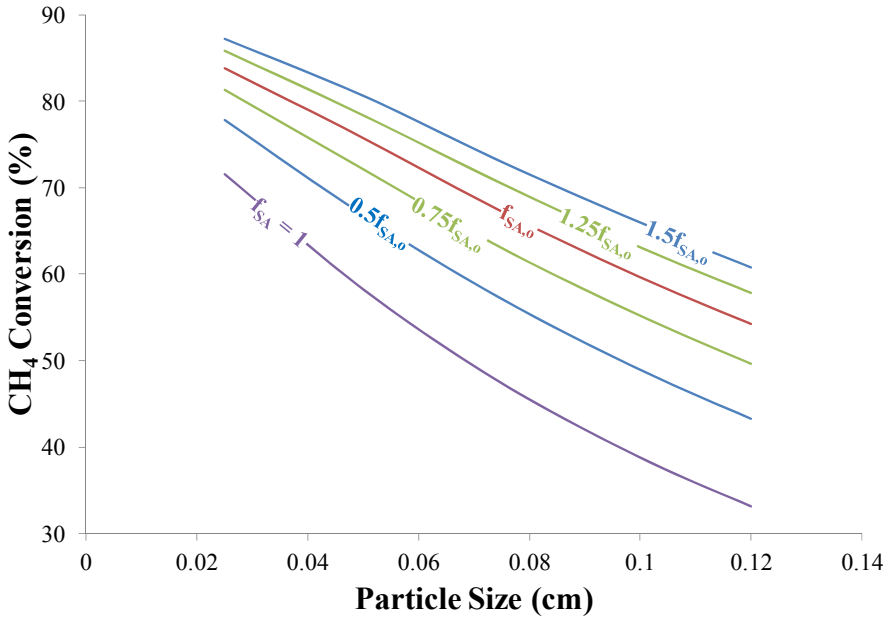

Fig. 4-24: Effect of number of active sites on variations of methane conversion with particle size.

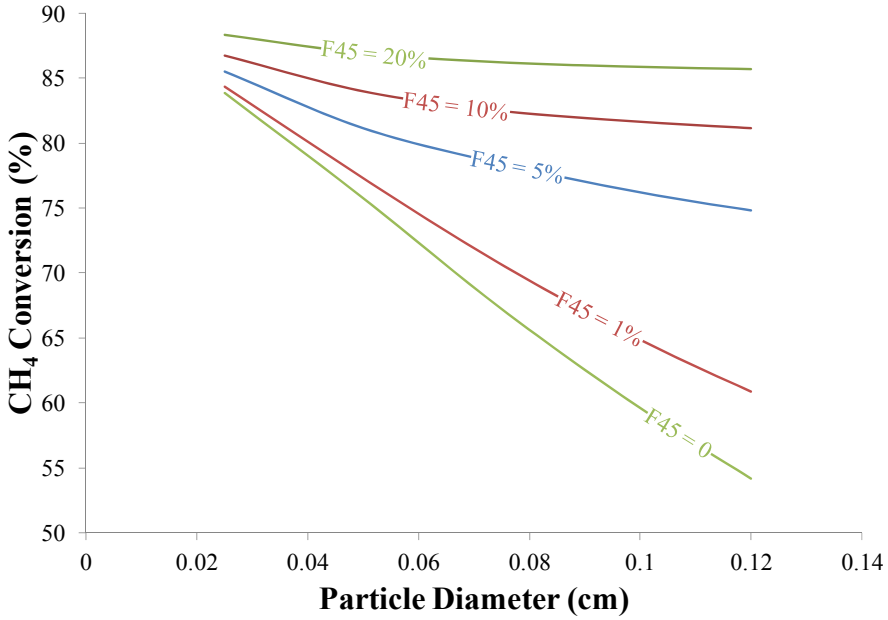

Fig. 4-25: Effect of the addition of fines on variations of methane conversion with particle size.

of conversion when the size of particles is changed from 0.12 to 0.025 cm is around 55% point, while in a bed with 20% fines this decrease is around 3% point. The main reason is that when fines are included in the bed, the change in the catalyst particle does not affect the average diameter as much as cases where fines are not present. Therefore, the changes in minimum fluidization and residence time are also smaller, which explains the trend observed in this figure.

4.6. Pore volume

The pore volume is a determining factor for the density of porous particles like carbon catalysts. It therefore has a noticeable effect on the hydrodynamics of fluidization. Particles with large pore volumes usually have a higher surface area; however, the objective of this section is to investigate the effect of pore volume alone and the surface area is assumed to be constant. Increasing the pore volume causes a decrease in the apparent density of the particle, and affects the residence time. Similar to previous sections, four cases are considered to study the effect of the pore volume on residence time. In the first case, the residence time is maintained constant by changing the mass of the catalyst. In cases 2 and 3, the inlet volumetric flow and catalyst mass are considered constant and the residence time changes due to the variations of pore volume can be obtained as follow:

$$\tau_{\rho 2} = \frac{\tau_{\rho 1}\rho_{p1}(1-\varepsilon_1)}{\rho_{p2}(1-\varepsilon_2)} \qquad \textbf{(4-7)}$$

Since the changes in the void fraction are usually small, the residence time is almost inversely proportional with the density. In case 2, the reactor operates with minimum fluidization conditions, while a specific reactor size is used in case 3 resulting in a constant velocity. In order to maintain the fluidization condition in all the range investigated in case 3, the velocity is set equal to the minimum fluidization velocity obtained with the highest particle density.

In cases 4, the reactor has a specific size while the volumetric flow rate changes to attain the minimum fluidization velocity. The variable residence time in this case is obtained as follow:

$$\tau_{\rho 2} = \frac{\tau_{\rho 1} u_{mf1} \rho_{p1} (1 - \varepsilon_{mf1})}{u_{mf2} \rho_{p2} (1 - \varepsilon_{mf2})} \quad \textbf{(4-8)}$$

This equation shows that the residence time is inversely proportional to the density of the particle and the minimum fluidization velocity.

In this study, the effect of pore volume on conversion is investigated by increasing and decreasing this value up to 50%. It is also noted that since the Archimedes number, which is used to determine the limits between Geldart's group A and B, increases with the density of the particle, using a smaller pore volumes can place the particle in Geldart's group B. Therefore, the smallest density considered in this study is chosen at the limit of Geldart's group A and B.

The effect of changing the pore volume in the limit described above was investigated on the four cases of residence time variations. In case 1, the constant volume of catalyst that is required to attain a constant residence time creates the need to decrease the amount of particles when the pore volume is increased. In contrast to other sections, where the constant residence time was obtained with small changes in the mass of the catalyst, when the variations of pore volume are investigated this change is considerable. The consequent lower surface sites produce a drop in conversion, as observed in Fig. 4-4, which is around 12% in the limits investigated. This figure also shows that changes of conversion decrease with an increase in the residence time. As an example, the conversion increases by 28% point in the range of pore volume investigated when a small residence time of 1 second is used, while the change is only 6% point with a residence time of 50 seconds. Since a large mass of catalyst is used for high residence times, the addition of mass to compensate the increase in density has a smaller effect.

Using a specific amount of catalyst with higher densities in cases 2 and 3 causes a smaller bed volume which has two opposite effects on the conversion: the residence time decreases, which has a negative effect on the conversion, while the probability of surface reactions increases due to the higher fraction of surface sites and gas molecules. Calculations show that the effect of the latter is slightly higher and results in an overall minor increase in conversion, with a small difference between the two cases due to the difference in velocity.

In case 4, the changes of residence time are also dependant on the velocity as observed in Equation (4-8), and since the minimum fluidization velocity and density both decrease with larger pore volumes, the residence time and conversion increase noticeably. In this study, the increase in conversion in case 4 is around 8%.

Similar to previous sections, the effect of different factors on the variations of conversion with the pore volume are investigated in a reactor with a specific size in which the onset of fluidization is maintained by changing the inlet flow rate.

Temperature

The changes of conversion with pore volume at different temperatures are shown in Fig. 4-11. It can be observed that as temperature rises, the effect of pore volume considerably decreases. The increase of pore volume in the range investigated causes a change of 66% point at 1150 K, while the variations are around 3% point at 1400 K. While a higher pore volume creates a higher residence time, the change in residence time with the pore volume are the same in different temperatures. Since according to Fig. 4-1 the amount of changes in conversion with residence time is lower when high temperatures are used, the effect of changing the pore volume decreases with temperature.

Velocity

The effect of changing the velocity from the minimum fluidization to minimum bubbling conditions on the changes of conversion with pore volume is observed in Fig. 4-16. It is observed that using particles with a larger pore volume increases the conversion at the onset of fluidization, and slightly decreases this value at the onset of bubbling. The increase in pore volume is equivalent to a lower density, which results in a smaller minimum fluidization velocity and considerably higher residence time, which causes the increase in conversion. The use of particles with smaller densities also causes the ratio of catalyst surface area to gas volume to drop, which in turn can cause a decrease in conversion. However, the effect of residence time is more prominent in the minimum fluidization conditions, and the conversion increases as observed in Fig. 4-16. On the other hand, with the minimum bubbling conditions, the changes in velocity and residence time with density are very small and the decrease of the ratio of catalyst surface area to the gas volume with larger pore volumes

results in smaller conversions. The increase in particle pore volume in the range studied causes the conversion to rise by 13% point at the onset of fluidization, while this value drops by 2% at the onset of bubbling.

Gas Composition

As it is observed in Fig. 4-20, the change in conversion with pore volume decreases when argon is added to the feed gas. The increase in conversion in the range of particle pore volume investigated is 13% point when pure methane is used and 5% point when the feed gas is composed of 80% argon. The increase of conversion with pore volume is due to the increase in residence time, and since the residence time is higher when argon is part of the feed gas, the changes are less important in this condition, according to Fig. 4-2.

Catalyst Size

Using smaller catalyst particles decreases the effect of particle pore volume on conversion as observed in Fig. 4-23. The residence time is larger for small particles, and according to Fig. 4-4 the change in pore volume produces a smaller increase in conversion. Another factor that affects the changes of conversion with pore volume is the ratio of gas to the surface of the catalyst. Larger particle pore volumes create a larger void volume which has a negative effect on the conversion. This factor has a minor effect on conversion variations when larger particles are used. However, the changes of this ratio are considerable for smaller particles, and create a noticeable decrease. The combined effect of this ratio and the residence time cause the conversion to be almost constant with a particle diameter of 0.025 cm, while this value changes by 25% point with the largest particle used.

Number of Active Sites

Fig. 4-26 shows the variations of conversion with pore volume when catalyst particles with different number of active sites are used. It is observed that the changes in conversion are larger for smaller number of active sites. Increasing the pore volume in the range investigated creates variations of 10% point when the particles have the highest number of active sites, while these variations are 20% point when half of the nominal value is used. This trend can be explained by considering that the amount of residence time and its changes are similar for

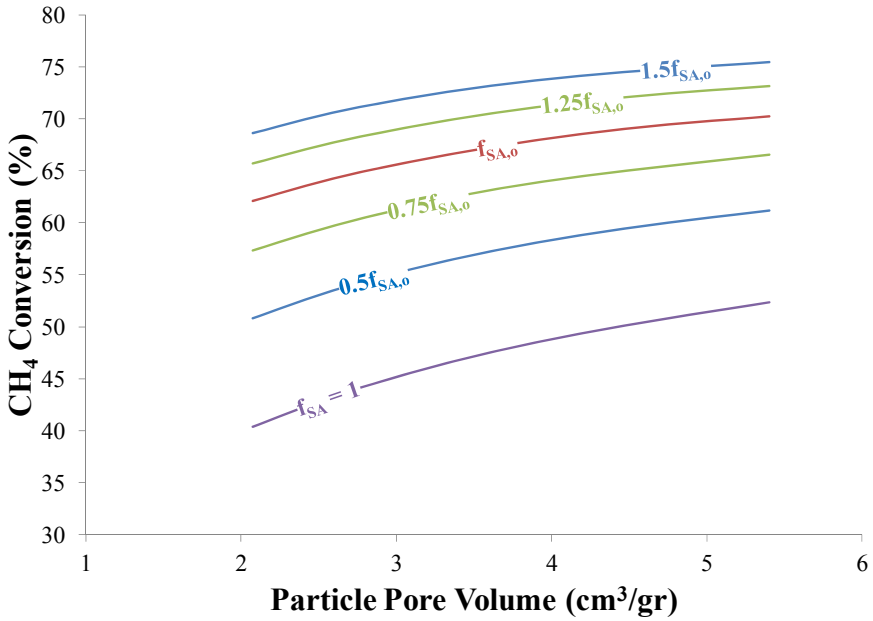

Fig. 4-26: Effect of number of active sites on the variations of methane conversion with particle pore volume.

all the number of active sites, and according to Fig. 4-5 this change creates a larger increase in conversion when smaller surface areas are used.

Fine Particles

Fig. 4-27 shows the variations of conversion with particle pore volume with different amounts of fines in the bed. The effect of adding fine to the bed is similar to the use of smaller particles. Low amounts of fines create a small residence time which causes a high increase in conversion with pore volume, according to Fig. 4-6. Conversely, high amounts of fines have a high residence with smaller effects on the conversion, with a simultaneous decrease in the ratio of catalyst surface area to gas which ultimately results in a constant conversion. It is observed that the inclusion of more than 10% of fines in the bed eliminates the effect of using particles with larger pore volumes on conversion, which can cause an increase of 10% point in conversion in the range investigated when no fines are in the bed.

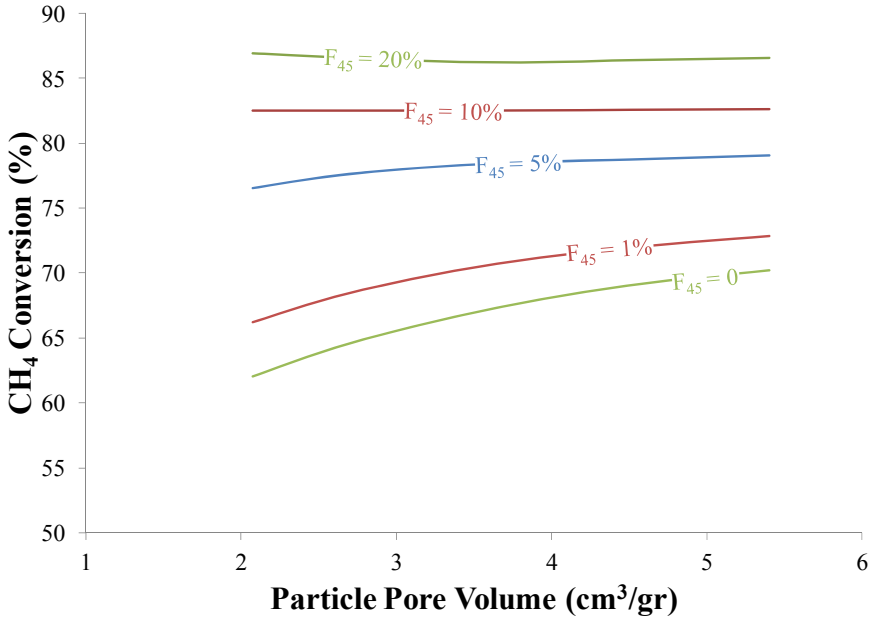

Fig. 4-27: Effect of the addition of fines on the variations of methane conversion with particle pore volume.

4.7. Number of Active Sites

The number of active sites is one of the important properties of the catalyst that changes the amount of hydrogen produced by affecting the kinetics of the process. Increasing this parameter has a positive effect on hydrogen production, since it increases the probability of surface reactions. The difference in the number of active sites is either due to the difference in the crystal structure of catalysts, or their specific surface area. Consequently, the change in the number of active sites often occurs along variations in other properties of the catalyst. For example, in most cases, catalyst particles with large specific surface area have a large pore volume. However, the properties of each catalyst particle depend on its specific structure, and there is no direct correlation between them. In this section, the variations in the number of active sites caused by a change a change of up to ±50% in the number density are investigated, and it is assumed that these changes do not affect any other property of the catalyst, including the specific surface area. The effect of different operating parameters and catalyst properties on the trend of the variations is also studied. It is noted that increasing either the number density of active sites or the specific surface area of the catalyst have the same effect on the kinetics of the process when other properties are assumed constant.

Therefore, the result obtained in this section can also be used to describe the variations of conversion with the specific surface area.

The effect of increasing the number of active sites on conversion in different residence times can be observed in Fig. 4-5. This figure shows that the increase of conversion obtained by using a catalyst particle with a larger number of active sites is more considerable at short residence times. For example, at a short residence time of 1 second the change of conversion obtained by changing the residence time in the range shown is 45% point, while at a residence time of 50 seconds the variation is 10% point.

Temperature

Fig. 4-12 shows that the positive effect of the increase of this factor on the conversion decreases when higher temperatures are used. Increasing the specific surface area 3 times raises the conversion by 70% point at 1150 K, and 17% point at 1400 K. The changes of the number of surface sites does not affect the residence time and void fraction, and the changes in conversion are solely due to the variations in the rate of surface reactions. At low temperatures, the reaction rates are relatively small and the change in active sites has a large effect on the conversion. However, at higher temperatures the rate of surface reactions are high and the changes caused by this factor are not as significant.

Velocity

The changes of conversion with the number of active sites at different fluidization conditions can be observed from Fig. 4-18. This figure shows that the variations of conversion increases when higher velocities are used. However, the rate of these variations is approximately the same in different velocities. The conversion change between the two limits of number of active sites used is 33 and 28% point at the onset of bubbling and fluidization, respectively.

Gas Composition

Fig. 4-21 shows that the relative increase in conversion obtained by using a catalyst with a higher number of active sites decreases when argon is present in the feed gas. In the range of specific surface areas investigated, the conversion increases by 28% point with pure methane and slightly decreases to 22% point when the feed gas is composed of 80% argon. It is

observed that the composition of the inlet gas has a small effect on these variations and. It is also noted that the rate of conversion change with the number of active sites is almost similar in different compositions.

Catalyst Size

It is observed from Fig. 4-24 that decreasing the size of the catalyst particles has a negative effect on the increase of conversion with surface area. The largest particle size used in the calculations causes an increase of 40% point in conversion when the specific surface area is changed between the two limits, while this change is only 12% point when the smallest particle size is used. Since the number of active sites does not affect the fluidization behavior, this change is due to the kinetics of the reaction.

Pore volume

Fig. 4-26 shows that the rate of increase in conversion is higher for particles with a small pore volume. The increase in conversion in the range investigated is 35% and 23% point with the smallest and largest pore volumes, respectively. When the pore volume is constant, the changes in the ratio of the number of active sites of catalyst to the volume of gas cause the increase in conversion and the residence time is constant. Therefore, when particles with smaller pore volumes are used, the residence time is smaller and, according to the results of Fig. 4-5, the effect of the change of this ratio results in a more prominent increase of conversion.

Fine Particles

Fig. 4-28 shows the changes of conversion with the number of active sites of the particles with different amounts of fines in the reactor. This figure shows that the changes of conversion with active sites decrease when the bed includes higher amounts of fines. In the nominal case, the change in conversion due to the increase of the number of active sites between the two limits considered in this study is around 28% point, while replacing 20% of the catalyst particles with fines decreases this value to 10% point. The number of active sites does not cause any change in the residence time and these variations are caused by the change in kinetic rates due to the increase of the number of reactive sites. It is also noted that

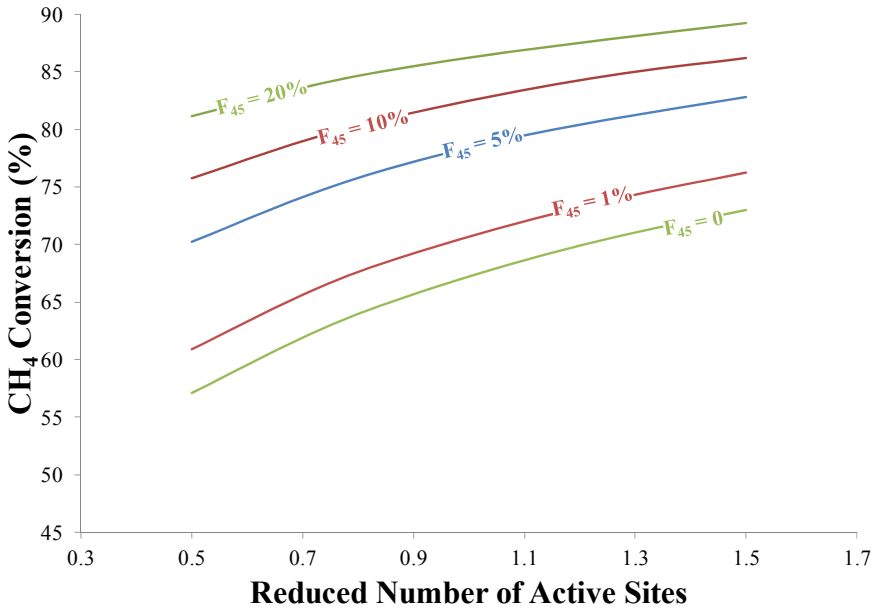

Fig. 4-28: Effect of the addition of fines on the variations of methane conversion with the number of active sites.

the reduced number of active sites is defined as the ratio of the actual to the nominal value of the number of active sites.

4.8. Fine Particles

The addition of fine particle to a bed of Geldart's group A particles improves the fluidization of the reactor by expanding the extent in which the bed stays in the homogeneous expansion phase. It can be observed in the equation used for the calculation of minimum bubbling velocity, Equation (3-22), that this variable is proportional to the exponential of the amount of fine particles smaller than 45 μm added to the bed. Also, the addition of fine particles decreases the average particle diameter and therefore causes a reduction in the minimum fluidization velocity and void fraction. Considering the variations of velocity with the addition of fine particles, the residence time is also affected by this parameter. The same cases studied in previous sections for determining the changes of residence time and its effect on the conversion are used in this section as well. The variable residence time is calculated with equations similar to those in section 4.4.

The changes of conversion with the inclusion of fine particles in the bed are investigated while considering the four different cases of residence time variations. The results show that, in case 1, the presence of fines in the bed increases the void fraction and therefore causes a decrease in the probability of surface reactions by lowering the ratio of gas in the reactor to the surface sites available. The conversion is therefore decreased as observed in Fig. 4-6. When 20% of fine particles with a diameter of 45 μm are included in the bed, this drop is around 8.5% in nominal conditions. It is also observed in Fig. 4-6 that as the residence time increases, the reduction of conversion decreases. The decrease in conversion with residence times of 1 and 50 seconds are 16 and 6% point, respectively. In cases 2, according to Equation (4-5), the residence time increases by adding fines due to the increase of void fraction. The increases of residence time and voidage have opposite effects and result in a negligible change in conversion. Case 3 is not applicable due to the large variations of minimum fluidization and minimum bubbling velocity with the addition of fines. Case 4 has a relatively high impact on conversion, since the residence time considerably increases due to the decrease in minimum fluidization velocity when fines are added to the bed. The increase in conversion is around 19% when 20% of fines are included in the bed in nominal conditions. It is observed that the highest variation in conversion is again obtained in the last case. In this section, the effect of different parameters is studied on the changes of conversion in case 4 with the inclusion of up to 20% monodispersed fines with a diameter of 45 μm in the bed.

Temperature

The variation of conversion with the percentage of fines at different temperatures can be observed from Fig. 4-13. Similar to the case of particle size change, the total residence time change with the addition of fines is similar in different temperatures. Also, the minimum fluidization velocity decreases with the addition of fines, causing an increase in residence time. According to the results of Fig. 4-1, the change in conversion with a similar residence time is larger at low temperatures. Therefore, when fines are added to the bed, the increase in conversion is much larger at lower temperatures, which is observed in Fig. 4-13. For example, at 1150 K adding 20% particles of 45 μm to the catalyst bed increases the conversion more than two times, while the increase is only 12% point at 1400 K.

Velocity

Fig. 4-18 is used to compare the changes of conversion with the percentage of fine particles in the bed at the onset of fluidization and bubbling. It is observed from this figure that the increase in conversion with the amount of fines is slightly larger at the minimum fluidization velocity compared to higher velocities. Replacing 20% of the catalyst particles in the bed with fine particles results in an increase of 29% point and 19% point at the onset of fluidization and bubbling, respectively. This trend is due to the large changes in fluidization velocity with the addition of fines compared to the change of the minimum bubbling velocity. A larger variation in residence time is observed in the former case, which results in a higher effect on conversion.

Gas Composition

It is observed from Fig. 4-22 that the trend of conversion change is similar when different amounts of argon are added to the inlet gas. However, the effect of the percentage of fines is slightly smaller when the amount of argon increases. The amount of increase of conversion obtained by adding 20% of fines to the bed with a flow of pure methane is 30% point, and this value decreases to 14% point when the inlet flow comprises 80% of argon. Calculations show that the relative changes in residence time with the percentage of fines are similar in different feed gas compositions. However, the residence time is longer when the feed gas that contains larger amounts of argon. Since the changes of conversion with shorter residence times are larger, as observed in Fig. 4-2, they are also larger when the percentage of argon in the feed gas is small, which explains the trend observed in Fig. 4-22.

Catalyst Size

Fig. 4-25 shows that the addition of fines is more effective when larger particles are used. A bed of catalyst with 20% of fines increases the original conversion by around 60% point when the particle diameter is 0.12 cm, and when particles of 0.025 cm are used, the increase is only 6%. This is mainly due to the considerably larger decrease of the high minimum fluidization velocity of a bed of large particles when fines are added. This causes a large increase in short residence times, and the trend observed in Fig. 4-3 explains the high increase of conversion with large particles. It is also noted that the rate of conversion change

is much larger when small amounts of fines are added. With particles of a diameter of 0.12 cm, the increase of conversion with the addition of 10% of fines is 50% point, while adding 10% more fines only causes a 6% point increase. This occurs since the addition of fines decreases the minimum fluidization velocity and therefore increases the residence time, and it is known form Fig. 4-3 that the rate of increase of conversion is higher at low residence times.

Pore volume

It is observed in Fig. 4-27 that increasing the pore volume of particle decreases the effect of fines on conversion. The conversion change due to the inclusion of 20% fine particles is 32% point with the smallest pore volume, and 17% point with the highest one. When particles with smaller pore volumes are used, the residence time is small and its changes create a higher increase in conversion according to Fig. 4-4. With larger pore volumes, not only the residence is higher with a smaller effect on conversion, but the ratio of catalyst surface area to the gas in the bed also decreases, and the combination of these effects ultimately leads to a smaller increase in conversion.

Number of Active Sites

Fig. 4-28 shows that as the number of active sites increases a lower increase in conversion is obtained. Particles with the highest number of active site used cause an increase of 22% point when 20% of fines are present in the bed, while using a catalyst with a third of these active sites area creates an increase of 42% point. This trend can be explained using the results of Fig. 4-5 and considering that the amount and changes of residence time with different amount of fines are not affected by the number of active sites.

4.9. Summary and Conclusions

The effect of different operating parameters and catalyst properties were investigated on the amount of methane conversion in the thermocatalytic decomposition of methane. The changes observed in conversion result from the combination of the variations of the reaction kinetics, and the hydrodynamic characteristics of the fluidized bed. The main hydrodynamics characteristic that is responsible for the variations of conversion is the residence time. This

value changes with the variations of all of the factors considered in this study, except the number of active sites. This change is mainly due to the influence of the main factors on the minimum fluidization velocity. Considering the variations in this velocity, and due to the restraints of the reactor to operate in the particulate regime, the velocity of the gas should be regulated to be in the specific limit required. This action can be performed by modifying the reactor size or gas flow rate. These variables, as well as the mass of the catalyst in the reactor, affect the changes in residence time with the main factors. Therefore, the method used to control the velocity of the gas, and the extent of the variations of these three variables should be determined before investigating the changes of conversion with the main factors. Accordingly, four different cases have been considered in this study. In the first case, the reactor operates at the onset of fluidization while the residence time remains constant using different amounts of catalyst. In case 2, a constant normal inlet flow rate is considered, and the minimum fluidization velocity is obtained by modifying the reactor size. In case 3, the inlet volumetric flow rate and reactor size are constant, while the velocity is allowed to change within the limits of the particulate fluidization. In case 4, a variable inlet flow rate is used to maintain the onset of fluidization velocity in a reactor with a specific size. With the exception of the variation in temperature and particle pore volume, the changes of conversion with the main factors are minimal and almost similar in cases 1 to 3. On the other hand, the advantage of changing the different factors creates a more noticeable effect in case 4, which is therefore investigated thoroughly in this study.

The effect of the main factors on the conversion of methane in a reactor of a specific size operating at the onset of fluidization was investigated, and the results are summarized in Table 4-1. The terms used in this table are displayed in Fig. 4-29. When investigating the effect of each factor, other parameters in Table 4-1, except the residence time, are constant. The results presented in this table are also represented in a graphic form in Fig. 4-30. It can be observed that in the nominal conditions and in the range of variables considered, the residence time has the highest effect on methane conversion. A wide range of variation is achievable for the residence time by changing the amount of the catalyst in the reactor and its dimensions. However, an increase in the initial and operating cost is evident with larger residence time which should be considered for an ultimate decision. The results show that the size of the catalyst is the second important factor, and the application of smaller particles has

Table 4-1: Variations of conversion with each main factor (variable V_1) in nominal conditions and the effect of changing other factors (variable V_2) on these variations*.

Variable V_2; V_{2ref}, ΔV_2 \ Variable V_1; Range of Change		**Residence Time** 3 to 50 s $\frac{\Delta X_{V1}(V_{2ref})}{X(V_{1ref}, V_{2ref})} = 31\%$	**Temperature** 1250 to 1400 K	**Velocity** u_{mf} to u_{mb}	**Argon in Feed Gas** 0 to 10%	**Fines** 0 to 10%	**Particle Size** 0.075 to 0.025cm	**Pore volume** 3.6 to 5.4 cm^3/gr	**Number of Active Sites** Equ. (3-7) to +50%
Temperature 1250 K, 150 K	$\Delta X_{V1}(V_{2o})/X(V_{1ref}, V_{2o})$	346	$\frac{\Delta X_{V1}(V_{2ref})}{X(V_{1ref}, V_{2ref})} = 19\%$	-23	14	92	102	23	20
	$\Delta X_{V1}(V_{2f})/X(V_{1ref}, V_{2f})$	16		-5	2	10	11	1	6
Velocity u_{mf}, u_{mb}-u_{mf}	$\Delta X_{V1}(V_{2o})/X(V_{1ref}, V_{2o})$	-	-	$\frac{\Delta X_{V1}(V_{2ref})}{X(V_{1ref}, V_{2ref})} = -9\%$	-	-	-	-	-
	$\Delta X_{V1}(V_{2f})/X(V_{1ref}, V_{2f})$	33	24		2	15	18	-1	10
Argon in Feed Gas 0, 10%	$\Delta X_{V1}(V_{2o})/X(V_{1ref}, V_{2o})$	-	-	-	$\frac{\Delta X_{V1}(V_{2ref})}{X(V_{1ref}, V_{2ref})} = 4\%$	-	-	-	-
	$\Delta X_{V1}(V_{2f})/X(V_{1ref}, V_{2f})$	32	16	-11		20	21	4	8
Fines 0, 10%	$\Delta X_{V1}(V_{2o})/X(V_{1ref}, V_{2o})$	-	-	-	-	$\frac{\Delta X_{V1}(V_{2ref})}{X(V_{1ref}, V_{2ref})} = 23\%$	-	-	-
	$\Delta X_{V1}(V_{2f})/X(V_{1ref}, V_{2f})$	36	7	-15	2		5	0	5
Particle Size 0.075 cm, 0.05 cm	$\Delta X_{V1}(V_{2o})/X(V_{1ref}, V_{2o})$	38	6	-14	2	3	$\frac{\Delta X_{V1}(V_{2ref})}{X(V_{1ref}, V_{2ref})} = 25\%$	0	4
	$\Delta X_{V1}(V_{2f})/X(V_{1ref}, V_{2f})$	33	33	0	7	50		9	12
Pore volume 3.6 cm^3/gr, 50%V_{2ref}	$\Delta X_{V1}(V_{2o})/X(V_{1ref}, V_{2o})$	25	26	-1	6	32	36	$\frac{\Delta X_{V1}(V_{2ref})}{X(V_{1ref}, V_{2ref})} = 4\%$	11
	$\Delta X_{V1}(V_{2f})/X(V_{1ref}, V_{2f})$	39	15	-15	4	17	20		7.5
Number of Active Sites Equ. (3-7), 50%V_{2ref}	$\Delta X_{V1}(V_{2o})/X(V_{1ref}, V_{2o})$	44	26	-12	6	32	36	7	$\frac{\Delta X_{V1}(V_{2ref})}{X(V_{1ref}, V_{2ref})} = 9\%$
	$\Delta X_{V1}(V_{2f})/X(V_{1ref}, V_{2f})$	25	16	-8	4	18	20	3	

* The terms used in this table are defined in Fig. 4-29.

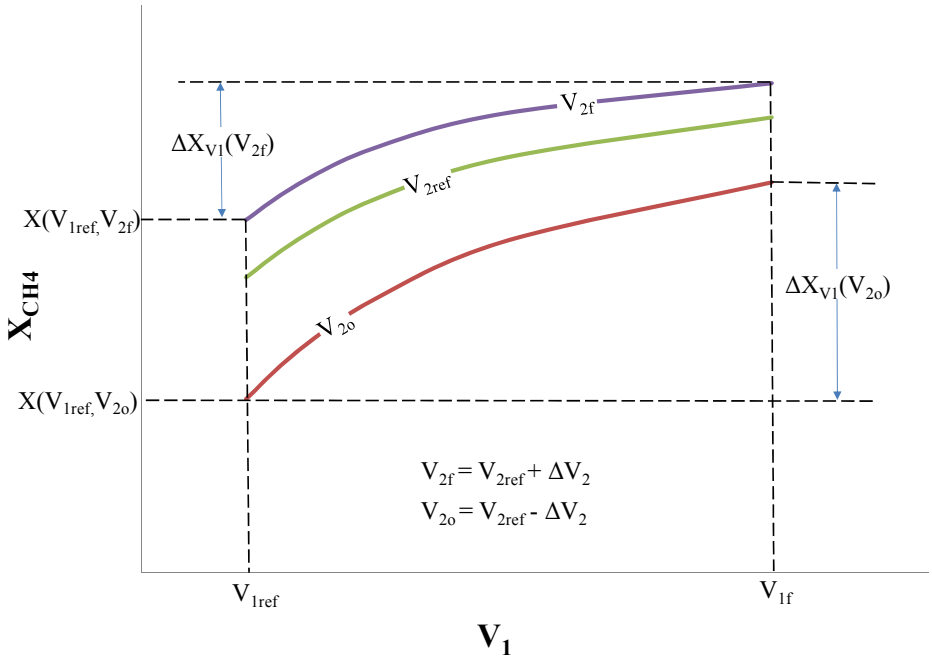

Fig. 4-29: Representation of the terms used in Table 4-1.

a high positive effect on methane conversion. Therefore, using a process for decreasing the size of the particles before or during the operation is an important step in improving or maintaining the amount of conversion. The cost of this process should be weighed against the advantage of higher conversion to decide about the suitable solution for a specific case. It should also be noted that due to the low fluidization velocity of small particles, although the conversion is high, the rate of the produced hydrogen might be smaller. In this case a larger reactor is required to produce a specific yield. Adding fine particles to the catalyst bed also has a considerable effect on the conversion. This procedure decreases the average particles size and has an effect similar to decreasing the size of the particles. Thus, large conversions can be obtained while using large particles. The temperature of the reactor is also an important parameter in improving the conversion of methane. However, the additional operating cost associated with the high temperatures and the increase in the initial cost of the reactor are among factors to be considered when operation at elevated temperatures is sought. Table 4-1 also shows that using a catalyst with a large number of active sites has a considerable effect on conversion. The increase in the number of active sites can be obtained by using catalysts with higher specific surface areas, or with a more disordered structure. Employing catalysts with large pore volumes and changing the feed gas composition by

adding an inert gas such as argon to the flow of methane are the last factors affecting the conversion. It is noted that when argon is present in the inlet gas the inlet flow of methane is reduced, and a larger reactor is required to produce a certain amount of hydrogen yield, which increases the initial cost of the process. Also, the generation of the larger inlet flow rate due to the presence of argon and the separation of this gas from the outlet flow are associated with a higher operating cost. Consequently, considering that the improvement in conversion with the variations of the feed gas composition is small, the application of this factor in the range investigated is unlikely to be beneficial. It should be emphasised that the results displayed in Table 4-1 represent the effect of the changes of one factor, while other parameters are kept constant. However, in most cases the properties that cause a high number of active sites in catalysts are associated with large pore volumes, and the combined effect of these two catalyst properties has a larger effect than the results presented in this study. The results of this study also show that the conversion decreases around 10% when the conditions are changed from minimum fluidization to minimum bubbling, which shows that application of the former is beneficial. Therefore, if a higher hydrogen yield is required, maintaining the onset of fluidization while increasing the size of the reactor would result in higher conversions, while economic factors should be considered to make the final decision.

Table 4-1 also shows how changing one factor affects the variations of conversion with another one. In the range used in this study, when the onset of fluidization is maintained by regulating the inlet flow rate in a specific reactor, decreasing the temperature has the highest positive effect on the variations of conversion with other factors. It is observed that although the amount of methane conversion is much higher at elevated temperatures, the improvement of conversion with the changes in other factors is much more significant at low temperatures. At the lower temperature limit, the variations of conversion with different factors increase in a wide range compared to the nominal value. The highest increase occurs with the pore volume, followed by the particle size and the amount of fine particles. As a result, similar to the nominal conditions, the particles size remains the most important factor, followed closely by the effect of adding fines. Although using high temperatures also considerably reduces the improvement in conversion obtained from other factors, decreasing the particle size and the addition of fines have the highest negative effect on this improvement. The increase in conversion at the higher temperature limit is reduced from 0.25 to 0.7 its nominal value, and

the order of importance of the different factors remains closely the same as the nominal conditions. Using small particles decreases the effect of other variables by a factor of up to 8. It is also noted that the amount and trend of the negative effect observed with small particles is almost similar to that of adding fine particles to the bed. Although using small particles and adding fine particles both have a positive effect on conversion when used individually, using other factors after applying each of these two factors creates a very small improvement for the conversion. In this case, the parameter that has the highest effect as a secondary factor is the temperature, which can create an additional increase in conversion of around 7%. Using larger particles has the second highest positive effect on the changes in conversion with other factors. These variations are around 1.5 to 2.25 times those at the nominal condition. The largest effect is on the particle pore volume and temperature, followed by the addition of fine particles. Consequently, when large particles are used, the addition of fines has the highest effect, and is followed by the temperature and the number of active sites. Table 4-1 also show that changing the pore volume and number of active sites to their boundary values results in similar variations of conversion with other factors. The variation of conversion increases up to 1.6 times the nominal value when the lower limits are used, and decreases down to 0.75 times the nominal value at the higher limit. When the number of active sites is modified, the effect of pore volume has the largest variations. When the particles have a large pore volume, the effects of the particle size, percentage of fines and temperature increase the most, while small pore volumes mainly affect the effect of the percentage of fines and temperature. The results show that the changes of the variations in the conversion with different number of active site and different pore volumes does not affect the order of importance of the main factors, which remains similar to that at the nominal conditions. The factor having the smallest effect on decreasing the improvement of conversion with other parameters is the addition of argon to the inlet flow. The highest effect is on the particle porosity, followed by the temperature and percentage of fines. In this case, the particle size and percentage of fines are the secondary parameter with the highest effect on conversion. It is also noted that the conversion could be further increased by changing the residence time of the reactor, especially at low temperatures. The velocity has different impacts on the increase of conversion with other factors. It reduces the effect of the particle size, fines, and inlet gas composition in a range from 0.5 to 0.8 their initial values, while it

completely eliminates the positive effect of the pore volume. It is also interesting to note that higher velocities improve the effect of temperature and number of active sites. The results also point that if a higher velocity is required, it is optimal to produce this change by modifying the size of the reactor, or by changing other variables to maintain the residence time constant. If this is not achievable, the negative effect of using high velocities can almost be eliminated by increasing the size of the particle or decreasing its pore volume.

The results presented in this chapter can be used as a guideline to choose between several catalysts considering their characteristics, or to suggest appropriate operating conditions. Further discussion is addressed in the next chapter.

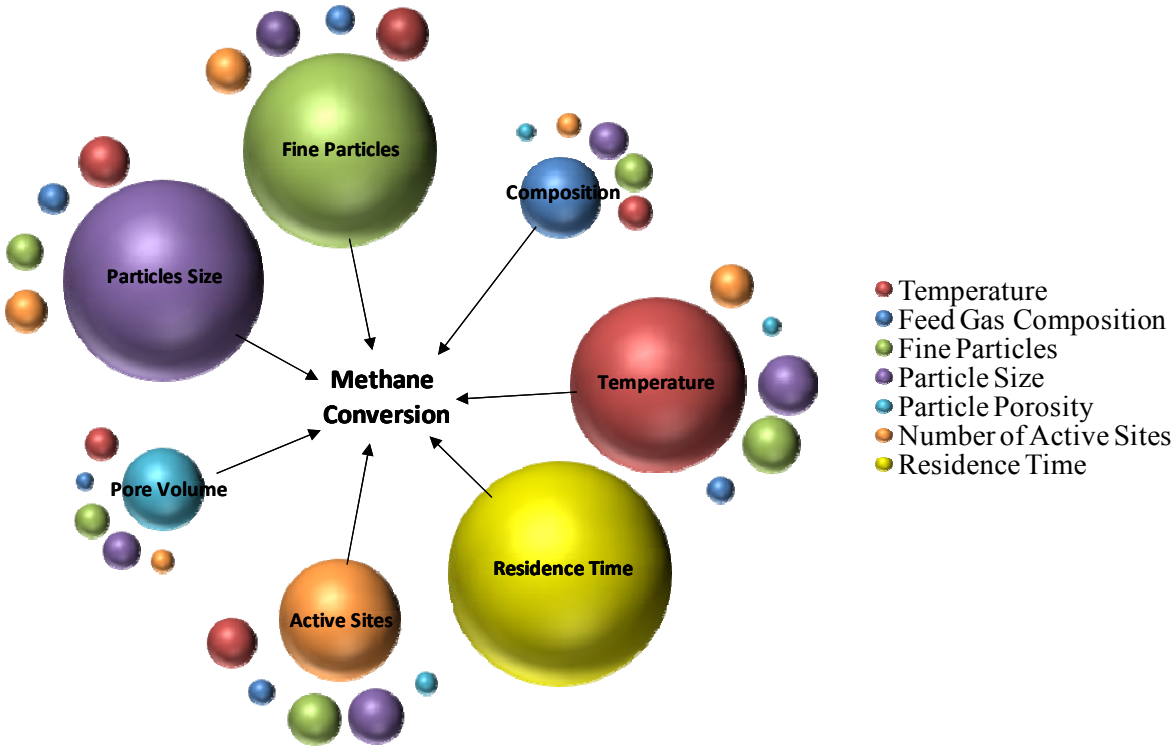

Fig. 4-30: Graphic representation of results in Table 4-1.

Chapter 5
Conclusions and Recommendations

5.1. Conclusions

A model was developed for the thermocatalytic decomposition of methane in a fluidized bed of carbon particles. Since the aim of using this process is the production of hydrogen, the amount of methane conversion to hydrogen was used as the parameter to evaluate the performance. This value was obtained with a detailed kinetic model. In contrast to the rate law that is generally employed for representing the kinetics of this process, the detailed model developed in this study comprises the main properties of carbon catalysts. Therefore, one of the advantages of this model is that it allows the investigation of the effect of the catalyst properties on the performance. The kinetic model takes into consideration the effect of the interaction of gas-phase species, and the additional hydrogen production due to the presence of catalyst particles. The interaction of gas phase species was modeled with a reaction mechanism obtained using several major combustion models, which were modified using experimental data specific to hydrogen production. The effect of the catalyst was added with a mechanism of surface reactions. One of the important and distinctive benefits of this model is the use of the number of active sites of carbon particles in the equations of the reaction rates. Experimental investigations have recognized this property as one of the main reasons of the variations between the activities of different types of carbon. However, it has not been properly quantified or used in any model. In this study, a method was presented to

use experimental data and the theoretical model developed with the consideration of the number of active sites to estimate this value. Accordingly, the initial number of active surface sites of three commercial carbon blacks, BP120, XC72, and BP2000 were determined. It was shown that the effect of the number of active sites has a high importance in the model, and neglecting this parameter can cause large errors. Another important feature of this model is the use of correlations to predict the hydrodynamic characteristics of the fluidized bed to eliminate the requisite to obtain these values from experimental data. The hydrodynamics of the reactor was modeled in a particulate fluidized bed. Considering the size and properties of the carbon particles, this bubble-free regime is obtained between the onset of fluidization and the formation of bubbles. It is preferable to operate the reactor in this regime since it provides good mixing and a high contact area between the gas and catalyst. The main fluidized bed characteristics required in this study are the void fraction of the bed, as well as the minimum fluidization and minimum bubbling velocities. The appropriate correlations used to obtain these values were selected based on comparison of their results with experimental data.

The model was used to study the effect of operating parameters and catalyst properties on the amount of methane conversion. A nominal value is attributed to each factor, and the changes in conversion caused by their variations in a certain range are investigated individually. The combined effects of two factors are also studied. The operating parameters studied are the temperature in a range from 1100 to 1400 K, and the residence time, which was changed from 1 to 50 s. The effect of changing the velocity of the gas from minimum fluidization velocity to minimum bubbling velocity was investigated. The composition of the feed gas was also changed by adding up to 10% of argon to the flow of pure methane. The catalyst properties considered are the particle size, which varies from 0.025 to 0.12 cm, as well as the particle pore volume and number of active sites with variations of up to 50% their nominal values. The last effect investigated is that of including up to 10% of fine particles in the bed. The nominal values are those of a fluidized bed reactor operating at the onset of fluidization with a residence time of around 3 seconds. The inlet gas is pure methane at atmospheric pressure, and the temperature of the bed is 1250 K. The catalyst used in this reactor is the carbon black BP2000. Since most of the factors investigated affect the onset of fluidization, the velocity of the gas is regulated by changing the inlet flow rate in a reactor of a specific size. The results show that, in the range of variations investigated, the procedures

that cause the highest improvement in conversion are: increasing the residence time, decreasing the size of the particles, adding fine particles to the bed, increasing the temperature, using catalysts with high surface areas or large number of active sites, adding argon to the inlet gas, and using catalysts with large pore volumes, respectively.

One of the most important variables affecting the performance is the residence time. The results show that at a low residence time, even small increases can lead to a significantly higher amount of hydrogen production, whereas changing large residence times is not as effective. The residence time can be mainly modified by changing the velocity of the gas, the mass of the catalyst, and the size of the reactor. It is noted that the residence time varies with most of the other main factors due to their effect on the minimum fluidization velocity.

Using catalyst particles with small diameters can also improve the conversion. Adding fine particles to the bed can create the same effect. When very small particles are used, or fine particles are added to the bed, applying other factors only changes the conversion slightly. However, the temperature can still have a noticeable effect. On the other hand, if a large particle is used, the effect of other factors rises. In this case, the addition of fine particles has the largest effect, followed by the temperature.

Increasing the temperature can considerably improve the conversion of methane. However, a higher initial and operating cost is associated with this change due to the additional energy required. When the reactor operates at high temperatures, small particles can be used to increase the conversion further. If the size of the catalyst cannot be decreased, addition of fine particles has a positive effect on the performance. When a reactor with a lower temperature is used to decrease the cost, smaller catalyst particles with larger pore volumes and number of active sites can be used to compensate for the effect of temperature.

The application of a catalyst with a high number of active sites, which can be due to a high specific surface area or disordered surface, increases the conversion. In contrast to other parameters discussed so far, when this variable has a high value, the effect of other factors on conversion is still considerable. When particles with a small number of active sites are used, changing the size and adding fines still have the highest effects.

The pore volume and the inlet gas composition have the smallest effect on conversion within the ranges of parameters investigated. When argon is added to the inlet flow of

methane, the use of particles with small diameters, the addition of fines to the bed and raising the temperature can be applied respectively to further increase the conversion. When the pore volume increases up to 50% from the nominal value, the effect of other factors decreases but remains relatively high. On the other hand, the main factors have a higher effect on the conversion with small pore volumes. In both cases of pore volume changes, the particle size, the percentage of fines and the temperature have the highest effect on conversion.

If additional values of hydrogen yield are required, the velocity can be increased up to the bubbling velocity. However, this causes a decrease in the conversion. This negative effect in negligible if high temperatures and large particles are used. This decrease can also be reduced by keeping the residence time constant.

The results obtained in this study can be used as a guideline to choose between several catalysts considering their characteristics, or to suggest appropriate operating conditions. The model developed can be used to find the optimum operating and design parameters of the process. However, it should be mentioned that a complete optimization can only be performed when other parameters such as economic factors are considered. It is also noted that the results obtained in this study are related to the initial activity of the catalysts. To perform a complete comparison between the different catalysts the rate of deactivation should be added to the model.

5.2. Recommendations

The following suggestions are recommended for future works:

- **Determining the variations of the catalysts dynamic properties during the process**: The results presented in this study were obtained for the initial activity of the catalyst. However a complete comparison of different factors affecting the performance of the process with various catalysts can only be performed when the initial activity and the conversion through the process are both available. Although the code was written for a transient process, this feature cannot be used due to lack of information on the changes of the properties of the catalyst during the progress of the process. The code can be completed with a correlation for the

variations of surface area and pore volume, which can be obtained with a series of oriented experiments.

- **Inclusion of economic factors**: Although the trend of several factors was investigated on the conversion, the application of the results to improve the performance is usually associated with an increase in the initial or operating cost. Therefore, economic factors should be considered and an economic analysis should be conducted to determine the proper values of these factors to achieve an optimum performance. This step will direct the study to be more practicable.
- **Finding the number of active sites of different types of carbon blacks and active carbons**: The model was used with experimental data to obtain the initial number of active sites in three carbon blacks of BP2000, BP120, and XC75. Different types of carbon blacks and active carbons can be used as the catalyst in this process. Finding the number of surface sites of these particles with the method developed in this study will enable the comparison of the conversion using catalysts with a wide range of properties.
- **Modeling a bubbling bed of carbon particles**: The particles of the carbon catalyst were determined to be from Geldart's group A particles, and the reactor can therefore operate in a particulate regime. The application of this regime is optimal as it provides a homogeneous mixture and adequate contact between the catalyst and the gas. However, the need to obtain higher yields of hydrogen can necessitate the use of higher flow rates that result in a bubbling bed. It is therefore recommended to complete the model by adding the effect of using a bubbling fluidized bed. This model can provide a good understanding about the consequences of using this regime, and will enable the comparison of different factors in it.
- **Considering different types of particles**: The addition of fine particles was shown to have a considerable effect on the conversion. However, the fine particles were assumed to have the same properties as the catalyst. Since fines with the same properties as the catalyst might not be practically available, investigation on the effect of fines with different properties would be beneficial.

This would require some changes in the model to enable the calculation related to particles with different properties.

- **Investigation on the catalytic decomposition of methane in solar reactors**: A method used in solar reactors to improve the conversion is adding a trace of fine carbon particles to the flow of methane. Since the kinetics of this process has been obtained, the variations of methane conversion in this type of reactor can be investigated by applying proper changes to the existing model.

References

[1] Muradov, N. Z., and Veziroglu, T. N., 2005, "From Hydrocarbon to hydrogen–carbon to Hydrogen Economy," International Journal of Hydrogen Energy, **30**(3) pp. 225-237.

[2] Rosen, M. A., 2010, "Advances in Hydrogen Production by Thermochemical Water Decomposition: A Review," Energy, **35**(2) pp. 1068-1076.

[3] Ursua, A., Gandia, L. M., and Sanchis, P., 2012, "Hydrogen Production from Water Electrolysis: Current Status and Future Trends," Proceedings of the IEEE, **100**(2) pp. 410-426.

[4] Parthasarathy, P., and Narayanan, K. S., 2014, "Hydrogen Production from Steam Gasification of Biomass: Influence of Process Parameters on Hydrogen Yield – A Review," Renewable Energy, **66**(9) pp. 570-579.

[5] Tanksale, A., Beltramini, J. N., and Lu, G. M., 2010, "A Review of Catalytic Hydrogen Production Processes from Biomass," Renewable and Sustainable Energy Reviews, **14**(1) pp. 166-182.

[6] Abánades, A., Rubbia, C., and Salmieri, D., 2013, "Thermal Cracking of Methane into Hydrogen for a CO2-Free Utilization of Natural Gas," International Journal of Hydrogen Energy, **38**(20) pp. 8491-8496.

[7] Dufour, J., Serrano, D. P., Gálvez, J. L., 2009, "Life Cycle Assessment of Processes for Hydrogen Production. Environmental Feasibility and Reduction of Greenhouse Gases Emissions," International Journal of Hydrogen Energy, **34**(3) pp. 1370-1376.

[8] Muradov, N. Z., and Veziroglu, T. N., 2008, "“Green” Path from Fossil-Based to Hydrogen Economy: An Overview of Carbon-Neutral Technologies," International Journal of Hydrogen Energy, **33**(23) pp. 6804-6839.

[9] Marban, G., and Valdes-Solis, T., 2007, "Towards the Hydrogen Economy?" International Journal of Hydrogen Energy, **32**(12) pp. 1625-1637.

[10] Abbas, H. F., and Wan Daud, W. M. A., 2010, "Hydrogen Production by Methane Decomposition: A Review," International Journal of Hydrogen Energy, **35**(3) pp. 1160-1190.

[11] Dincer, I., 2012, "Green Methods for Hydrogen Production," International Journal of Hydrogen Energy, **37**(2) pp. 1954-1971.

[12] Yan, W., and Hoekman, S. K., 2014, "Production of CO 2-Free Hydrogen from Methane Dissociation: A Review," Environmental Progress & Sustainable Energy, **33**(1) pp. 213-219.

[13] Muradov, N., 2002, "Thermocatalytic CO_2-free production of hydrogen from hydrocarbon fuels," Proceedings of the 2002 US DOE Hydrogen Program Review, NREL/CP-610–32405, .

[14] Muradov, N. Z., 1998, "CO_2-Free Production of Hydrogen by Catalytic Pyrolysis of Hydrocarbon Fuel," Energy & Fuels, **12**(1) pp. 41-48.

[15] Steinberg, M., 1999, "Fossil Fuel Decarbonization Technology for Mitigating Global Warming," International Journal of Hydrogen Energy, **24**(8) pp. 771-777.

[16] Frusteri, F., Italiano, G., Espro, C., 2012, "H2 Production by Methane Decomposition: Catalytic and Technological Aspects," International Journal of Hydrogen Energy, **37**(21) pp. 16367-16374.

[17] Pinilla, J. L., Moliner, R., Suelves, I., 2007, "Production of Hydrogen and Carbon Nanofibers by Thermal Decomposition of Methane using Metal Catalysts in a Fluidized Bed Reactor," International Journal of Hydrogen Energy, **32**(18) pp. 4821-4829.

[18] Guil-Lopez, R., Botas, J. A., Fierro, J. L. G., 2011, "Comparison of Metal and Carbon Catalysts for Hydrogen Production by Methane Decomposition," Applied Catalysis A, General, **396**(1-2) pp. 40-51.

[19] Rodat, S., Abanades, S., Sans, J., 2010, "A Pilot-Scale Solar Reactor for the Production of Hydrogen and Carbon Black from Methane Splitting," International Journal of Hydrogen Energy, **35**(15) pp. 7748-7758.

[20] Rodat, S., Abanades, S., and Flamant, G., 2009, "High-Temperature Solar Methane Dissociation in a Multitubular Cavity-Type Reactor in the Temperature Range 1823-2073 K," Energy & Fuels, **23**(5) pp. 2666-2674.

[21] Robertson, S. D., 1970, "Carbon Formation from Methane Pyrolysis Over some Transition Metal surfaces—I. Nature and Properties of the Carbons Formed," Carbon, **8**(3) pp. 365-374.

[22] Muradov, N. Z., 2003, "In a Moving Bed Reactor using Carbon-Based Catalysts in Air and/or Water-Free Environment," University of Central Florida, **09/824437**(United States Patent #6670058) pp. 1-12.

[23] Al-Hassani, A. A., Abbas, H. F., and Wan Daud, W. M. A., 2014, "Hydrogen Production Via Decomposition of Methane Over Activated Carbons as Catalysts: Full Factorial Design," International Journal of Hydrogen Energy, **39**(13) pp. 7004-7014.

[24] Chen, W., Liou, H., and Hung, C. I., 2013, "Kinetics Development and Numerical Simulation of Methane Thermocatalytic Decomposition at the Early Stage and Steady State," International Journal of Hydrogen Energy, **38**(13) pp. 5270-5284.

[25] Dunker, A. M., and Ortmann, J. P., 2006, "Kinetic Modeling of Hydrogen Production by Thermal Decomposition of Methane," International Journal of Hydrogen Energy, **31**(14) pp. 1989-1998.

[26] Muradov, N., Chen, Z., and Smith, F., 2005, "Fossil Hydrogen with Reduced CO_2 Emission: Modeling Thermocatalytic Decomposition of Methane in a Fluidized Bed of Carbon Particles," International Journal of Hydrogen Energy, **30**(10) pp. 1149-1158.

[27] Ozalp, N., Ibrik, K., and Al-Meer, M., 2013, "Kinetics and Heat Transfer Analysis of Carbon Catalyzed Solar Cracking Process," Energy, **55**(Complete) pp. 74-81.

[28] Caliot, C., Flamant, G., Patrianakos, G., 2012, "Two-Dimensional Model of Methane Thermal Decomposition Reactors with Radiative Heat Transfer and Carbon Particle Growth," AICHE Journal, **58**(8) pp. 2545-2556.

[29] Patrianakos, G., Kostoglou, M., and Konstandopoulos, A. G., 2012, "Effect of Seeding on Hydrogen and Carbon Particle Production in a 10 MW Solar Thermal Reactor for Methane Decomposition," International Journal of Hydrogen Energy, **37**(21) pp. 16570-16580.

[30] Patrianakos, G., Kostoglou, M., and Konstandopoulos, A., 2011, "One-Dimensional Model of Solar Thermal Reactors for the Co-Production of Hydrogen and Carbon Black from Methane Decomposition," International Journal of Hydrogen Energy, **36**(1) pp. 189-202.

[31] Ozalp, N., and Shilapuram, V., 2010, "Step-by-Step Methodology of Developing a Solar Reactor for Emission-Free Generation of Hydrogen," International Journal of Hydrogen Energy, **35**(10) pp. 4484-4495.

[32] Maag, G., Lipinski, W., and Steinfeld, A., 2009, "Particle–gas Reacting Flow Under Concentrated Solar Irradiation," International Journal of Heat and Mass Transfer, **52**(21-22) pp. 4997-5004.

[33] Trommer, D., Hirsch, D., and Steinfeld, A., 2004, "Kinetic Investigation of the Thermal Decomposition of CH_4 by Direct Irradiation of a Vortex-Flow Laden with Carbon Particles," International Journal of Hydrogen Energy, **29**(6) pp. 627-633.

[34] Serrano, D. P., Botas, J. A., Fierro, J. L. G., 2010, "Hydrogen Production by Methane Decomposition: Origin of the Catalytic Activity of Carbon Materials," Fuel, **89**(6) pp. 1241-1248.

[35] Lázaro, M. J., Pinilla, J. L., Suelves, I., 2008, "Study of the Deactivation Mechanism of Carbon Blacks used in Methane Decomposition," International Journal of Hydrogen Energy, **33**(15) pp. 4104-4111.

[36] Lee, S. Y., Ryu, B. H., Han, G. Y., 2008, "Catalytic Characteristics of Specialty Carbon Blacks in Decomposition of Methane for Hydrogen Production," Carbon, **46**(14) pp. 1978-1986.

[37] Suelves, I., Lazaro, M. J., Moliner, R., 2007, "Hydrogen Production by Methane Decarbonization: Carbonaceous Catalysts," International Journal of Hydrogen Energy, **32**(15) pp. 3320-3326.

[38] Ryu, B. H., Lee, S. Y., Lee, D. H., 2007, "Catalytic Characteristics of various Rubber-Reinforcing Carbon Blacks in Decomposition of Methane for Hydrogen Production," Catalysis Today, **123**(1-4) pp. 303-309.

[39] Muradov, N., Smith, F., and T-Raissi, A., 2005, "Catalytic Activity of Carbons for Methane Decomposition Reaction," Catalysis Today, **102-103**pp. 225-233.

[40] Kim, M. H., Lee, E. K., Jun, J. H., 2004, "Hydrogen Production by Catalytic Decomposition of Methane Over Activated Carbons: Kinetic Study," International Journal of Hydrogen Energy, **29**(2) pp. 187-193.

[41] Lee, E. K., Lee, S. Y., Han, G. Y., 2004, "Catalytic Decomposition of Methane Over Carbon Blacks for CO_2-Free Hydrogen Production," Carbon, **42**(12-13) pp. 2641-2648.

[42] Ikuma, Y., and Bessho, H., 2007, "Effect of Pt Concentration on the Production of Hydrogen by a TiO2 Photocatalyst," International Journal of Hydrogen Energy, **32**(14) pp. 2689-2692.

[43] Vagia, E. C., and Lemonidou, A. A., 2007, "Thermodynamic Analysis of Hydrogen Production Via Steam Reforming of Selected Components of Aqueous Bio-Oil Fraction," International Journal of Hydrogen Energy, **32**(2) pp. 212-223.

[44] Westermann, P., Jorgensen, B., Lange, L., 2007, "Maximizing Renewable Hydrogen Production from Biomass in a bio/catalytic Refinery," International Journal of Hydrogen Energy, **32**(17) pp. 4135-4141.

[45] Ni, M., Leung, D. Y. C., and Leung, M. K. H., 2007, "A Review on Reforming Bio-Ethanol for Hydrogen Production," International Journal of Hydrogen Energy, **32**(15) pp. 3238-3247.

[46] Zedtwitz, P. v., Petrasch, J., Trommer, D., 2006, "Hydrogen Production Via the Solar Thermal Decarbonization of Fossil Fuels," Solar Energy, **80**(10) pp. 1333-1337.

[47] Pena, M. A., Gomez, J. P., and Fierro, J. L. G., 1996, "New Catalytic Routes for Syngas and Hydrogen Production," Applied Catalysis A, General, **144**(1-2) pp. 7-57.

[48] Steinberg, M., and Cheng, H. C., 1989, "Modern and Prospective Technologies for Hydrogen Production from Fossil Fuels," International Journal of Hydrogen Energy, **14**(11) pp. 797-820.

[49] Stevens, S., and Gale, J., 2000, "Geologic CO_2 Sequestration," Oil & Gas Journal, **98**pp. 40-44.

[50] Bachu, S., 2008, "CO2 Storage in Geological Media: Role, Means, Status and Barriers to Deployment," Progress in Energy and Combustion Science, **34**(2) pp. 254-273.

[51] Gough, C., 2008, "State of the Art in Carbon Dioxide Capture and Storage in the UK: An Experts' Review," International Journal of Greenhouse Gas Control, **2**(1) pp. 155-168.

[52] Calahan, M., 1972, "Thermo-catalytic hydrogen generation from hydrocarbon fuels," From electrocatalysis to fuel cells, G. Sanstede, ed. Battelle Seattle Research Center by the University of Washington Press, Seattle and London, **18,** pp. 189.

[53] Holmen, A., Rokstad, O., and Solbakken, A., 1976, "High-Temperature Pyrolysis of Hydrocarbons. I. Methane to Acetylene," Industrial & Engineering Chemistry Process Design and Development, **15**pp. 439-444.

[54] Koerts, T., Deelen, M. J. A. G., and van Santen, R. A., 1992, "Hydrocarbon Formation from Methane by a Low-Temperature Two-Step Reaction Sequence," Journal of Catalysis, **138**(1) pp. 101-114.

[55] Aiello, R., Fiscus, J. E., zur LoyeCo-corresponding author., H., 2000, "Hydrogen Production Via the Direct Cracking of Methane Over Ni/SiO2: Catalyst Deactivation and Regeneration," Applied Catalysis A: General, **192**(2) pp. 227-234.

[56] Muradov, N., 2001, "Catalysis of Methane Decomposition Over Elemental Carbon," Catalysis Communications, **2**(3-4) pp. 89-94.

[57] Lázaro, M. J., Pinilla, J. L., Utrilla, R., 2010, " H_2− CH_4 Mixtures Produced by Carbon-Catalyzed Methane Decomposition as a Fuel for Internal Combustion Engines " Energy & Fuels, **24**(6) pp. 3340-3345.

[58] Botas, J. A., Serrano, D. P., Guil-López, R., 2010, "Methane Catalytic Decomposition Over Ordered Mesoporous Carbons: A Promising Route for Hydrogen Production," International Journal of Hydrogen Energy, **35**(18) pp. 9788-9794.

[59] Serrano, D. P., Botas, J. A., and Guil-Lopez, R., 2009, "H_2 Production from Methane Pyrolysis Over Commercial Carbon Catalysts: Kinetic and Deactivation Study," International Journal of Hydrogen Energy, **34**(10) pp. 4488-4494.

[60] Muradov, N., 2001, "Hydrogen Via Methane Decomposition: An Application for Decarbonization of Fossil Fuels," International Journal of Hydrogen Energy, **26**(11) pp. 1165-1175.

[61] Moliner, R., Suelves, I., Lázaro, M. J., 2005, "Thermocatalytic Decomposition of Methane Over Activated Carbons: Influence of Textural Properties and Surface Chemistry," International Journal of Hydrogen Energy, **30**(3) pp. 293-300.

[62] Suelves, I., Pinilla, J. L., Lazaro, M. J., 2008, "Carbonaceous Materials as Catalysts for Decomposition of Methane," Chemical Engineering Journal, **140**(1-3) pp. 432-438.

[63] Bai, Z., Chen, H., Li, B., 2005, "Catalytic Decomposition of Methane Over Activated Carbon," Journal of Analytical and Applied Pyrolysis, **73**(2) pp. 335-341.

[64] Lee, K. K., Han, G. Y., Yoon, K. J., 2004, "Thermocatalytic Hydrogen Production from the Methane in a Fluidized Bed with Activated Carbon Catalyst," Catalysis Today, **93–95**(0) pp. 81-86.

[65] Lee, S. Y., Kwak, J. H., Han, G. Y., 2008, "Characterization of Active Sites for Methane Decomposition on Carbon Black through Acetylene Chemisorption," Carbon, **46**(2) pp. 342-348.

[66] Kinoshita, K., 1988, "Carbon: Electrochemical and Physicochemical Properties," John Wiley Sons, New York, pp. 560-560.

[67] Hashimoto, A., Suenaga, K., Gloter, A., 2004, "Direct Evidence for Atomic Defects in Graphene Layers," Nature, **430**pp. 870-873.

[68] Popov, V. N., Henrard, L., and Lambin, P., 2009, "Resonant Raman Spectra of Graphene with Point Defects," Carbon, **47**(10) pp. 2448-2455.

[69] Liang, C., Xie, H., Schwartz, V., 2009, "Open-Cage Fullerene-Like Graphitic Carbons as Catalysts for Oxidative Dehydrogenation of Isobutane," Journal of the American Chemical Society, **131**(22) pp. 7735-7741.

[70] El-Barbary, A. A., Telling, R. H., Ewels, C. P., 2003, "Structure and Energetics of the Vacancy in Graphite," Physical Review B, **68**(14) pp. 144107-144114.

[71] Carlsson, J. M., and Scheffler, M., 2006, "Structural, Electronic, and Chemical Properties of Nanoporous Carbon," Physical Review Letters, **96**(4) pp. 046806-1-046806-4.

[72] Mahecha-Botero, A., Grace, J. R., Elnashaie, S. S. E. H., 2009, "Advances in Modeling of Fluidized-Bed Catalytic Reactors: A Comprehensive Review," Chemical Engineering Communications, **196**(11) pp. 1375-1405.

[73] Geldart, D., 1973, "Types of Gas Fluidization," Powder Technology, **7**(5) pp. 285-292.

[74] Serrano, D. P., Botas, J. Á., Pizarro, P., 2013, "Kinetic and Autocatalytic Effects during the Hydrogen Production by Methane Decomposition Over Carbonaceous Catalysts," International Journal of Hydrogen Energy, **38**(14) pp. 5671-5683.

[75] Bautista, O., Méndez, F., and Treviño, C., 2008, "Theoretical Analysis of the Direct Decomposition of Methane Gas in a Laminar Stagnation-Point Flow: CO2-Free Production of Hydrogen," International Journal of Hydrogen Energy, **33**(24) pp. 7419-7426.

[76] Hirsch, D., and Steinfeld, A., 2004, "Radiative Transfer in a Solar Chemical Reactor for the Co-Production of Hydrogen and Carbon by Thermal Decomposition of Methane," Chemical Engineering Science, **59**(24) pp. 5771-5778.

[77] Pinilla, J. L., Suelves, I., Lazaro, M. J., 2008, "Kinetic Study of the Thermal Decomposition of Methane using Carbonaceous Catalysts," Chemical Engineering Journal, **138**(1-3) pp. 301-306.

[78] Abbas, H. F., and Daud, W. M. A. W., 2009, "Deactivation of Palm Shell-Based Activated Carbon Catalyst used for Hydrogen Production by Thermocatalytic Decomposition of Methane," International Journal of Hydrogen Energy, **34**(15) pp. 6231-6241.

[79] Abbas, H. F., and Wan Daud, W. M. A., 2009, "Thermocatalytic Decomposition of Methane using Palm Shell Based Activated Carbon: Kinetic and Deactivation Studies," Fuel Processing Technology, **90**(9) pp. 1167-1174.

[80] Solymosi, F., Erdohelyi, A., Cserenyi, J., 1994, "Decomposition of CH4 Over Supported Pd Catalysts," Journal of Catalysis, **147**(1) pp. 272-278.

[81] Amin, A. M. L., 2011, "Modeling and Experimental Study of Methane Catalytic Cracking as A Hydrogen Production Technology," Doctoral Dissertation, University of Waterloo, Chemical Engineering Department, pp. 249.

[82] Hazra, M., Croiset, E., Hudgins, R. R., 2009, "Experimental Investigation of the Catalytic Cracking of Methane Over a Supported Ni Catalyst," Canadian Journal of Chemical Engineering, **87**(1) pp. 99-105.

[83] Appel, J., Bockhorn, H., and Frenklach, M., 2000, "Kinetic Modeling of Soot Formation with Detailed Chemistry and Physics: Laminar Premixed Flames of C2 Hydrocarbons," Combustion and Flame, **121**(1-2) pp. 122-136.

[84] Gidaspow, D., Jung, J., and Singh, R. K., 2004, "Hydrodynamics of Fluidization using Kinetic Theory: An Emerging Paradigm," Powder Technology, **148**(2-3) pp. 123-141.

[85] Tsuji, Y., Kawaguchi, T., and Tanaka, T., 1993, "Discrete Particle Simulation of Two-Dimensional Fluidized Bed," Powder Technology, **77**(1) pp. 79-87.

[86] Kunii, D., and Levenspiel, O., 1991, "Fluidization Engineering," Butterworth-Heinemann, pp. 491.

[87] Leva, M., 1959, "Fluidization," McGraw Hill, New York, pp. 327.

[88] Davidson, J.F., and Harrison, D., 1971, "Fluidization," Academic Press, London, pp. 847.

[89] Geldart, D., and Wong, A. C. Y., 1984, "Fluidization of Powders Showing Degrees of cohesiveness—I. Bed Expansion," Chemical Engineering Science, **39**(10) pp. 1481-1488.

[90] Lim, K. S., Zhu, J. X., and Grace, J. R., 1995, "Hydrodynamics of Gas-Solid Fluidization," International Journal of Multiphase Flow, **21**pp. 141-193.

[91] Kameya, Y., and Hanamura, K., 2012, "Carbon Black Texture Evolution during Catalytic Methane Decomposition," Carbon, **50**(10) pp. 3503-3512.

[92] Bai, Z., Chen, H., Li, W., 2006, "Hydrogen Production by Methane Decomposition Over Coal Char," International Journal of Hydrogen Energy, **31**(7) pp. 899-905.

[93] Serrano, D. P., Botas, J. Á., Pizarro, P., 2008, "Ordered Mesoporous Carbons as Highly Active Catalysts for Hydrogen Production by CH_4 Decomposition," Chemical Communications, pp. 6585-6587.

[94] Costandy, J., El Ghazal, N., Mohamed, M. T., 2012, "Effect of Reactor Geometry on the Temperature Distribution of Hydrogen Producing Solar Reactors," International Journal of Hydrogen Energy, **37**(21) pp. 16581-16590.

[95] Younessi Sinaki, M., Matida, E. A., and Hamdullahpur, F., 2011, "Development of a Reaction Mechanism for Predicting Hydrogen Production from Homogeneous Decomposition of Methane," International Journal of Hydrogen Energy, **36**(4) pp. 2936-2944.

[96] Brown, P. N., Byrne, G. D., and Hindmarsh, A. C., 1989, "VODE, A Variable-Coefficient ODE Solver," SIAM Journal on Scientific and Statistical Computing, **10**(5) pp. 1038-1051.

[97] Konnov A.A., 2000, "Detailed Reaction Mechanism for Small Hydrocarbons Combustion," Http://homepages.Vub.Ac.be/~akonnov/, pp. 1-24.

[98] Smith, G. P., Golden, D. M., Frenklach, M., 1997, " GRI-Mech 3.0," .

[99] Dagaut, P., and Nicolle, A., 2005, "Experimental and Detailed Kinetic Modeling Study of Hydrogen-Enriched Natural Gas Blend Oxidation Over Extended Temperature and Equivalence Ratio Ranges," Proceedings of the Combustion Institute, **30**(2) pp. 2631-2638.

[100] Hughes, K. J., Turányi, T., Clague, A. R., 2001, "Development and Testing of a Comprehensive Chemical Mechanism for the Oxidation of Methane," International Journal of Chemical Kinetics, **33**(9) pp. 513-538.

[101] Hidaka, Y., Sato, K., Henmi, Y., 1999, "Shock-Tube and Modeling Study of Methane Pyrolysis and Oxidation," Combustion and Flame, **118**(3) pp. 340-358.

[102] Back, M. H., and Back, R. A., 1983, "Pyrolysis: Theory and Industrial Practice," Academic Press, pp. 1-24.

[103] Murphy, D. B., Carroll, R. W., and Klonowski, J. E., 1997, "Analysis of Products of High-Temperature Pyrolysis of various Hydrocarbons," Carbon, **35**(12) pp. 1819-1823.

[104] Shah, N., Panjala, D., and Huffman, G. P., 2001, "Hydrogen Production by Catalytic Decomposition of Methane," Energy & Fuels, **15**(6) pp. 1528-1534.

[105] Frenklach, M., Wang, H., Goldenberg, M., 1995, "GRI-Mech-An Optimized Detailed Chemical Reaction Mechanism for Methane Combustion," Gas Research Institute, GRI-95/0058, .

[106] McBride, B.J., Gordon, S., and Reno, M.A., 1993, "Coefficients for Calculating Thermodynamic and Transport Properties of Individual Species," NASA, TM-4513, .

[107] Lutz, A.E., Kee, R.J., and Miller, J.A., 1997, "SENKIN: A Fortran Program For Predicting Homogeneous Gas Phase Chemical Kinetics With Sensitivity Analysis. " Sandia National Laboratories, SAND87-8248, MS-9051, Livermore.

[108] Billaud, F., Gueret, C., and Weill, J., 1992, "Thermal Decomposition of Pure Methane at 1263 K. Experiments and Mechanistic Modelling," Thermochimica Acta, **211**(0) pp. 303-322.

[109] Burgess, D. R., Allison, T. C., Manion, J. A., "NIST Chemical Kinetic Combustion Model Database," .

[110] Sheen, D. A., You, X., Wang, H., 2009, "Spectral Uncertainty Quantification, Propagation and Optimization of a Detailed Kinetic Model for Ethylene Combustion," Proceedings of the Combustion Institute, **32**(1) pp. 535-542.

[111] Glaude, P. A., Warth, V., Fournet, R., 1998, "Modeling of the Oxidation of n-Octane and n-Decane using an Automatic Generation of Mechanisms," International Journal of Chemical Kinetics, **30**(12) pp. 949-959.

[112] Gupta, G. K., Hecht, E. S., Zhu, H., 2006, "Gas-Phase Reactions of Methane and Natural-Gas with Air and Steam in Non-Catalytic Regions of a Solid-Oxide Fuel Cell," Journal of Power Sources, **156**(2) pp. 434-447.

[113] Curran, H. J., Gaffuri, P., Pitz, W. J., 1998, "A Comprehensive Modeling Study of n-Heptane Oxidation," Combustion and Flame, **114**(1–2) pp. 149-177.

[114] Held, T. J., Marchese, A. J., and Dryer, F. L., 1997, "A Semi-Empirical Reaction Mechanism for n-Heptane Oxidation and Pyrolysis," Combustion Science and Technology, **123**(1-6) pp. 107-146.

[115] Babushok, V. I., and Tsang, W., 2004, "Kinetic Modeling of Heptane Combustion and PAH Formation," Journal of Propulsion and Power, **20**(3) pp. 403-414.

[116] Meeks, E., Naik, C.V., Puduppakkam, K.V., 2009, "Experimental and Modeling Studies of Combustion Characteristics of Conventional and Alternative Jet Fuels. " NASA, CR NNC07CB45C-Final Report 1, .

[117] Dunker, A. M., Kumar, S., and Mulawa, P. A., 2006, "Production of Hydrogen by Thermal Decomposition of Methane in a Fluidized-Bed Reactor-Effects of Catalyst, Temperature, and Residence Time," International Journal of Hydrogen Energy, **31**(4) pp. 473-484.

[118] Levine, I.N., 2009, "Physical chemistry " McGraw Hill, New York, pp. 1008.

[119] Frenklach, M., 1996, "On Surface Growth Mechanism of Soot Particles," Symposium (International) on Combustion, **26**(2) pp. 2285-2293.

[120] Pinilla, J. L., Suelves, I., Utrilla, R., 2007, "Hydrogen Production by Thermo-Catalytic Decomposition of Methane: Regeneration of Active Carbons using CO_2," Journal of Power Sources, **169**(1) pp. 103-109.

[121] Frenklach, M., and Wang, H., 1991, "Detailed Modeling of Soot Particle Nucleation and Growth," Symposium (International) on Combustion, **23**(1) pp. 1559-1566.

[122] Younessi-Sinaki, M., and Hamdullahpur, F., 2014, "Numerical Investigation on the Number of Active Surface Sites of Carbon Catalysts in the Decomposition of Methane," AICHE Journal, **60**(6) pp. 2228-2234.

[123] Frenklach, M., and Harris, S. J., 1987, "Aerosol Dynamics Modeling using the Method of Moments," Journal of Colloid and Interface Science, **118**(1) pp. 252-261.

[124] Richardson, J. F., and Zaki, W. N., 1954, "The Sedimentation of a Suspension of Uniform Spheres Under Conditions of Viscous Flow," Chemical Engineering Science, **3**(2) pp. 65-73.

[125] Hoffmann, A. C., and Finkers, H. J., 1995, "A Relation for the Void Fraction of Randomly Packed Particle Beds," Powder Technology, **82**(2) pp. 197-203.

[126] Ergun, S., 1952, "Fluids Flow through Packed Column," Chemical Engineering Progress, **48**(2) pp. 89-94.

[127] Wen, C. Y., and Yu, Y. H., 1966, "A Generalized Method for Predicting the Minimum Fluidization Velocity," AICHE Journal, **12**(3) pp. 610-612.

[128] Grace, J.R., 1982, "Fluidized Bed Hydrodynamics," Hemisphere, Washington, pp. 1024.

[129] Bin, A. K., 1994, "Prediction of the Minimum Fluidization Velocity," Powder Technology, **81**(2) pp. 197-199.

[130] Zhiping, Z., Yongjie, N., and Qinggang, L., 2007, "Effect of Pressure on Minimum Fluidization Velocity," Journal of Thermal Science, **16**(3) pp. 264-269.

[131] Adánez, J., and Abanades, J. C., 1991, "Minimum Fluidization Velocities of Fluidized-Bed Coal-Combustion Solids," Powder Technology, **67**(2) pp. 113-119.

[132] Hartman, M., Trnka, O., and Svoboda, K., 2000, "Fluidization Characteristics of Dolomite and Calcined Dolomite Particles," Chemical Engineering Science, **55**(24) pp. 6269-6274.

[133] Reina, J., Velo, E., and Puigjaner, L., 2000, "Predicting the Minimum Fluidization Velocity of Polydisperse Mixtures of Scrap-Wood Particles," Powder Technology, **111**(3) pp. 245-251.

[134] Fletcher, J. V., Deo, M. D., and Hanson, F. V., 1992, "Re-Examination of Minimum Fluidization Velocity Correlations Applied to Group B Sands and Coked Sands," Powder Technology, **69**(2) pp. 147-155.

[135] Subramani, H. J., Mothivel Balaiyya, M. B., and Miranda, L. R., 2007, "Minimum Fluidization Velocity at Elevated Temperatures for Geldart's Group-B Powders," Experimental Thermal and Fluid Science, **32**(1) pp. 166-173.

[136] Gauthier, D., Zerguerras, S., and Flamant, G., 1999, "Influence of the Particle Size Distribution of Powders on the Velocities of Minimum and Complete Fluidization," Chemical Engineering Journal, **74**(3) pp. 181-196.

[137] Thonglimp, V., 1985, "Fluidization," Academic Press, London, pp. 31-33.

[138] Doichev, K., and Akhmakov, N. S., 1979, "Fluidisation of Polydisperse Systems," Chemical Engineering Science, **34**(11) pp. 1357-1359.

[139] Xu, C. C., and Zhu, J., 2008, "Prediction of the Minimum Fluidization Velocity for Fine Particles of Various Degrees of Cohesiveness," Chemical Engineering Communications, **196**(4) pp. 499-517.

[140] Abrahamsen, A. R., and Geldart, D., 1980, "Behaviour of Gas-Fluidized Beds of Fine Powders Part I. Homogeneous Expansion," Powder Technology, **26**(1) pp. 35-46.

[141] Yang, F., Thornton, C., and Seville, J., 2013, "Effect of Surface Energy on the Transition from Fixed to Bubbling Gas-Fluidised Beds," Chemical Engineering Science, **90**(1-2) pp. 119-129.

[142] Pinilla, J. L., Suelves, I., Lázaro, M. J., 2009, "Influence on Hydrogen Production of the Minor Components of Natural Gas during its Decomposition using Carbonaceous Catalysts," Journal of Power Sources, **192**(1) pp. 100-106.

[143] Todd, B., and Young, J. B., 2002, "Thermodynamic and Transport Properties of Gases for use in Solid Oxide Fuel Cell Modelling," Journal of Power Sources, **110**(1) pp. 186-200.

[144] Lemmon, E. W., and Jacobsen, R. T., 2004, "Viscosity and Thermal Conductivity Equations for Nitrogen, Oxygen, Argon, and Air," International Journal of Thermophysics, **25**(1) pp. 21-69.

[145] Ye, M., Van der Hoef, M. A., and Kuipers, J. A. M., 2005, "The Effects of Particle and Gas Properties on the Fluidization of Geldart A Particles," Chemical Engineering Science, **60**(16) pp. 4567-4580.

[146] Levenspiel, O., 1999, "Chemical Reaction Engineering," John Wiley & Sons, New York, pp. 688.